PHYSICS REPORTS (Review Section of Physics Letters) 177, Nos. 5 & 6 (1989) 319–405. North-Holland, Amsterdam

SPIN EFFECTS AT SUPERCOLLIDER ENERGIES

C. BOURRELY, J. SOFFER

Centre de Physique Théorique, CNRS, Luminy, Case 907, F-13288 Marseille Cedex 9, France*

F.M. RENARD

*Laboratoire de Physique Mathématique**, USTL, Place E. Bataillon, F-34060 Montpellier Cedex, France*

P. TAXIL***

Division TH, CERN, CH-1211 Geneva 23, Switzerland

Received December 1988

Contents:

* Laboratoire propre du CNRS LP 7061.
** Unité associée au CNRS no. 040768.
*** Permanent address: Centre de Physique Théorique, CNRS, Case 907, Luminy, F-13288 Marseille Cedex 9, France.

Single orders for this issue

PHYSICS REPORTS (Review Section of Physics Letters) 177, Nos. 5 & 6 (1989) 319–407.

Copies of this issue may be obtained at the price given below. All orders should be sent directly to the Publisher. Orders must be accompanied by check.

Single issue price Dfl. 66.00, postage included.

0 370-1573/89/$30.45

SPIN EFFECTS AT SUPERCOLLIDER ENERGIES

C. BOURRELY, J. SOFFER

Centre de Physique Théorique, CNRS, Luminy, Case 907, F-13288 Marseille Cedex 9, France

F.M. RENARD

Laboratoire de Physique Mathématique, USTL, Place E. Bataillon, F-34060 Montpellier Cedex, France

and

P. TAXIL

Division TH, CERN, CH-1211 Geneva 23, Switzerland

NORTH-HOLLAND – AMSTERDAM

Abstract:

Polarization studies have proven to be relevant at current accelerator energies, providing valuable experimental information in different areas of particle physics, some of which is a real challenge for dynamical theories. The purpose of this review is to answer the question: does hadron supercollider physics need polarized beams? We present in the framework of gauge theories, Standard Model and beyond it, many original calculations of single or double helicity asymmetries for a large number of interesting processes. These results, some of which are spectacular, emphasize the significant advantages of the full use of polarized proton beams for signal detection in the exploration of the 1 TeV scale.

1. Introduction

Hopefully there will be several multi-TeV hadronic machines in operation in the next decade. The chances are high that in the United States a Superconducting Super Collider (SSC) with an energy of 20 TeV per beam and a luminosity of $10^{33}\,\mathrm{cm}^{-2}\,\mathrm{s}^{-1}$ will be built. Europe is planning a Large Hadron Collider (LHC), to be hosted in the LEP tunnel, with a proton beam energy of 8 TeV or so and a luminosity up to $10^{34}\,\mathrm{cm}^{-2}\,\mathrm{s}^{-1}$. There are many fundamental reasons why particle physics needs high energy, high luminosity and why these new hadron colliders will be major research facilities. Within the framework of the Standard Model we still have to discover the Higgs boson, whose mass is unknown, and we must get a physical understanding of why and how the electroweak symmetry is broken. We would like to know if heavier quarks and leptons exist and if there is a deep reason for having a particular number of generations. Although parity violation has been known for many years, an important question remains: is parity violation of the Standard Model a low-energy property of nature? The answer to this question may be given by extending the standard gauge structure, for example by restoring right–left symmetry. Other extensions have also been proposed in the framework of grand unified theories or inspired by superstring models. There is some hope to go beyond the Standard Model and to hit new areas in particle physics where new particles and new interactions would show up. For example, one would like to discover supersymmetry, a further symmetry in nature relating fermion and boson states, or to detect any structure quarks and leptons could have, another attractive possibility.

To open windows for new physics these future machines should be able to search for quite high masses, say in the TeV range, and given the fact that quarks or gluons often carry only a small fraction of the hadron momentum, a beam energy of several TeV is certainly required. Moreover, the cross section for producing a new particle of mass 1 TeV/c^2 is of the order of $10^{-36}\,\mathrm{cm}^2$ or smaller (assuming the interaction coupling constant is of the order of 0.1), so one should achieve a luminosity of $10^{33}\,\mathrm{cm}^{-2}\,\mathrm{s}^{-1}$, which will allow one to reach cross sections as small as $10^{-40}\,\mathrm{cm}^2$ with a running time of 10^7 s/year. Knowing that this interesting physics will lie in small cross sections and that signal detection will be the hardest part of data analysis, further means are needed to disentangle new physics and polarized beams might be one way to do it.

Spin has been shown to be very useful at lower energies [BOU80, YOK80, CRA83, BRO82, MAR84, SER86, MIN88], providing elegant and powerful methods in various instances, some of which are worth recalling:

– the precise measurement of the mass of the upsilon mesons using resonance depolarization of the polarized beam in a e^+e^- storage ring [ART82], a method which was used earlier at Novosibirsk for the phi meson [BUK78];

– the use of the transverse polarization of the beams in a e^+e^- storage ring both at Spear [SCH75] and Petra [ORI79] up to $\sqrt{s} = 30$ GeV to confirm the spin 1/2 nature of the quarks, from the azimuthal φ

distribution of charged and neutral hadrons in $e^+e^- \to hX$, which has minima for $\varphi = \pm\pi/2$ as shown in fig. 1.1;
- the famous SLAC experiment [PRE78, PRE79] in deep inelastic ep scattering with a polarized electron beam on an unpolarized target to detect a parity violation effect from γ–Z interference in beautiful agreement with the prediction of the electroweak theory;
- the observation in hadronic collisions of several interesting effects in exclusive reactions at large angles, which are a real challenge for dynamical models, and also of strong polarization effects in inclusive hyperon production growing with transverse momentum.

Concerning this last point, let us recall that in pp elastic scattering at 28 GeV/c, the analyzing power A is of the order of 5% in the small-angle region but increases to a much higher positive value for $\theta_{cm} \sim 45°$ as shown in fig. 1.2. This is evidence for the serious need of non-perturbative effects in a kinematic region where perturbative QCD is believed to be relevant [SOF87]. For inclusive hyperon production by unpolarized 400 GeV/c protons, the experimental situation of the transverse polarization of the final baryon in the proton fragmentation region is summarized in fig. 1.3. It is negative for Λ, Ξ^0 and Ξ^-, positive for $\Sigma^\pm$ and zero for $\bar{\Lambda}$. For illustration we also show, in fig. 1.4, the Λ polarization in $K^-p \to \Lambda X$ in the K^- fragmentation region, which is now positive, larger than in the previous case and essentially independent of the incident beam energy. Some qualitative features of these data are consistent with simple semiclassical theoretical ideas [AND83, DEG85], but we are still missing a serious understanding of the subtle dynamical origin of this important phenomenon where experiment is far ahead of theory.

Finally let us mention an unexpected effect for π^0 production in the central region with a polarized target, where a large transverse spin asymmetry has been observed as shown in fig. 1.5 in π^-p and π^-d collisions at 40 GeV/c, which was first discovered at CERN in pp collisions [ANT80].

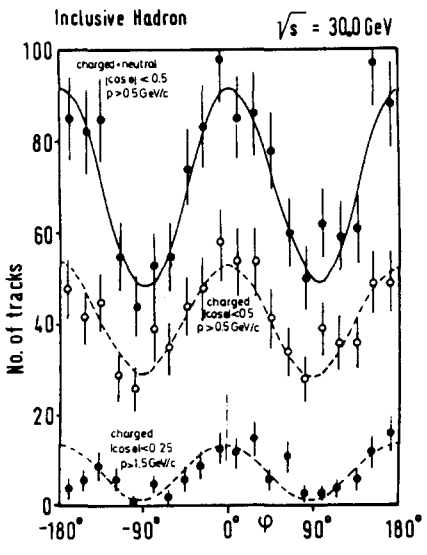

Fig. 1.1. Azimuthal ϕ distribution in inclusive e^+e^- hadron production with various cuts at $\sqrt{s} = 30$ GeV, from [ORI79].

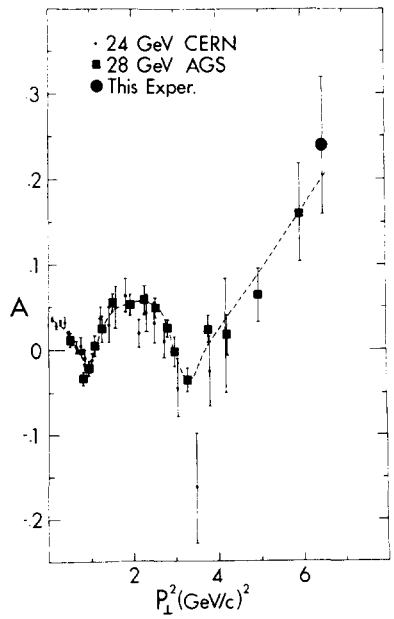

Fig. 1.2. The analyzing power A for pp elastic scattering versus $p_\perp^2$, taken from [CAM85]. The curve is hand-drawn to guide the eye.

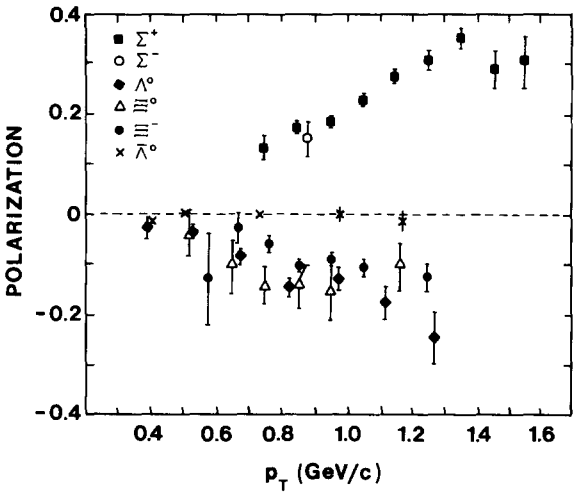

Fig. 1.3. Transverse polarizations of different hyperons produced by 400 GeV/c protons on Be versus p_T, taken from [WIL87] and references therein.

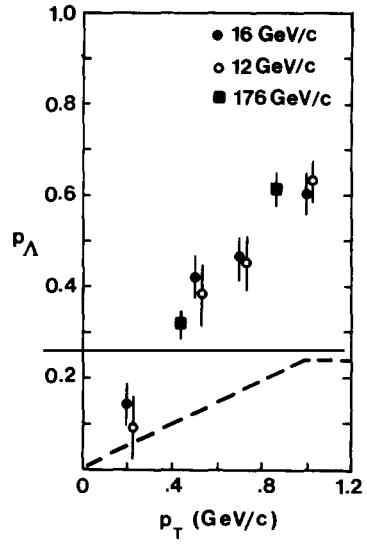

Fig. 1.4. Transverse Λ polarization in $K^-p \to \Lambda X$ versus p_T at 12 GeV/c and 16 GeV/c, taken from [ARM85], and at 176 GeV/c, from [GOU86]. The dashed line shows for comparison the magnitude of P_Λ in proton induced reactions.

Clearly, these transverse polarization effects, which make all the excitement in an energy range much below 1 TeV, are too complicated to be explained in terms of lowest-order calculations. However, these calculations are useful to evaluate helicity effects and, as we will see, they are very interesting in the multi-TeV energy range, where life is simpler. There are probably also higher-order effects which may come as surprises but we will restrict our study to the discussion of the lowest-order ones.

In present day hadronic machines there is some real effort to continue the existing experimental programs, both at BNL and Serpukhov, or to undertake new programs at higher energies, like the construction of the polarized proton beam obtained from Λ decay at FNAL, which has already

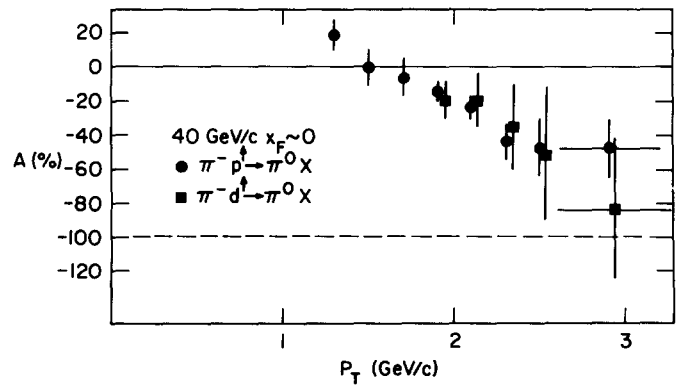

Fig. 1.5. Results on single transverse spin asymmetry versus p_T, taken from [VAS88].

produced some data [FNA88], and at CERN the future installation of a polarized gas target by the UA6 collaboration [CER88]. For future machines, polarization is a major concern; in particular HERA will have polarized electrons, which is perhaps one of its most attractive features; SLC will also have polarized electrons and people seem to be convinced now that LEP should have polarized beams [BLO87, ALE88]. This would improve greatly our ability to get an accurate determination of the Standard Model parameters. Moreover, a precise measurement of the left–right helicity asymmetry at the Z^0 peak would allow one, through virtual effects, to get some information about the top quark and Higgs boson masses as well as possible manifestations of new physics. Future e^+e^- machines in the TeV energy range are being seriously considered (CLIC at CERN, TLC at SLAC, VLEPP in the USSR) and a recent report [AHN88] shows that the e^+e^- physics community is already aware that "... one should plan for polarization as an integral part of the collider design ...".

The goal of this paper is to show that there are fundamental physics issues which can be illuminated by the use of polarized beams in future hadron colliders, so such an option should be taken seriously in the design of these planned facilities. We will follow the spirit of the work of Eichten, Hinchliffe, Lane and Quigg [EIC84] (henceforth referred to as EHLQ) and we will try to provide reliable estimates of spin asymmetries both for the physics of the Standard Model and for new physics implied by various exciting speculations. We will consider the pp, and not $\bar{p}p$, option, which has the merits on the one hand to reach a higher luminosity and on the other hand to give access to double spin asymmetries, since nobody knows today how to make a multi-TeV polarized $\bar{p}$ beam.

On the contrary, such a proton beam seems feasible and section 2 will be devoted to a short review on this question, where we will recall the essential arguments according to the experts in this field, based in particular on the Siberian Snake concept. In section 3 we will give analytic expressions for a plausible set of unpolarized and polarized parton distributions and we will calculate the parton differential luminosities, which are very useful for a quick estimate of the production rates at supercollider energies. In section 4 we will discuss, as first applications, direct photon production and hadron jet phenomena described in terms of hard scattering constituent interactions. When the subprocess center of mass energy is above 200 GeV or so, weak interactions and consequently large parity violating asymmetries are expected. They will be presented in some detail in section 5 in the framework of the electroweak Standard Model, in particular spin tests in lepton pair, single gauge boson production and pair production of gauge bosons. We will also give some asymmetries involving the production of the most important particle which remains to be found, namely the scalar Higgs boson.

We will then turn to new physics and we will treat in section 6 the minimal extension of the standard model with new quarks, new leptons and new gauge bosons. Compositeness including technicolor will be discussed in section 7, where new couplings among leptons, quarks and vector bosons will be considered, in particular taking into account residual interactions with contact terms. Let us stress already that the chirality structure of such a new interaction is arbitrary: it may well violate parity and this could trigger new spectacular spin effects. In section 8 we will investigate the usefulness of spin as a tool to reveal the existence of SUSY particles. Section 9 will be devoted to a new type of processes, WW collisions, which has a growing interest at supercolliders. We will try to draw some conclusions of our study in section 10.

Finally, the recent results of the EMC experiment [ASH88] on deep inelastic scattering of polarized muons on a polarized target has motivated a large number of theoretical papers on the subject of the proton spin, so we ought to review the present situation. This will be done in appendix A, where we

also mention briefly what HERA will miss without proton polarization. This is followed by appendices B to G, where we give several useful but lengthy formulae.

2. Technical feasibility of multi-TeV polarized protons

Our purpose is to give a brief summary of reports made by experts in this domain and we just stress what is reasonably expected from the new technical developments [MON84, TER83, COU84].

The present capability to accelerate a polarized proton beam has been proved to a lab energy of 22 GeV/c with a polarization of 46% at the Brookhaven AGS [KRI85], so a big gap has to be bridged in the future to obtain a polarized proton beam with an energy of several TeV. Among the different projects presented in the literature the most probable configuration designed to get a multi-TeV polarized beam contains the following parts: a polarized ion source from which polarized protons are injected into a Linac; the beam is then accelerated and stored in one or two boosters to reach an energy around 1 TeV; next the beam comes into the rings of the main collider, where a new boost produces the final beam energy (fig. 2.1). At first sight this structure looks similar to a standard unpolarized beam accelerator; however, to keep a bunch of protons with all their spins aligned in the same direction is the main difficulty, because there exists a strong tendency for the protons to depolarize when interacting with the electromagnetic fields created by the different magnets installed in an accelerator.

The first component of this chain of devices is an efficient polarized proton source [SCH84]. There exist several types of polarized sources like Lamb shift (metastable) sources, atomic (ground state) sources, ultracold atomic sources and optically pumped sources; all these are currently in use and still

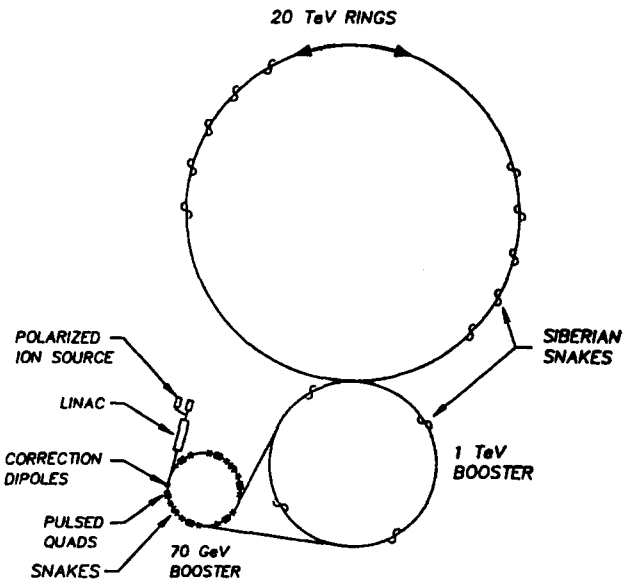

Fig. 2.1. Acceleration of polarized protons at the SSC (not to scale) [KRI85].

under development. It is expected in the near future that $\vec{H}^-$ dc currents of 100 μA will be obtained, as compared with 10 to 20 μA obtainable now. Moreover, a booster such as the one now being constructed at the AGS will increase the useable polarized beam intensity by an additional factor of about 25. High-intensity currents (1 mA) will be necessary to construct a beam of 10^{12} polarized protons in order to produce a reasonable total number of events/year for most of the scattering processes of interest.

The main concern when accelerating a polarized beam to high energy is to avoid depolarization resonances, so let us outline how this phenomenon occurs. We consider a circular accelerator in which vertically polarized particles are kept on their orbit by a vertical magnetic field; in that case each particle will precess about the vertical axis, and thus the vertical projection of the spin vector is preserved; as a result no depolarization occurs. However, in order to maintain particles close to the calculated orbit focusing fields are necessary, in particular horizontal magnetic fields; consequently the spin precesses out of the vertical direction, inducing a depolarization. It is shown that depolarization becomes important when the spin precession frequency of the particle is equal to an integer multiple of the frequency with which the particle sees horizontal magnetic fields as it circles the accelerator with the cylotron frequency. If such a condition is realized then a depolarizing resonance occurs; in fact, after each turn a small precession around the horizontal axis adds in phase with those of the previous turns [RUT84].

One distinguishes two major types of depolarizing resonances: the intrinsic depolarization resonances, which are caused by the horizontal magnetic fields of the quadrupole magnets, and the imperfection depolarizing resonances, due to misalignments and imperfect magnets. The number of resonances a particle has to cross in an accelerator of 20 GeV is about 30; this number increases to 200 for an energy up to 100 GeV and in the case of the SSC there will be around 30 000 imperfection depolarizing resonances to correct in each ring!

For low-energy accelerators like the ZGS and the AGS intrinsic resonances are destroyed by the technique of "resonance jumping" using fast quadrupole magnets; in the case of imperfection depolarizing resonances, correction dipole magnets are applied to the beam. All these techniques work well up to energies of 30 GeV; their extension to higher energy seems inappropriate because one has to deal with hundreds of resonances. A solution to the problem of depolarizing resonances was invented by Derbenev and Kondratenko [DER77]; this solution is known as the "Siberian Snake".

The basic idea of a Siberian Snake is to use a string of six to ten magnets which precesses the spin by 180° around the longitudinal direction after one turn around the accelerator and at the same time yields no net orbit deflection (the magnets give an important beam motion so the orbit follows a twisted path like a snake). During the circulation of the beam any spin rotation which occurs after the first turn is then canceled by the identical rotation which occurs during the second turn. There are different possibilities to combine several Siberian Snakes; for instance, one Snake rotates spin by 180° about the longitudinal direction (type I Snake), while another one rotates it by 180° about the horizontal direction (type II Snake). In that case the precession frequency is 1/2, but the equilibrium spin is now up in one half of the accelerator and down in the other, the main advantage of the Siberian Snake technique being that the effect is energy independent. Let us notice that for the SSC a number of 50 Snakes are probably required in each ring to maintain a well-polarized beam. An experimental model of the Siberian Snake is presently being tested at the IUCF proton cooler ring [KRI87, TER88].

In conclusion, accelerating a polarized proton beam up to 20 TeV seems feasible at a reasonable cost (a few percent of the cost of an accelerator with unpolarized beams), provided one confirms that the Siberian Snake technique works experimentally.

3. Parton distributions and luminosities

3.1. Unpolarized and polarized parton distributions

A high-energy proton beam is an unseparated beam of constituent partons and all fundamental hadronic interactions, which are probed in pp collisions by testing the Standard Model or by producing new particles, involve the collisions of quarks and gluons at short distances. As an example, let us consider the hard scattering hadronic process

$$a + b \to c \text{ (or jet)} + X, \tag{3.1}$$

which is described in terms of two to two parton subprocesses as shown in fig. 3.1. In the QCD parton model, the corresponding inclusive cross section, provided factorization holds, is given by

$$d\sigma(a + b \to c + X) = \sum_{ij} \frac{1}{1+\delta_{ij}} \int dx_a\, dx_b\, [f_i^{(a)}(x_a, Q^2) f_j^{(b)}(x_b, Q^2) + (i \leftrightarrow j)]\, d\hat{\sigma}_{ij}\,. \tag{3.2}$$

The summation runs over all contributing parton configurations; the parton distribution $f_i^{(a)}(x_a, Q^2)$ is the probability that hadron a contains a parton i carrying a fraction x_a of the hadron's momentum. It represents the parton flux available in the colliding hadron, which is universal, that is, process independent. Clearly the parton distributions play a crucial role because they allow the connection between hadron–hadron collisions and elementary subprocesses. $d\hat{\sigma}_{ij}$ is the cross section for the interaction of two partons i and j, which can be calculated perturbatively. The total energy of the partons in the subprocess center of mass frame is

$$\sqrt{\hat{s}} = \sqrt{x_a x_b s}\,, \tag{3.3}$$

where $\sqrt{s}$ denotes the total center of mass energy of the initial hadrons. Finally Q^2, which is defined in terms of the invariants of the subprocess, characterizes the physical momentum scale. The distributions $f_i(x, Q^2)$ are extracted from deep inelastic data at low Q^2 and their Q^2 dependence, which is logarithmic, is predicted in perturbative QCD by the Altarelli–Parisi equations [ALT77] based on the renormalization group. For supercollider energies the relevant Q^2 range is $10^2 < Q^2 < 10^8$ GeV^2. The

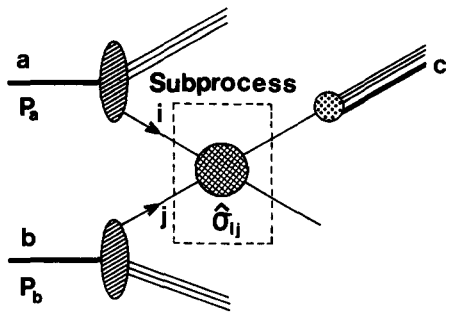

Fig. 3.1. Parton model representation of a hadron–hadron collision at short distances.

distributions fall rapidly with x at fixed Q^2 and for increasing Q^2, $f_i(x, Q^2)$ become very important at small x, where more and more partons can be produced. If we want to detect a small invariant mass, say 100 GeV, one sees from eq. (3.3) that we also need small x values, say $x \leq 10^{-3}$ for $\sqrt{s} = 40$ TeV; so at supercollider energies the hadron energy is less efficiently used and one should keep in mind that the kinematic region of interest is $10^{-5} < x < 10^{-1}$. These small values of x, even at low Q^2, are not probed by current experiments, which only extend to $x > 10^{-2}$. However, this present limited knowledge is not so critical because uncertainties are reduced for higher Q^2. Following recent studies [GRI83, COL84] we will take for granted that, modulo some reasonable approximations, the small-x behavior of the parton distributions at large Q^2 can be safely obtained analytically from perturbative QCD.

Rather than referring to any of the various numerical solutions available in the literature, we will provide our own set of parton distributions in terms of a simple parametrization of their x and Q^2 dependences, already used in [BOU87]. For the gluon distribution we take

$$xG(x, S) = K(S) \exp[12\sqrt{(S/b)\ln(1/x)}]\,(1-x)^6\,, \tag{3.4}$$

with

$$K(S) = 50.36[\exp(S) - 0.957]\exp(-7.597\sqrt{S})$$

and $t = \ln(Q^2/\Lambda^2)$ with $\Lambda = 200$ MeV and $S(Q^2) = \ln(t/t_0)$, where t_0 corresponds to the initial momentum value $Q_0^2 = 5$ GeV^2. As usual $b = 33 - 2N_f$, N_f being the number of quark flavors. This expression, except for the factor $(1-x)^6$ related to the large-x behavior of the distribution, was originally proposed in [RAL86]. It gives an excellent approximation up to $x = 0.1$, to the solutions provided by EHLQ in [EIC84]. Similarly by using the results quoted in [EIN86] for the valence u-quark distribution we will take

$$xu_v(x, S) = K'(S) \exp[4\sqrt{2}\sqrt{(S/b)\ln(1/x)}]\,x^{0.65}(1-x)^3\,, \tag{3.5}$$

with

$$K'(S) = 2\sqrt{S}\exp(-1.5S)\,.$$

For the valence d-quark distribution we will take

$$xd_v(x, S) = 0.5(1-x)xu_v(x, S)\,. \tag{3.6}$$

By comparing eq. (3.4) and eqs. (3.5) and (3.6) we see that the gluon distribution dominates over valence quark distributions at small x, because gluons carry a large fraction of the proton momentum due to the high probability of emission of soft gluons. This fact will have strong consequences for the evaluation of the production rates as will be discussed later.

For the sea u-quark distribution, following [RAL86] we will take[1)]

$$xu_s(x, S) = \tfrac{1}{2}[(S/b)\ln(1/x)]^{1/2}xG(x, S)\,, \tag{3.7}$$

[1)] The factor $\sqrt{3}$ in eq. (2) of [BOU87] is a misprint.

and like EHLQ we assume that the sea is isosymmetric, that is, $u_s = d_s$. One can also find heavy quarks inside a proton with a probability which becomes significant at high Q^2. For a heavy quark of mass m_q, $f_q(x, Q^2) = 0$ unless $Q^2 > m_q^2$ and for very high Q^2, above all mass thresholds, we will simply take

$$xq_s(x, S) = q_s x u_s(x, S) , \tag{3.8}$$

with

$$u_s : s_s : c_s : b_s : t_s = 1 : 0.82 : 0.33 : 0.23 : 0.14 .$$

A better determination of heavy quark distributions will be needed for a description of interactions such that heavy flavor couplings are enhanced, e.g. for Higgs production (see section 5).

So far we have ignored the spin of the initial protons, but if we consider the case of polarized beams one can define correspondingly polarized parton distributions. For a given parton (quark, antiquark or gluon) we denote by $f_\pm(x, Q^2)$ the parton distributions in a polarized nucleon either with helicity parallel (+) or antiparallel (−) to the parent nucleon helicity. As usual, we define the *unpolarized distribution* $f = f_+ + f_-$ and the *parton helicity asymmetry* $\Delta f = f_+ - f_-$. Let us recall that for the inclusive reaction (3.1) with both initial hadrons longitudinally polarized, the double helicity hadron asymmetry A_{LL}, defined as

$$A_{LL} = \frac{d\sigma_{a(+)b(+)} - d\sigma_{a(+)b(-)}}{d\sigma_{a(+)b(+)} + d\sigma_{a(+)b(-)}} , \tag{3.9}$$

is given by

$$A_{LL}\, d\sigma = \sum_{ij} \frac{1}{1+\delta_{ij}} \int dx_a\, dx_b\, [\Delta f_i^{(a)}(x_a, Q^2)\, \Delta f_j^{(b)}(x_b, Q^2) + (i \leftrightarrow j)] \hat{a}_{LL}^{ij}\, d\hat{\sigma}_{ij} , \tag{3.10a}$$

assuming the factorization property, where $d\sigma$ is given by eq. (3.2) and $\hat{a}_{LL}^{ij}$ denotes the subprocess double helicity asymmetry for initial partons i and j[2]. The explicit expressions of these quantities for various subprocesses are given in section 4. To get a rough estimate of A_{LL} one can use the following approximation:

$$A_{LL} \sim \sum_{ij} \langle \Delta f_i / f_i \rangle \langle \Delta f_j / f_j \rangle \hat{a}_{LL}^{ij} , \tag{3.10b}$$

in terms of the average of the *parton polarizations* defined as $\Delta f_i / f_i$. This shows that, even if at the parton level $\hat{a}_{LL}^{ij}$ is as large as $\pm 100\%$, it is expected to be diluted twice at the hadron level since, as we will see below, the parton polarizations are much less than one in the relevant kinematic region.

Our experimental knowledge on the quark helicity asymmetries Δq_i comes from deep inelastic scattering of polarized charged lepton beams from polarized targets. One measures the virtual photon–nucleon asymmetry defined as

[2] Here we have assumed parity conservation for the parton distributions, namely the probability for a parton with a given helicity (+ or −) inside a polarized nucleon with a given helicity (+ or −) is the same if both parton and nucleon helicities are reversed.

$$A_1(x) = \frac{\Sigma_i e_i^2 \Delta q_i(x)}{\Sigma_i e_i^2 q_i(x)} \,. \tag{3.11}$$

In fig. 3.2 we show the data on A_1 versus x for polarized protons from a SLAC–Yale experiment [BAU83] and from the recent EMC experiment [ASH88] in the limited Q^2 range ($Q^2 < 70\,\mathrm{GeV}^2$). This graph also shows the results of some theoretical calculations. The dotted curve corresponds to a model based on the three-quark SU(6) wave function [BAB79]. In this case the helicity of the proton is carried by its valence quarks and the gluon does not contribute. The solid curve, in better agreement with the data, corresponds to the model of Carlitz and Kaur [CAR77] introducing SU(6) breaking effects based on the idea that valence quarks carry most of the proton helicity *only* at large x values. In this case the gluon carries 25% of the proton helicity. The dashed–dotted curve corresponds to a model [CHI85] which generalizes the Carlitz–Kaur model and leads to a closer consistency with the data near $x = 0$ due to a larger contribution of the gluon to the proton helicity. Finally the dashed curve is the prediction of the MQM/QGD approach [GIA85], where the gluon is believed to play no role, which gives a fair description of the data *both* at small and large x. These new EMC data have generated a large number of theoretical papers [SOF87a, GLU88, LEA88, PRE88, CLO88, BRO88, EFR88], most of them devoted to the discussion of the validity of the sum rules [ELL74, BJO66] one is able to test by using the data (see appendix A). The interpretation of these *low-Q^2* data is controversial and remains to be clarified by the measurement of A_1 on polarized neutrons, which will indeed be very crucial. A better knowledge of the strange sea quark polarization [PRE88] and of the gluon polarization [GUI88] is also essential. In spite of these uncertainties, if one adopts a conservative attitude, it is possible to give at *high Q^2* a consistent set of parton helicity asymmetries, which will be used to evaluate hadron helicity asymmetries.

For the gluon helicity asymmetry the small-x behavior has been derived in [EIN86] and by fitting the numerical results of [CHI87] we obtain the simple expression

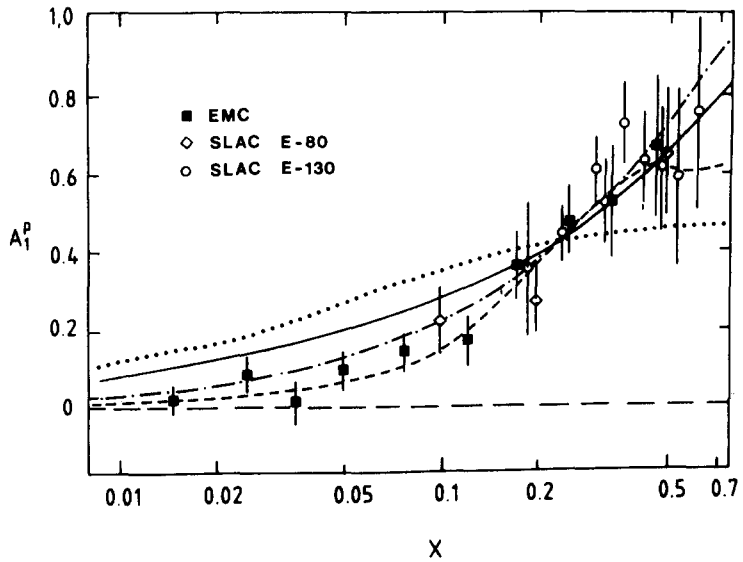

Fig. 3.2. Data on A_1 versus x from [ASH88], with various theoretical calculations (see text).

$$x\,\Delta G(x, S) = K''(S)x \exp[4(10 + \sqrt{64 - 6N_f})^{1/2}\sqrt{(S/b)\ln(1/x)}]\,(1-x)^6\,, \tag{3.12}$$

with $K''(S) = \exp(-4.5\sqrt{S})$.

For the valence quark helicity asymmetries we will use the approach introduced in [CHI85] as model I. So we take

$$\begin{aligned} \Delta u_v(x, S) &= \cos 2\theta_u\, u_v(x, S) - \tfrac{2}{3}\cos 2\theta_d\, d_v(x, S)\,, \\ \Delta d_v(x, S) &= -\tfrac{1}{3}\cos 2\theta_d\, d_v(x, S)\,, \end{aligned} \tag{3.13}$$

which are directly expressed in terms of the unpolarized parton distributions by means of two dilution factors $\cos 2\theta_u$ and $\cos 2\theta_d$ given by the following simple formulae:

$$\begin{aligned} \cos 2\theta_u &= [1 + H_0^u(1-x)^2\sqrt{x}]^{-1}\,, \quad H_0^u = 0.09 - 0.04S\,, \\ \cos 2\theta_d &= [1 + H_0^d(1-x)/\sqrt{x}]^{-1}\,, \quad H_0^d = 0.03 - 0.01S\,. \end{aligned} \tag{3.14}$$

In this model the sea quark helicity asymmetry remains positive and it increases with larger x and higher Q^2. For the u sea quark it can be parametrized as follows:

$$\Delta u_s(x, S) = (0.7 + 0.5\ln S)x u_s(x, S)\,, \tag{3.15}$$

while the other flavors are obtained by using the same rules as for the unpolarized parton distributions. These parton helicity asymmetries are required to satisfy important constraints like the Bjorken sum rule at the level of parton model [BJO66, BJO70] or with a QCD correction [KOD79] and also various new sum rules established recently [EIN86, BOU87a], as a test of their correct Q^2 evolution. These requirements, which help to reduce the theoretical uncertainty, are indeed fulfilled by eqs. (3.12) to (3.15).

The resulting parton polarizations versus x are shown in figs. 3.3 to 3.6 for u-quark, d-quark, gluon and sea quark for $Q^2 = 10^4$ GeV^2 and 10^8 GeV^2. They are positive except for the d-quark as a direct

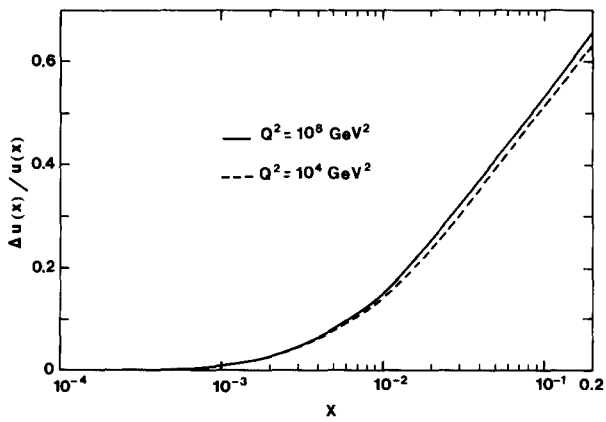

Fig. 3.3. u-quark polarization versus x for $Q^2 = 10^4$ and 10^8 GeV^2.

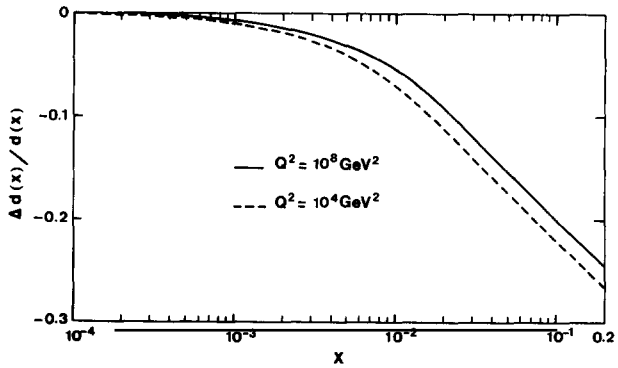

Fig. 3.4. d-quark polarization versus x for $Q^2 = 10^4$ and 10^8 GeV^2.

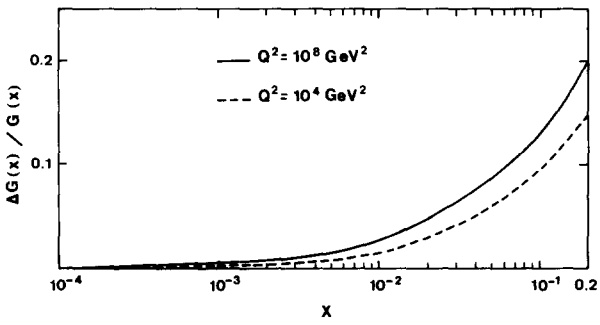

Fig. 3.5. Gluon polarization versus x for $Q^2 = 10^4$ and 10^8 GeV^2.

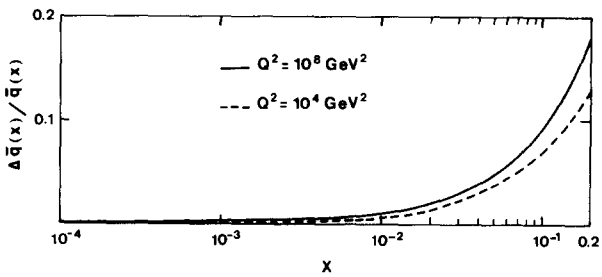

Fig. 3.6. Sea quark polarization versus x for $Q^2 = 10^4$ and 10^8 GeV^2.

consequence of eq. (3.13). They all grow with increasing x and slowly increase with larger values of Q^2. The u-quark polarization is the largest one, being over 50% for $x = 0.1$.

3.2. Parton–parton luminosities

The parton distributions derived above will be used to compute differential cross sections and helicity asymmetries for various reactions of interest at supercollider energies. We have checked that our unpolarized distributions (eqs. 3.4–3.8) follow the numerical solutions provided by EHLQ within 10 to 15% except for Q^2 as low as 10 GeV^2, so they lead to a reasonable determination of hadronic cross sections. Event rates given by EHLQ should be reliable to a factor two or better and we expect the same uncertainties for event rates with polarized beams, but they should be smaller in helicity asymmetries, which are cross section ratios. To evaluate these hadronic cross sections let us consider a convenient quantity introduced by EHLQ, the differential parton–parton luminosity, defined as

$$\tau \frac{\mathrm{d}\mathscr{L}_{ij}}{\mathrm{d}\tau} = \frac{\tau}{1+\delta_{ij}} \int_{\tau}^{1} \frac{\mathrm{d}x}{x} \left[f_i^{(a)}(x, \hat{s}) f_j^{(b)}(\tau/x, \hat{s}) + (i \leftrightarrow j) \right]. \tag{3.16}$$

It represents the number of parton i–parton j collisions per unit of τ with subprocess energy squared $\hat{s} = \tau s$. Thus the differential cross section with respect to the scaling variable τ for the reaction (3.1), using eqs. (3.2) and (3.16), is given by

$$\frac{\mathrm{d}\sigma}{\mathrm{d}\tau} = \sum_{ij} \tau \frac{\mathrm{d}\mathscr{L}_{ij}}{\mathrm{d}\tau} \hat{\sigma}_{ij}. \tag{3.17}$$

By dimensional analysis one has $\hat{\sigma}_{ij} = k/\hat{s}$, with coupling strength k, so the quantity $(\tau/\hat{s})\,\mathrm{d}\mathscr{L}_{ij}/\mathrm{d}\tau$, which has the dimension of a cross section, can be used to estimate the total number of events/year N_{ij} for a given subprocess,

$$N_{ij} = L_{\mathrm{h}} k(\tau/\hat{s})\,\mathrm{d}\mathscr{L}_{ij}/\mathrm{d}\tau, \tag{3.18}$$

knowing k and the hadron–hadron luminosity L_h, which is typically 10^{40} cm^{-2} at SSC[3]. This notion of parton luminosity can be generalized to the case of a hadronic reaction with *one or two* polarized beams by replacing in eq. (3.16) *one or two* unpolarized distributions f by the corresponding parton helicity asymmetries Δf. Therefore we define the following two useful quantities, namely the singly polarized luminosity

$$\tau \frac{d\mathscr{L}_{\Delta ij}}{d\tau} = \tau \int_\tau^1 \frac{dx}{x} \Delta f_i^{(a)}(x, \hat{s}) f_j^{(b)}(\tau/x, \hat{s}), \tag{3.19}$$

when hadron a only is polarized, and the doubly polarized luminosity

$$\tau \frac{d\mathscr{L}_{\Delta i \Delta j}}{d\tau} = \frac{\tau}{1 + \delta_{ij}} \int_\tau^1 \frac{dx}{x} [\Delta f_i^{(a)}(x, \hat{s}) \Delta f_j^{(b)}(\tau/x, \hat{s}) + (i \leftrightarrow j)], \tag{3.20}$$

when both initial hadrons a and b are polarized.

We show all these parton luminosities for gluon–gluon interactions at $\sqrt{s} = 40$ TeV in fig. 3.7a and at $\sqrt{s} = 10$ TeV in fig. 3.7b. Clearly for higher energy all parton luminosities increase and one should note at small $\sqrt{\hat{s}}$ a strong reduction of the (singly or doubly) polarized luminosities. We also show various parton luminosities for several other parton–parton interactions in figs. 3.8 to 3.13. By comparing fig.

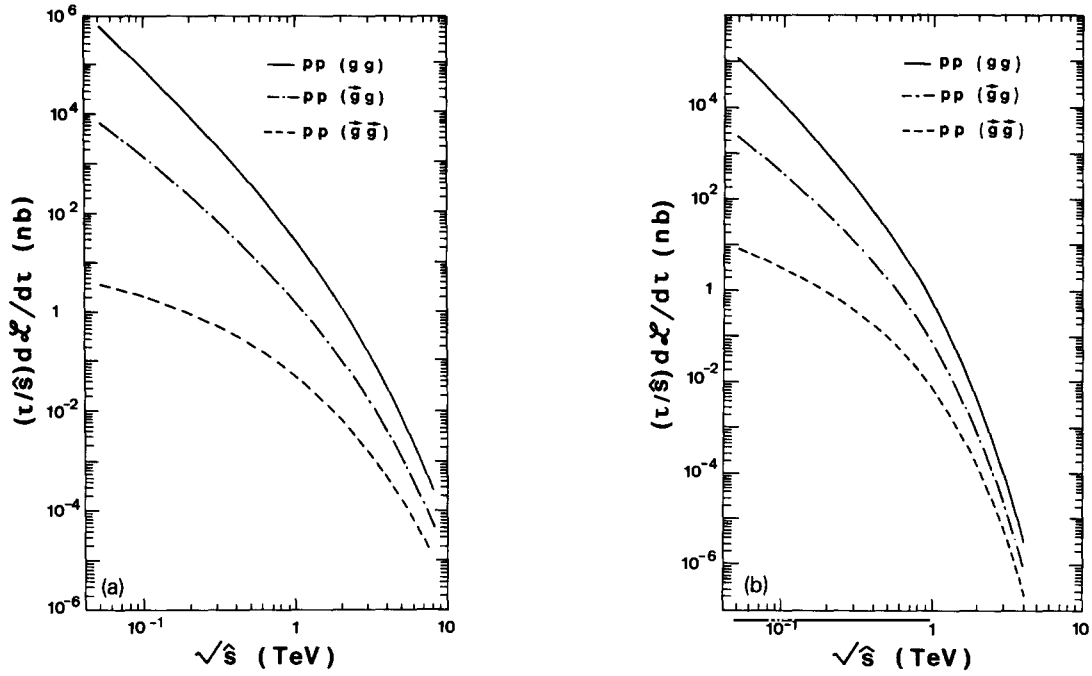

Fig. 3.7. The quantity $(\tau/\hat{s})\, d\mathscr{L}/d\tau$ (in nanobarns) versus $\sqrt{\hat{s}}$ for gg interactions in pp collisions (a) at $\sqrt{s} = 40$ TeV, (b) at $\sqrt{s} = 10$ TeV. Solid curve, unpolarized gluon distributions; dashed–dotted curve, singly polarized gluon distributions; dashed curve, doubly polarized gluon distributions.

[3] Throughout the paper we will give event rates assuming this luminosity for the SSC with polarized beams.

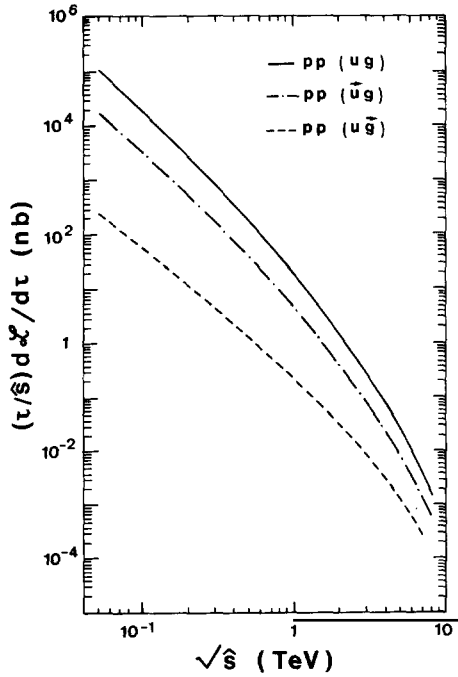

Fig. 3.8. The quantity $(\tau/\hat{s})\,\mathrm{d}\mathcal{L}/\mathrm{d}\tau$ (in nanobarns) versus $\sqrt{\hat{s}}$ for ug interactions in pp collisions at $\sqrt{s} = 40$ TeV. Solid curve, unpolarized distributions; dashed-dotted curve, polarized u-quark distributions; dashed curve, polarized gluon distributions.

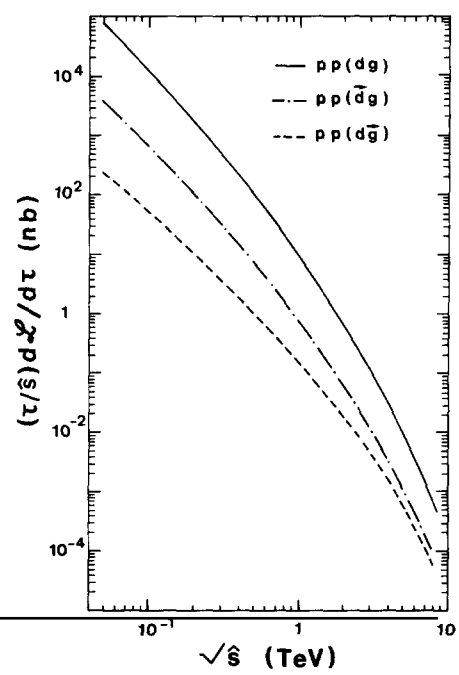

Fig. 3.9. Same as fig. 3.8 for dg interactions. Note that the dashed-dotted curve has been changed in sign, because the d-quark helicity asymmetry is negative.

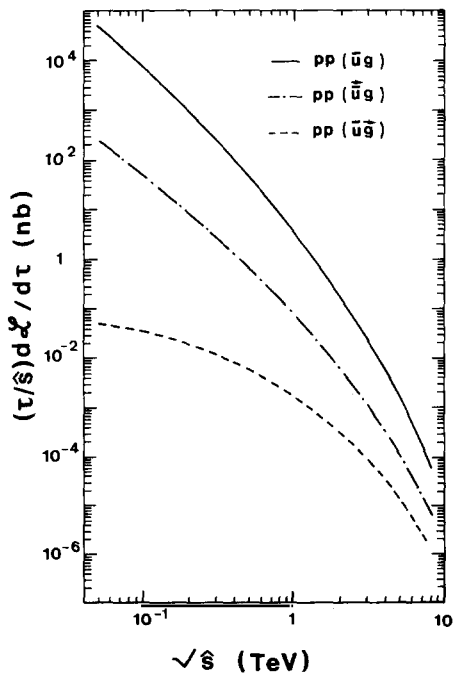

Fig. 3.10. Same as fig. 3.8 for ūg interactions.

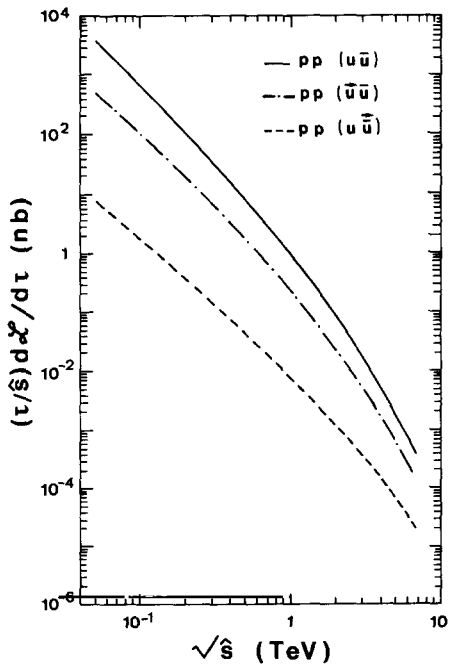

Fig. 3.11. Same as fig. 3.8 for uū interactions.

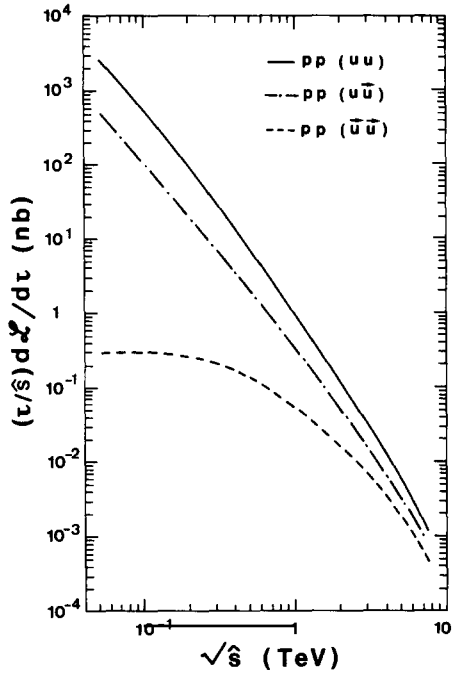

Fig. 3.12. Same as fig. 3.8 for uu interactions.

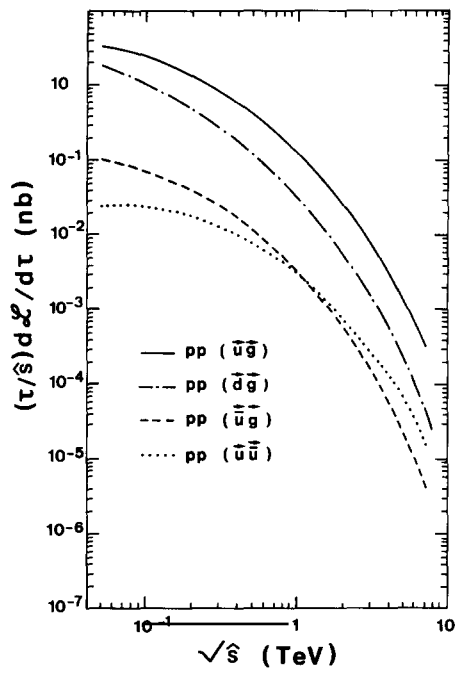

Fig. 3.13. Doubly polarized luminosities for various parton–parton interactions in pp collisions at $\sqrt{s} = 40$ TeV. Note that the dashed-dotted curve has been changed in sign because the d-quark helicity asymmetry is negative.

3.7a and fig. 3.8 we see that gluon–gluon induced reactions will occur more copiously than u-quark–gluon induced reactions, except at the edge of the accessible kinematic region, but gluons are less efficient than u-quarks in building up asymmetries. There is a similar effect for d-quark–gluon induced reactions (see fig. 3.9), but since the d-quark helicity asymmetry is negative, it will reduce the hadron asymmetries. The luminosities involving sea quarks are even smaller.

By making ratios of the (singly or doubly) polarized luminosity to the unpolarized luminosity, one can estimate how much a (single or double) subprocess asymmetry will contribute to the corresponding helicity asymmetry in hadron–hadron collisions due to the dilution effect of the parton distributions. This is more accurate than using the parton polarizations mentioned above [see eq. (3.10b)]. As a simple example let us consider a reaction with one beam longitudinally polarized, whose cross sections are $d\sigma^{(\pm)}/d\tau$ [see eq. (3.17)]; the single helicity hadron asymmetry defined as

$$A_L = \frac{d\sigma^{(-)}/d\tau - d\sigma^{(+)}/d\tau}{d\sigma^{(-)}/d\tau + d\sigma^{(+)}/d\tau} \tag{3.21}$$

can be evaluated by means of these ratios. Let us denote by $\hat{a}_L^{ij}$ ($\hat{a}_L^{ji}$) the subprocess helicity asymmetry where parton i (j) is polarized. If the cross section is dominated by a subprocess induced by the collision of parton i and parton j and if $\hat{a}_L^{ij}$ and $\hat{a}_L^{ji}$ are constant one has

$$A_L \simeq a_i(j)\hat{a}_L^{ij} + a_j(i)\hat{a}_L^{ji}, \tag{3.22}$$

where

$$a_i(j) = \frac{\tau\, \mathrm{d}\mathscr{L}_{\Delta ij}/\mathrm{d}\tau}{\tau\, \mathrm{d}\mathscr{L}_{ij}/\mathrm{d}\tau} \tag{3.23}$$

represents the polarization of parton i in interaction with the unpolarized parton j. This quantity is not necessarily related to the single helicity hadron asymmetry and its usefulness will become obvious in the specific cases we will study in the following sections. Some examples of $a_i(j)$ are displayed in figs. 3.14 to 3.17 for two different energies. By comparing these quantities we see that

$$a_u(g) \sim a_u(\bar{d})\,, \tag{3.24}$$

and it rises with $\sqrt{\hat{s}}$ in the same way as the u-quark polarization rises with x (see fig. 3.3). Similarly

$$a_d(g) \sim a_d(\bar{u})\,, \tag{3.25}$$

both are negative and behave like the d-quark polarization (see fig. 3.4), and

$$a_g(d) \sim a_g(u)\,, \tag{3.26}$$

which behave like the gluon polarization (see fig. 3.5). Finally we show $a_{\bar{q}}(u)$ in fig. 3.17, which has a fast rise at high $\sqrt{\hat{s}}$, reflecting the behavior of the sea quark polarization for large x (see fig. 3.6), and we find

$$a_{\bar{d}}(u) \sim a_{\bar{u}}(d)\,. \tag{3.27}$$

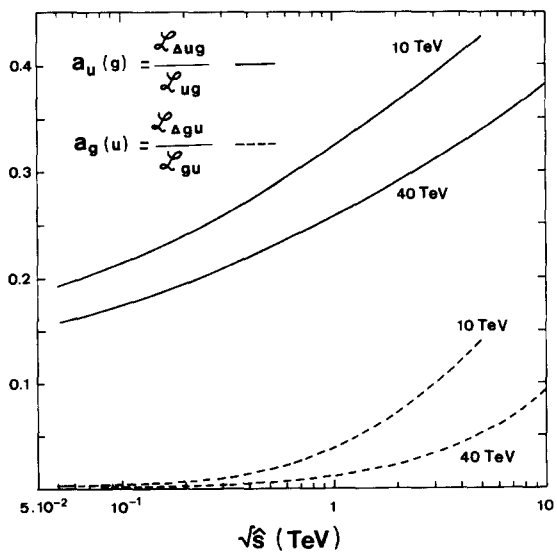

Fig. 3.14. $a_u(g)$ and $a_g(u)$ versus $\sqrt{\hat{s}}$ for $\sqrt{s} = 10$ and 40 TeV.

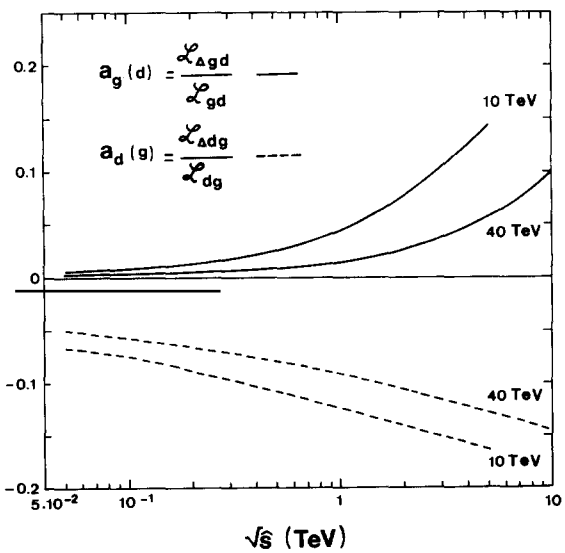

Fig. 3.15. $a_d(g)$ and $a_g(d)$ versus $\sqrt{\hat{s}}$ for $\sqrt{s} = 10$ and 40 TeV.

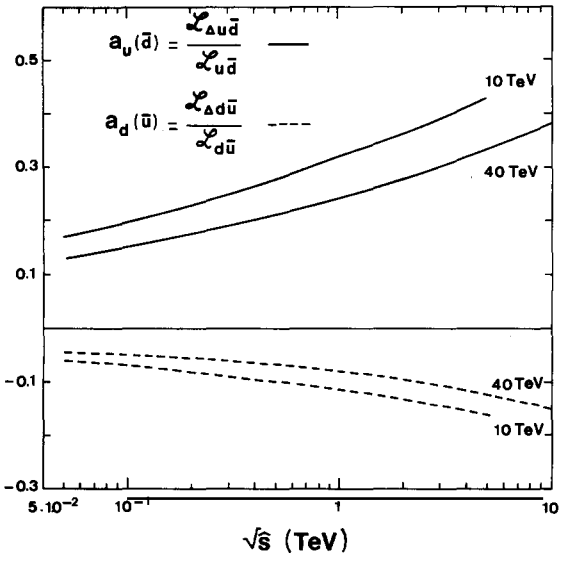

Fig. 3.16. $a_u(\bar{d})$ and $a_d(\bar{u})$ versus $\sqrt{\hat{s}}$ for $\sqrt{s} = 10$ and 40 TeV.

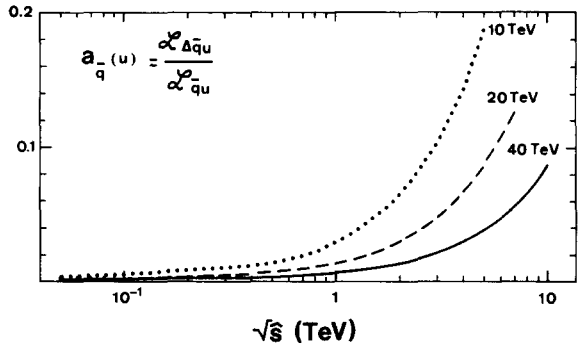

Fig. 3.17. $a_{\bar{q}}(u)$ versus $\sqrt{\hat{s}}$ for $\sqrt{s} = 10$, 20 and 40 TeV.

Clearly double helicity hadron asymmetries will be smaller than single helicity asymmetries due to the suppression of all doubly polarized luminosities, as shown in figs. 3.7 to 3.13. Some specific examples will be calculated explicitly in the next section, which is mainly devoted to QCD tests.

4. Hadronic jets and QCD tests

One of the major difficulties for testing QCD is the fact that experiments cannot be performed directly with the basic constituents quarks and gluons. Hadron–hadron processes are rather complicated at the level of the constituents because many subprocesses have to be summed over in the evaluation of the cross sections and the double helicity asymmetries [see eqs. (3.2) and (3.10a)]. These subprocesses lead to different cross sections and double helicity asymmetries as we will see below and it might be possible, in a given restricted range of the large transverse momentum kinematic region, to know which subprocesses are dominant. This is one way to test QCD and of course the correct knowledge of the parton distributions is also part of this test. At high energies most of the information at short distances is contained in hadronic jet physics, which has already exhibited some simple aspects at the CERN $Sp\bar{p}S$ collider. Jet production will be very copious at the SSC and with its expected luminosity there will be about one event per second yielding at least one jet with transverse momentum larger than 1 TeV/c. Therefore event rates will be very high and jets will be the main source of conventional background to new physics, so it is essential we understand as well as possible both their cross sections and their helicity asymmetries. By reaching enormous values of transverse momentum it will be possible to probe very short distances and, for example, to detect some evidence for quark compositeness, which leads to a definite signature in single helicity asymmetries resulting from the presence of an axial coupling which violates parity (see section 7). In this section, since we assume that parity is preserved, we will compute only double helicity asymmetries, which are expected to be small as explained previously. Although

direct photon production has a much lower cross section, it will be also considered because it is simpler and allows a direct probe of a smaller number of specific hard scattering processes.

4.1. Single-jet production

The invariant cross section for the production of a single jet of energy E (or rapidity y) and transverse momentum p_T reads after a simple phase space integration

$$E\frac{d^3\sigma}{dp^3} = \sum_{ij}\frac{1}{1+\delta_{ij}}\int_{x_0}^{1} dx_a \frac{2}{\pi}\frac{x_a x_b}{2x_a - x_T e^{y}}\left(f_i(x_a, Q^2) f_j(x_b, Q^2)\frac{d\hat{\sigma}_{ij}}{d\hat{t}}(\hat{s}, \hat{t}, \hat{u}) + (i \leftrightarrow j)\right),$$
$$x_T = \frac{2p_T}{\sqrt{s}}, \qquad x_0 = \frac{x_T e^{y}}{2 - x_T e^{-y}}, \qquad x_b = \frac{x_a x_T e^{-y}}{2x_a - x_T e^{y}}. \tag{4.1}$$

For large enough E the jet will be produced in the pp c.m. system at an angle θ_{cm} such that $y = \ln \operatorname{cotg} \theta_{cm}/2$. The subprocess cross section for initial partons i and j[1] giving different final states is $(d\hat{\sigma}_{ij}/d\hat{t})(\hat{s}, \hat{t}, \hat{u})$. Their Born expressions, with all possible exchanges in the three channels are recalled in table 4.1 in terms of the Mandelstam variables at the parton level

Table 4.1
List of the asymmetries $\hat{a}_{LL}^{ij}$ and corresponding Born cross sections in perturbative QCD. A factor of $\pi\alpha_s^2/\hat{s}^2$ has been factored out of the purely strong interaction cross sections and $\pi e_q^2 \alpha\alpha_s/\hat{s}^2$ out of the single-photon cross sections, where e_q denotes the quark charge ($\frac{2}{3}$ for u and $-\frac{1}{3}$ for d)

Process	$\hat{a}_{LL}^{ij}$	$\theta^* = \pi/2$	Cross section	$\theta^* = \pi/2$
$qq \to qq$	$\dfrac{(\hat{s}^2+\hat{u}^2)/\hat{t}^2 + (\hat{s}^2+\hat{t}^2)/\hat{u}^2 - \frac{2}{3}\hat{s}^2/\hat{t}\hat{u}}{(\hat{s}^2+\hat{u}^2)/\hat{t}^2 + (\hat{s}^2+\hat{t}^2)/\hat{u}^2 - \frac{2}{3}\hat{s}^2/\hat{t}\hat{u}}$	0.45	$\frac{4}{9}\left(\dfrac{\hat{s}^2+\hat{u}^2}{\hat{t}^2} + \dfrac{\hat{s}^2+\hat{t}^2}{\hat{u}^2} - \dfrac{2}{3}\dfrac{\hat{s}^2}{\hat{t}\hat{u}}\right)$	3.26
$q\bar{q}' \to q\bar{q}'$ $qq' \to qq'$	$(\hat{s}^2-\hat{u}^2)/(\hat{s}^2+\hat{u}^2)$	0.6	$\frac{4}{9}(\hat{s}^2+\hat{u}^2)/\hat{t}^2$	2.22
$q\bar{q} \to q'\bar{q}'$	-1		$\frac{4}{9}(\hat{t}^2+\hat{u}^2)/\hat{s}^2$	0.22
$q\bar{q} \to q\bar{q}$	$\dfrac{(\hat{s}^2-\hat{u}^2)/\hat{t}^2 - (\hat{t}^2+\hat{u}^2)/\hat{s}^2 + \frac{2}{3}\hat{u}^2/\hat{s}\hat{t}}{(\hat{s}^2+\hat{u}^2)/\hat{t}^2 + (\hat{t}^2+\hat{u}^2)/\hat{s}^2 - \frac{2}{3}\hat{u}^2/\hat{s}\hat{t}}$	0.37	$\frac{4}{9}\left(\dfrac{\hat{s}^2}{\hat{t}^2} + \dfrac{\hat{u}^2}{\hat{t}^2} + \dfrac{\hat{t}^2+\hat{u}^2}{\hat{s}^2} - \dfrac{2}{3}\dfrac{\hat{u}^2}{\hat{s}\hat{t}}\right)$	2.59
$q\bar{q} \to gg$	-1		$\frac{32}{27}(\hat{t}^2+\hat{u}^2)/\hat{u}\hat{t} - \frac{8}{3}(\hat{t}^2+\hat{u}^2)/\hat{s}^2$	1.04
$qg \to qg$	$(\hat{s}^2-\hat{u}^2)/(\hat{s}^2+\hat{u}^2)$	0.6	$(\hat{s}^2+\hat{u}^2)/\hat{t}^2 - \frac{4}{9}(\hat{s}^2+\hat{u}^2)/\hat{u}\hat{s}$	6.11
$gg \to q\bar{q}$	-1		$\frac{1}{2}[\frac{1}{3}(\hat{u}^2+\hat{t}^2)/\hat{u}\hat{t} - \frac{3}{4}(\hat{t}^2+\hat{u}^2)/\hat{s}^2]$	0.15
$gg \to gg$	$\dfrac{-3 + 2\hat{s}^2/\hat{u}\hat{t} + \hat{u}\hat{t}/\hat{s}^2}{3 - \hat{s}\hat{u}/\hat{t}^2 - \hat{s}\hat{t}/\hat{u}^2 - \hat{u}\hat{t}/\hat{s}^2}$	0.77	$\frac{9}{2}\left(3 - \dfrac{\hat{s}\hat{u}}{\hat{t}^2} - \dfrac{\hat{s}\hat{t}}{\hat{u}^2} - \dfrac{\hat{u}\hat{t}}{\hat{s}^2}\right)$	30.4
$qg \to q\gamma$	$(\hat{s}^2-\hat{u}^2)/(\hat{s}^2+\hat{u}^2)$	0.6	$-\frac{1}{3}\left(\dfrac{\hat{u}}{\hat{s}} + \dfrac{\hat{s}}{\hat{u}}\right)$	0.83
$q\bar{q} \to \gamma g$	-1		$\frac{8}{9}\left(\dfrac{\hat{u}}{\hat{t}} + \dfrac{\hat{t}}{\hat{u}}\right)$	1.77

[1] Clearly the permutation $(i \leftrightarrow j)$ in eq. (4.1) implies the interchange $(\hat{t} \leftrightarrow \hat{u})$ in the cross section.

$$\hat{s} = x_a x_b s\,, \qquad \hat{t} = -\tfrac{1}{2}\hat{s}(1-\cos\theta^*)\,, \qquad \hat{u} = -\tfrac{1}{2}\hat{s}(1+\cos\theta^*)\,, \tag{4.2}$$

where θ^* is the c.m. scattering angle, which can be expressed as

$$\cos\theta^* = \frac{x_a e^{-y} - x_b e^{y}}{x_a e^{-y} + x_b e^{y}}\,. \tag{4.3}$$

The scaling variable Q^2 which occurs in the parton distributions $f_i(x, Q^2)$ and in the running coupling constant $\alpha_s(Q^2)$ is taken to be $Q^2 = p_T^2/4$, which is a reasonable approximation suggested from a recent analysis of QCD radiative corrections [ELL86]. This choice is not unique and leads to some uncertainty in the calculation of the cross sections, which is also related to subtleties associated with next-to-leading order contributions [OWE87]. From table 4.1 we see that elastic processes give the main contributions, gluon–gluon scattering being largely dominant followed by gluon–quark and quark–quark scattering. A comparison with the single-jet production data obtained by UA1 and UA2 [ARN86, APP85] leads to a fair agreement with the predictions of lowest-order QCD [EIC84, OWE87]. So we expect that at future collider energies gluon–gluon scattering will dominate up to $p_T \simeq 1$ TeV/c, then gluon–quark will take over up to 5 TeV/c or so, where we start to reach the quark–quark regime.

The double helicity asymmetries follow from eq. (3.10a) and the explicit use of eq. (4.1). The expressions of the $\hat{a}_{LL}^{ij}$ are also given[2] in table 4.1 and are represented in fig. 4.1. According to a basic property of perturbative QCD, a quark and antiquark of a given flavor can annihilate into a gluon only if they have opposite helicities. It follows that all processes with $q\bar{q}$ either in the initial state or in the final state lead to $\hat{a}_{LL}^{ij} = -1$ as shown by curve E in fig. 4.1. For all the other cases $\hat{a}_{LL}^{ij}$ is found positive and corresponds to one of the four different curves A, B, C and D shown in fig. 4.1, where the

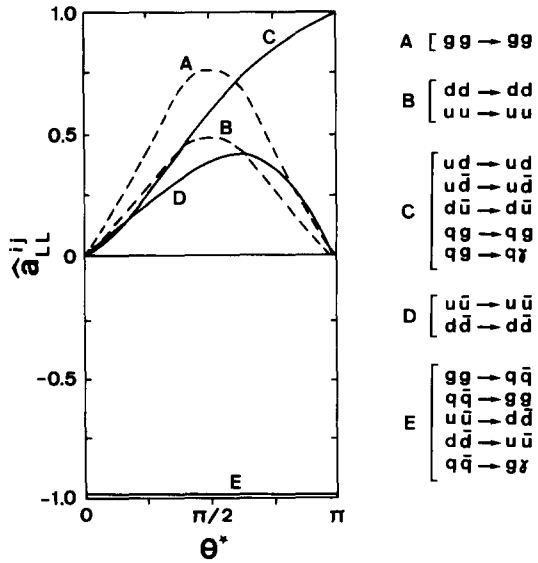

Fig. 4.1. The double helicity asymmetries $\hat{a}_{LL}^{ij}$ versus θ^* at the lowest order in perturbative QCD.

[2] They agree with [CRA83] but not with [BAL81] for qg→qg.

maximum effect near 90° occurs for gg→gg. So A_{LL} is expected to be positive in spite of the small contribution from the d-quarks, which have a negative helicity asymmetry Δd as we have seen in section 3. The result of our calculation for a jet produced at zero rapidity is shown in fig. 4.2 versus p_T for three different energies. The effect is of the order of a few percent, in agreement with a rough estimate based on eq. (3.10b) [SOF85]. Even for $p_T < 1\,\text{TeV}/c$, where gluon–gluon scattering dominates, A_{LL} is small because gluons are less efficient than quarks in building up polarizations (see figs. 3.14 and 3.15). A_{LL} decreases with increasing energy due to the rapid growth of the single-jet cross section with energy driven by the small-x behavior of the gluon distributions. A_{LL} rises with larger p_T because of the decrease of the cross section, which represents less and less background in this kinematic region, thus making it easier to detect new physics, which might also give signals in A_{LL} (e.g., see section 8). The curves in fig. 4.2 were not extended above p_T values for which the cross section drops below $10^{-40}\,\text{cm}^2/\text{GeV}$, corresponding to slightly less than one event per hour per TeV/c of p_T, which is still measurable.

4.2. Two-jet production

In the physics of hadronic jets one can also consider the production in the final state of two jets with rapidities y_1 and y_2 and with equal and opposite transverse momentum p_T. The differential cross section can be written as

$$\frac{d^3\sigma}{dy_1\,dy_2\,dp_T^2} = \tau \sum_{ij} \frac{1}{1+\delta_{ij}} \left(f_i(x_a, Q^2) f_j(x_b, Q^2) \frac{d\hat{\sigma}_{ij}}{d\hat{t}}(\hat{s}, \hat{t}, \hat{u}) + (i \leftrightarrow j) \right). \tag{4.4}$$

If we define

$$y^* = \tfrac{1}{2}(y_1 - y_2), \qquad y_{\text{boost}} = \tfrac{1}{2}(y_1 + y_2), \tag{4.5}$$

we have

$$x_a = \sqrt{\tau}\, e^{y_{\text{boost}}}, \qquad x_b = \sqrt{\tau}\, e^{-y_{\text{boost}}}, \qquad \tau = \frac{4p_T^2}{s} \cosh^2 y^*, \qquad \sin\theta^* = \frac{1}{\cosh y^*}. \tag{4.6}$$

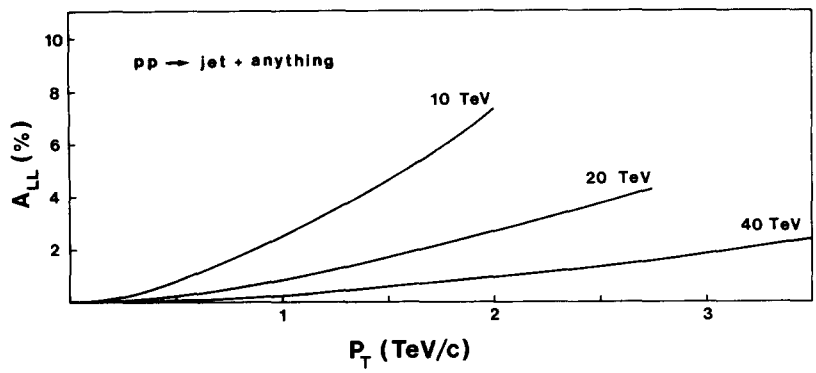

Fig. 4.2. Predictions for the double helicity hadron asymmetry A_{LL} in pp→jet + X at $y = 0$ versus p_T for three different energies.

So we see that large values of y^* correspond to the forward and backward directions at the parton level, where the dominant differential cross sections are strongly peaked. Therefore, to avoid overestimating the event rate, we must restrict ourselves to the central rapidity regions, that is

$$-Y \leq y_1, y_2 \leq Y, \tag{4.7}$$

where Y is of the order of one. For $y_1 = -y_2 = 1$ one has $y^* = 1$ corresponding to $\theta^* \sim 40°$. For y^* fixed around zero and for a given p_T, if one increases y_{boost}, then since x_a increases and x_b decreases, the cross section will fall due to the fast decrease of the parton distributions at large x. Gluon–gluon dominates at small y_{boost} whereas gluon–quark dominates at large y_{boost}. A larger cross section which can be obtained from eq. (4.4) after integration over the jet rapidities, is the invariant jet-pair mass distribution $d\sigma/dM$. The jet-pair mass is given by

$$M = 2p_T \cosh y^*, \tag{4.8}$$

and the invariant mass distribution reads

$$\frac{d\sigma}{dM} = \frac{M^3}{2s} \int_{-Y}^{Y} dy_1 \int_{y_{min}}^{y_{max}} dy_2 \sum_{ij} \frac{1}{(1+\delta_{ij}) \cosh^2 y^*} \left(f_i(x_a, Q^2) f_j(x_b, Q^2) \frac{d\hat{\sigma}_{ij}}{d\hat{t}} (\hat{s}, \hat{t}, \hat{u}) + (i \leftrightarrow j) \right), \tag{4.9}$$

where

$$y_{max} = \min(Y, -\log \tau - y_1), \qquad y_{min} = \max(-Y, \log \tau - y_1), \tag{4.10}$$

which reduce essentially to Y and $-Y$ for low mass values. The double helicity asymmetry A_{LL} versus the jet-pair mass is shown in fig. 4.3 at three different energies and it is even smaller than for single-jet production.

Finally we would like to remark that the magnitude of these asymmetries in hadronic jet production is related to the smallness of the gluon polarization, but they would be zero if the gluons were not polarized. They were found positive and recently the importance of this sign has been stressed

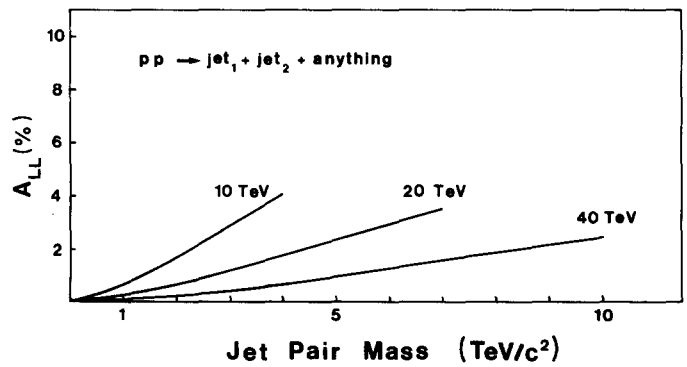

Fig. 4.3. Predictions for the double helicity hadron asymmetry A_{LL} for two-jet events in pp collisions versus the jet-pair mass for three different energies.

[RAM88] for the evaluation of the jet contribution to the total cross section and the corresponding double helicity asymmetry,

$$\Delta\sigma_L = \sigma_{tot}(p(+), p(+)) - \sigma_{tot}(p(+), p(-)) . \tag{4.11}$$

This quantity was measured at very low energy at the Argonne ZGS [AUE77] and was found negative. According to our calculation the jet contribution is expected to be $\sim +1\,\mu b$ at $\sqrt{s} = 0.02\,TeV$, the energy range of the Fermilab polarized proton beam[3] [MIL88], $\sim +10\,\mu b$ at $\sqrt{s} = 0.5\,TeV$ and $\sim +25\,\mu b$ at $\sqrt{s} = 10\,TeV$.

4.3. Direct photon production

Direct photon production at high p_T is also a useful probe of the underlying parton–parton interactions. Since the photon originates in the hard scattering subprocess and does not fragment, the cross section is also given by eq. (4.1). In the QCD parton model, in the absence of photon bremsstrahlung contributions, direct photons are produced via the quark–antiquark annihilation subprocess $q\bar{q} \to \gamma g$ and the quark–gluon Compton subprocess $qg \to q\gamma$, whose cross sections and double helicity asymmetries are recalled in table 4.1. The Compton subprocess has a positive $\hat{a}_{LL}$ (curve C in fig. 4.1), whereas for the annihilation one has $\hat{a}_{LL} = -1$ (curve E in fig. 4.1). We have calculated the unpolarized cross section at 90° and for different values of the c.m. production angle and we found consistency with the results of [OWE84]. Event rates are very small and for example one has $d^2\sigma/dy\,dp_T = 4 \times 10^{-40}\ cm^2/GeV$ for $p_T = 1\,TeV/c$ and $\theta_{cm} = 90°$. As it is well known, away from 90° the Compton subprocess dominates largely over annihilation except at very large p_T. The results we obtained for the double helicity asymmetry are shown in fig. 4.4 for $\theta_{cm} = 45°$ and 90°. In both cases A_{LL} is positive, which reflects the dominance of the Compton subprocess. However, u-quark–gluon and d-quark–gluon lead to opposite sign effects, which reduce the magnitude of A_{LL}. We also see that A_{LL} scales with x_T (eq. 4.1), but since the cross section does not, the measurement of A_{LL} at fixed x_T will be

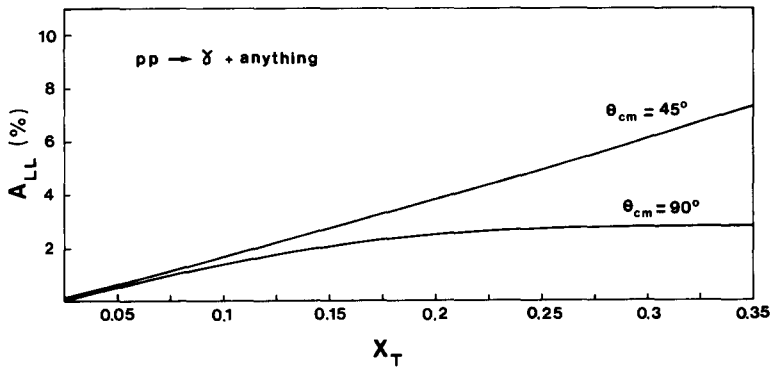

Fig. 4.4. Predictions for the double helicity hadron asymmetry A_{LL} in $pp \to \gamma X$ versus x_T, at very high energies ($\sqrt{s} \geq 10\,TeV$), for two different values of the c.m. production angle $\theta_{cm} = 45°$ and 90°.

[3] At $\sqrt{s} = 0.02\,TeV$, we have small Q^2 values so there is no reason to claim that a leading-twist calculation is reliable and to believe this sign for $\Delta\sigma_L$.

easier to measure for $\sqrt{s} = 10$ TeV than for $\sqrt{s} = 40$ TeV. At 45° A_{LL} rises with x_T, whereas it is flatter at 90°. This is due to the fact that at 90° the positive Compton asymmetry is reduced by the contribution of the negative annihilation asymmetry, which becomes more and more important for increasing x_T. A_{LL} becomes negative for $x_T \simeq 0.6$, where the cross section is not measurable at $\sqrt{s} = 10$ TeV, but this sign change is not predicted by much lower energy calculations [BAL81, CRA83].

In conclusion of this section and to summarize, we have seen that pure QCD processes lead to small double helicity asymmetries and any deviation in their measurements will give us a clear signal for some new physics. By measuring double helicity asymmetries with all spin configurations, one also gets for free single helicity asymmetries A_L. These single helicity asymmetries vanish for single-particle (or jet) inclusive production but not in the case where one observes at least two particles (or two jets) in the final state. They then involve a correlation between the transverse momentum and the angular distributions of the two objects produced. We have not calculated them but they are expected to be small compared to the A_L's related to the existence of a parity violating interaction at the subprocess level. Therefore pure QCD processes do not give any appreciable background to these single helicity asymmetries, which get large contributions from electroweak interactions as we will see now.

5. Spin tests of standard electroweak interactions

In this section we will study on the TeV scale spin phenomena associated to the Standard Model description of electroweak interactions [GLA61, WEI67, SAL68] based on the $SU(2)_L \times U(1)$ gauge symmetry broken by the minimal Higgs mechanism. The three quark and lepton doublets are assumed to interact through the charged left-handed vector bosons $W^{\pm}$ and the neutral vector boson Z^0, experimentally found at the CERN $S\bar{p}pS$ collider [ARN83, BAN83, BAG83], and a scalar Higgs boson H which remains to be discovered. One should emphasize here that one of the major physics goals of the next generation of hadron supercolliders is indeed to establish the existence of the Higgs particle. At SSC with $\mathscr{L} = 10^{33}$ cm^{-2} s^{-1}, one will be able to produce every second about 60 Z^0's and 200 $W^{\pm}$'s, so these impressive production rates will also be of great interest because, the standard production mechanism being known, they will allow a precise calibration of the parton distributions [CHA86]. In addition to gauge boson pair production it will be possible to study the influence of the three gauge boson couplings, which is a characteristic of non-abelian gauge theories. For example, approximately one thousand W^+W^- pairs per day will be produced at SSC and this rate, which is a direct consequence of the damping effect of the Z^0 contribution, is an obvious test to perform. Another feature of the standard model is the fact that gauge boson production at small angles is rather copious and will constitute the main background for an additional yield through a production mechanism involving new heavy particles.

The use of polarized beams will also lead to a reliable calibration of the polarized parton distributions. We will see that with the set previously proposed one expects large single helicity asymmetries, some of which are simply expressed in terms of parton polarizations $a_i(j)$ defined in eq. (3.23). Several characteristic aspects of these asymmetries will be discussed and in particular the effect of the three gauge boson couplings. One should also mention that all the corrections due to next-to-leading logarithm contributions [BAR88], which are usually discussed in terms of the so-called "K-factor", are expected to be less important for helicity asymmetries, which are cross section ratios. This is the case for the Drell–Yan mechanism [RAT83] and it is also known that in $e^+e^- \to q\bar{q} \to$ hadrons the single helicity asymmetry is insensitive to higher-order QCD corrections,

which preserve parity [LYN87]. We will treat successively massive dilepton production, single gauge boson production, pair production of gauge bosons and Higgs boson production.

5.1. Massive dilepton production

Let us consider the reaction

$$pp \to \ell^+\ell^- + \text{anything}, \tag{5.1}$$

where the production of high-mass e^+e^- and $\mu^+\mu^-$ pairs occurs through the lowest-order Drell–Yan mechanism $q\bar{q} \to \gamma, Z \to \ell^+\ell^-$. Unlike the processes we have studied above, this process does not involve initial gluons and allows one to measure the $\bar{q}$ content of the proton. As a consequence, the expected cross section for the invariant lepton pair mass M in the TeV region is rather low. More specifically it is of the order of 250 events/year for $0.9 < M < 1.1$ TeV/c^2 at SSC for each charged lepton species (see fig. 108 of EHLQ). This is minute compared to pure hadronic processes and it can be simply understood by recalling that the cross section averaged over quark colors, which reads

$$\frac{d\sigma}{dM} = \left(\frac{8\pi\alpha^2}{3M}\right)\frac{1}{3}\sum_i K_i\left(\frac{\tau}{M^2}\frac{d\mathcal{L}_{q_i\bar{q}_i}}{d\tau}\right), \tag{5.2}$$

is proportional to α^2 and not to α_s^2 and is directly expressed in terms of quark–antiquark luminosities, which are much smaller at a given M (or $\sqrt{\hat{s}}$) than gluon–gluon or gluon–quark luminosities as we have seen in section 3.2. Here $\tau = M^2/s$ is the usual scaling variable and K_i contains all the information about the underlying electroweak interactions. In the Standard Model, from the contribution of the photon and of the Z we have

$$K_i = e_i^2 - 2e_i a_\ell a_i M^2 \,\mathrm{Re}\, D_Z + (a_\ell^2 + b_\ell^2)(a_i^2 + b_i^2)M^4 |D_Z|^2, \tag{5.3}$$

where e_i is the electric charge of the quark q_i of flavor i, a_ℓ and b_ℓ (a_i and b_i) denote the vector and axial vector coupling constants of the lepton (quark i) to the Z boson. We have

$$\begin{aligned}
a_\ell &= \frac{4x_w - 1}{4x_w^{1/2}(1-x_w)^{1/2}}, \qquad b_\ell = \frac{-1}{4x_w^{1/2}(1-x_w)^{1/2}} \quad \text{for leptons},\\
a_i &= \frac{1 - \frac{8}{3}x_w}{4x_w^{1/2}(1-x_w)^{1/2}}, \qquad b_i = \frac{1}{4x_w^{1/2}(1-x_w)^{1/2}} \quad \text{for up quarks},\\
a_i &= \frac{-1 + \frac{4}{3}x_w}{4x_w^{1/2}(1-x_w)^{1/2}}, \qquad b_i = \frac{-1}{4x_w^{1/2}(1-x_w)^{1/2}} \quad \text{for down quarks},
\end{aligned} \tag{5.4}$$

where $x_w = \sin^2\theta_w$ is the weak mixing angle and we will use $x_w = 0.226$. Finally D_Z is the propagator of the Z boson with masss M_Z and width Γ_Z,

$$D_Z = (M^2 - M_Z^2 + iM_Z\Gamma_Z)^{-1}. \tag{5.5}$$

With one proton beam polarized in order to calculate the single helicity hadron asymmetry A_L defined in eq. (3.21) we need the expressions of the cross sections for $q_i(h_1) + \bar{q}_i(h_2) \to \ell^+\ell^-$, where h_1 is the helicity of the quark and h_2 that of the antiquark. The integrated subprocess cross section is

$$\hat{\sigma}_i(h_1, h_2) = \frac{4\pi\alpha^2}{3M^2}\left[(1 - h_1h_2)K_i + (h_2 - h_1)N_i\right], \tag{5.6}$$

where

$$N_i = -2e_ia_\ell b_iM^2 \,\mathrm{Re}\, D_Z + 2a_ib_i(a_\ell^2 + b_\ell^2)M^4|D_Z|^2 . \tag{5.7}$$

Since a_ℓ is very small, the sign of the asymmetry is that of a_ib_i, i.e. positive for both up and down quarks, and we see from eq. (5.6) that polarized quark–unpolarized antiquark annihilation and unpolarized quark–polarized antiquark annihilation give opposite contributions. We have

$$A_L = \frac{\sum_i N_i\left(\frac{\tau}{M^2}\frac{d\mathscr{L}_{\Delta q_i\bar{q}_i}}{d\tau} - \frac{\tau}{M^2}\frac{d\mathscr{L}_{q_i\Delta\bar{q}_i}}{d\tau}\right)}{\sum_i K_i\left(\frac{\tau}{M^2}\frac{d\mathscr{L}_{q_i\bar{q}_i}}{d\tau}\right)}, \tag{5.8}$$

and the results are shown in fig. 5.1 versus M at three different energies. A_L is only of the order of a few percent and this can be understood because it is driven by the u-quark polarization $a_u(\bar{u})$. With u-quark only, we would have

$$A_L \sim (N_u/K_u)a_u(\bar{u}), \tag{5.9}$$

and although $a_u(\bar{u})$ is large and grows with M, it is reduced by the factor N_u/K_u. It is also reduced by the effect of the d-quark polarization a_d, which is negative (see fig. 3.16), and by the subtraction of the

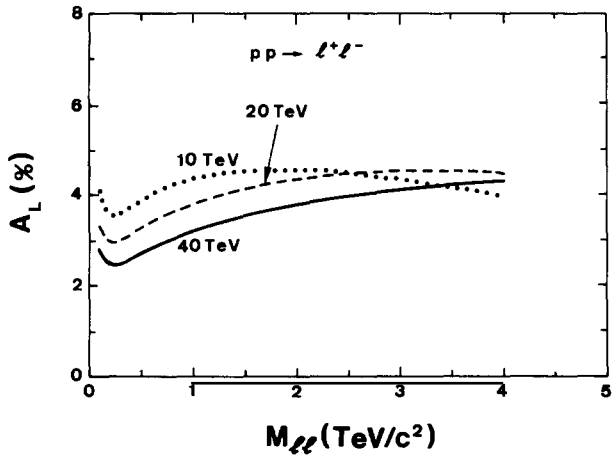

Fig. 5.1. A_L for Drell–Yan dilepton pair production versus M at $\sqrt{s} = 10$, 20 and 40 TeV.

antiquark polarizations $a_{\bar{u}}(u)$ and $a_{\bar{d}}(d)$. This last effect is more important at $\sqrt{s} = 10$ TeV because for higher M, $a_{\bar{q}}$ increases very quickly (see fig. 3.17)[1]. These are the predictions of the Standard Model but they could be different in magnitude and sign in the presence of right-handed currents [CHA85] or other deviations from the Standard Model as we will see later.

5.2. Single gauge boson production

The differential cross section for the reaction

$$pp \to W^{\pm} + \text{anything} \tag{5.10}$$

can be computed directly in the Drell–Yan picture in terms of the dominant quark–antiquark fusion reactions $u\bar{d} \to W^+$ and $\bar{u}d \to W^-$ and we have for the Standard Model W^+ production

$$\frac{d\sigma^{W^+}}{dy} = G_F \pi \sqrt{2} \tau \tfrac{1}{3}[u(x_a, M_W^2)\bar{d}(x_b, M_W^2) + (a \leftrightarrow b)] + \text{hfc}\,, \tag{5.11}$$

$$G_F = \frac{\pi\alpha}{\sqrt{2} M_W^2 x_w}\,, \qquad x_a = \sqrt{\tau} e^{y}\,, \qquad x_b = \sqrt{\tau} e^{-y}\,, \qquad \tau = M_W^2/s\,.$$

Here and in the following, hfc means that we include heavy flavor contributions ($c\bar{s}$, $t\bar{b}$) but since the mixing angles are small, contributions like $u\bar{s}$, etc. are largely suppressed. Quark flavors are interchanged in eq. (5.11) for W^- production. The y distribution is rather flat for $-4 < y < +4$ at $\sqrt{s} = 40$ TeV, corresponding to an angle $-2° < \theta_{cm} < +2°$, and then it drops very sharply (see fig. 112 of EHLQ).

In the Standard Model the W is a purely left-handed current, so the single helicity asymmetry in W^+ production reads simply

$$A_L = \frac{\Delta u(x_a, M_W^2)\, \bar{d}(x_b, M_W^2) - \Delta\bar{d}(x_a, M_W^2)\, u(x_b, M_W^2)}{u(x_a, M_W^2)\bar{d}(x_b, M_W^2) + \bar{d}(x_a, M_W^2) u(x_b, M_W^2) + \text{hfc}}\,, \tag{5.12}$$

assuming that only proton a is polarized. Note that the polarized hfc cancel in the numerator as a consequence of our proportionality assumption eqs. (3.8) and (3.15). This quantity, represented in figs. 5.2a and b for three different energies, is directly related to the u- and d-quark polarizations (see figs. 3.3 and 3.4) and for $y \sim 4$ it is dominated by $\Delta u/u$ at $x_a \sim 0.1$ for W^+ and by $\Delta d/d$ at $x_a \sim 0.1$ for W^-. For negative y, x_a is small and from the quark polarizations one expects also a very small A_L. At fixed y for increasing energy, since τ decreases, the magnitude of A_L also decreases as shown in the figures.

By integrating over y one gets higher event rates and the corresponding single helicity asymmetry for W^+ is

$$A_L = \frac{(\tau/M_W^2)(d\mathcal{L}_{\Delta u\bar{d}}/d\tau - d\mathcal{L}_{\Delta\bar{d}u}/d\tau)}{(\tau/M_W^2)\, d\mathcal{L}_{u\bar{d}}/d\tau + \text{hfc}}\,, \tag{5.13}$$

[1] The effect of the sea quark polarization has been studied in this process for $\sqrt{s} < 1$ TeV in [RIC86].

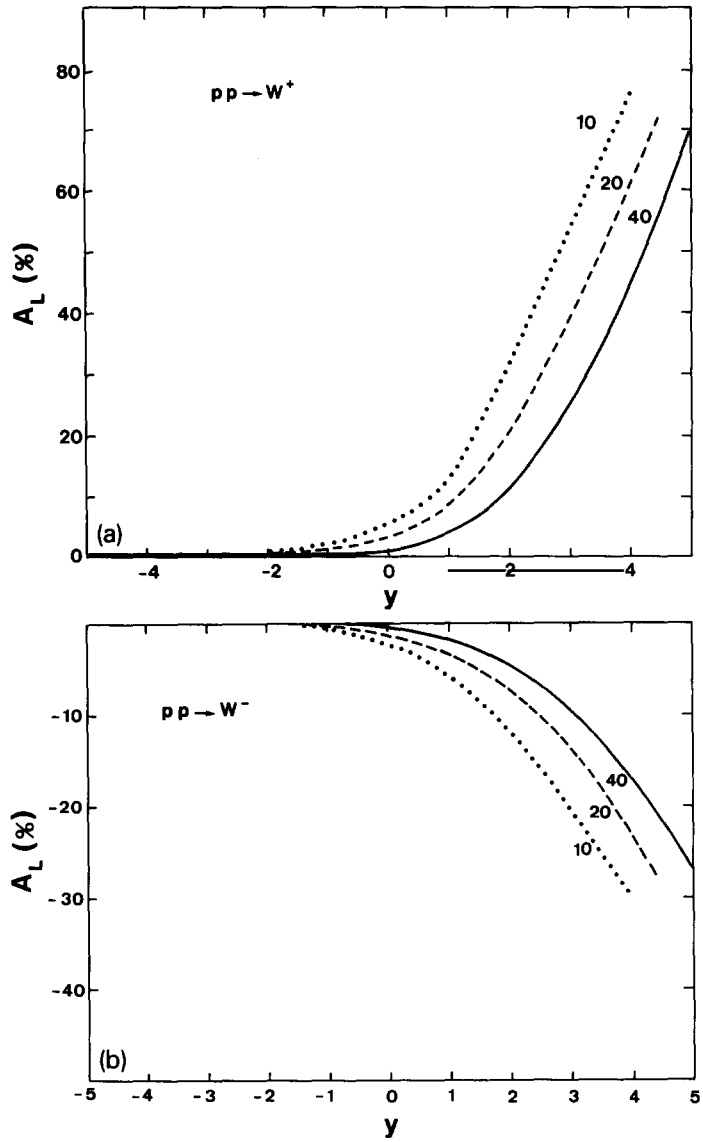

Fig. 5.2. A_L (a) in $pp \to W^+$, (b) in $pp \to W^-$, versus y for three different energies.

which becomes, neglecting the heavy flavor contribution in the denominator,

$$A_L \simeq a_u(\bar{d}) - a_{\bar{d}}(u) \quad \text{at } \sqrt{\hat{s}} = M_W\,, \tag{5.14a}$$

and for W^- by permuting u and d

$$A_L \simeq a_d(\bar{u}) - a_{\bar{u}}(d) \quad \text{at } \sqrt{\hat{s}} = M_W\,. \tag{5.14b}$$

The resulting A_L are shown in fig. 5.3 and they decrease very slowly with increasing energy consistently with fig. 3.16. The sea quark polarization $a_{\bar{q}}$ is very small at this $\sqrt{\hat{s}}$ value and effectively does not contribute.

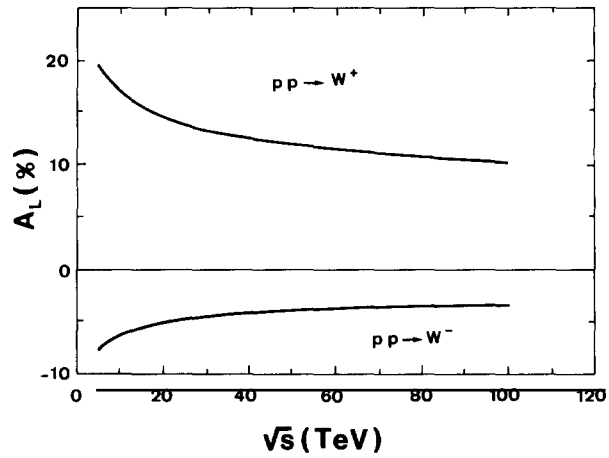

Fig. 5.3. Integrated A_L in $pp \to W^+$ and $pp \to W^-$ versus $\sqrt{s}$.

Similarly one can analyze the single-Z^0 production in the Drell–Yan picture and one finds that the helicity asymmetry as a function of y reads [see eqs. (5.3) and (5.7)]

$$A_L = \frac{\Sigma_i 2a_i b_i [\Delta q_i(x_a, M_Z^2)\, \bar{q}_i(x_b, M_Z^2) - \Delta\bar{q}_i(x_a, M_Z^2)\, q_i(x_b, M_Z^2)]}{\Sigma_i (a_i^2 + b_i^2)[q_i(x_a, M_Z^2)\bar{q}_i(x_b, M_Z^2) + (a \leftrightarrow b)]} . \tag{5.15}$$

We show the results of the calculation in fig. 5.4 and we observe that the trend is very similar to that of W^+ because it is dominated by the u-quark polarization, whose effect is reduced by the negative d-quark polarization and by the subtraction of the sea quark polarization, which was assumed to be

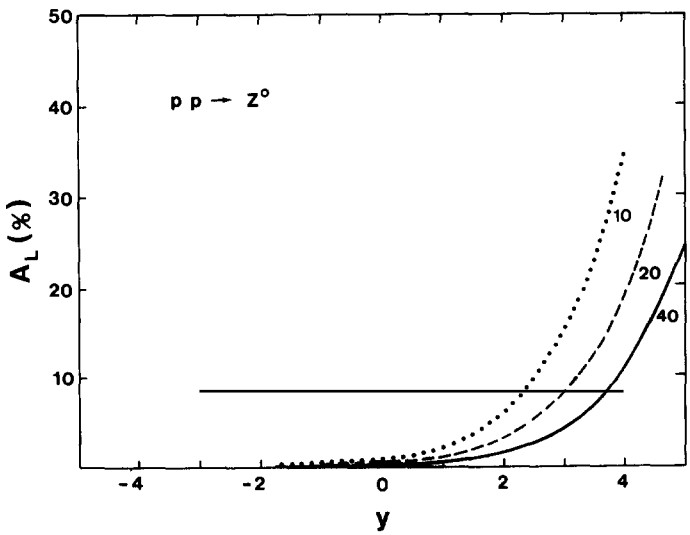

Fig. 5.4. A_L in $pp \to Z^0$ versus y for three different energies.

positive. As for the W's one can consider at each energy the cross section integrated over y and the corresponding asymmetry is

$$A_L = \frac{\sum_i 2a_i b_i \frac{\tau}{M_Z^2}\left(\frac{d\mathscr{L}_{\Delta q_i \bar{q}_i}}{d\tau} - \frac{d\mathscr{L}_{\Delta \bar{q}_i q_i}}{d\tau}\right)}{\sum_i (a_i^2 + b_i^2)\left(\frac{\tau}{M_Z^2}\frac{d\mathscr{L}_{q_i \bar{q}_i}}{d\tau}\right)}, \tag{5.16}$$

which is displayed in fig. 5.5. In this case the effect, which is at most 4%, much smaller than for W's, also decreases with increasing energy.

So far we have assumed that the W's and Z's are produced in the Drell–Yan picture, i.e. with a small transverse momentum p_T, but there are higher-order QCD processes where the gauge boson can be produced with a large p_T which is balanced by a hadronic jet. This is similar to the prompt photon production we have studied above (see section 4.3), but here one should consider the quark–antiquark annihilation subprocess $q_i\bar{q}_j \to Wg$ and the quark–gluon Compton subprocess $q_i g \to q_j W$ with $i \neq j$. From the decay distribution of the $W^{\pm}$ produced at large p_T it is possible to discriminate between the scalar and the vector nature of the gluon emitted in the final state [ART84]. By using this method based on the fact that, unlike the electromagnetic current, the axial current is not conserved, a scalar gluon was excluded at a 2σ level at the CERN collider [STU87]. Hopefully this will be confirmed by higher-statistics data.

The differential cross section for producing a W with p_T and rapidity y is

$$\frac{d\sigma}{dp_T\,dy} = 2p_T \sum_{ij} \int_{x_0}^{1} dx_a \frac{x_a x_b}{x_a - (m_T/\sqrt{s})e^{y}} \left(f_i(x_a, Q^2) f_j(x_b, Q^2) \frac{d\hat{\sigma}_{ij}}{d\hat{t}}(\hat{s}, \hat{t}, \hat{u}) + (i \leftrightarrow j) \right), \tag{5.17}$$

where the explicit M_W dependence appears in all the kinematic variables,

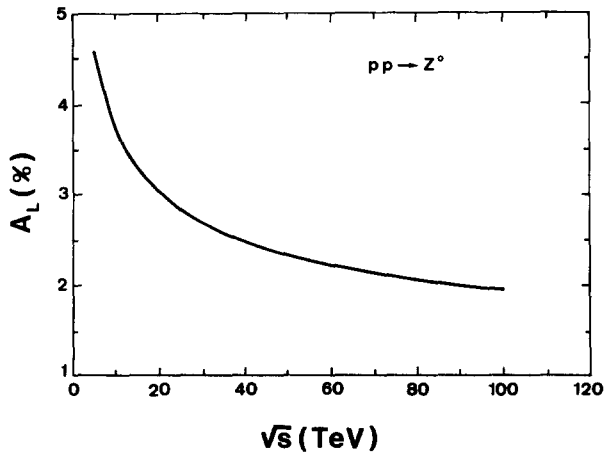

Fig. 5.5. Integrated A_L in $pp \to Z^0$ versus $\sqrt{s}$.

$$\hat{s} = x_a x_b s\,, \qquad \hat{t} - M_W^2 = -x_a\sqrt{s}m_T e^{-y}\,, \qquad \hat{u} - M_W^2 = -x_b\sqrt{s}m_T e^{-y}\,, \tag{5.18}$$

through the transverse mass $m_T = (M_W^2 + p_T^2)^{1/2}$ and where

$$x_b = \frac{x_a(m_T/\sqrt{s})e^{-y} - M_W^2/s}{x_a - (m_T/\sqrt{s})e^{y}}\,, \qquad x_0 = \frac{(m_T/\sqrt{s})e^{y} + M_W^2/s}{1 - (m_T/\sqrt{s})e^{-y}}\,.$$

To get a feeling for the event rates at $\sqrt{s} = 40$ TeV, the cross section at $y = 0$ and $p_T = 0.3$ TeV is found to be around 10^{-3} nb/GeV with $Q^2 = p_T^2$ (see fig. 118 of EHLQ). It is largely dominated by the Compton diagram and drops very rapidly with increasing p_T. For initial partons carrying a given helicity, let us recall that for annihilation $q(h_1)\bar{q}(h_2) \to Wg$ we have

$$\frac{d\hat{\sigma}^a}{d\hat{t}}(h_1, h_2) = \frac{2\pi\alpha\alpha_s}{9x_w\hat{s}^2}(1 - h_1)(1 + h_2)a(\hat{t})\,, \qquad a(\hat{t}) = \frac{(\hat{t} - M_W^2)^2 + (\hat{u} - M_W^2)^2}{\hat{u}\hat{t}}\,, \tag{5.19}$$

which is symmetric in $\hat{t}$ and $\hat{u}$, and for Compton scattering $q_i(h)g(\lambda) \to q_j W$ we have

$$\begin{aligned} &\frac{d\hat{\sigma}^c}{d\hat{t}}(h, \lambda) = \frac{\pi\alpha\alpha_s}{12x_w\hat{s}^2}(1 - h)[(1 - \lambda)c_1(\hat{t}) + \lambda c_2(\hat{t})]\,, \\ &c_1(\hat{t}) = -\frac{(\hat{s} - M_W^2)^2 + (\hat{u} - M_W^2)^2}{\hat{s}\hat{u}}\,, \qquad c_2(\hat{t}) = -\frac{2(\hat{u} - M_W^2)^2}{\hat{s}\hat{u}}\,. \end{aligned} \tag{5.20}$$

For $\bar{q}_i(h)g(\lambda) \to \bar{q}_j W$ the same formula holds but with $h \to -h$ and $\lambda \to -\lambda$. The corresponding single helicity asymmetries are $\hat{a}_L^a = \hat{a}_L^c = 1$ for polarized quarks, $\hat{a}_L^a = -1$ for polarized antiquarks and $\hat{a}_L^c = 1 - c_2/c_1$ for polarized gluons. This last quantity being rather small on average, the single hadron helicity asymmetry will be dominated by polarized quarks. The results of the calculation of A_L at $y = 0$ versus p_T for W^+ and W^- are shown in fig. 5.6 at three different energies[2]. Here again A_L is not sensitive to the gluon polarization a_g and is driven by a_u for W^+ and by a_d for W^-. At fixed p_T it decreases for increasing energy but it grows substantially for p_T in a kinematic region where the event rates are not negligible.

5.3. *Pair production of gauge bosons*

The first motivation for considering these processes is to study trilinear couplings in a sensitive kinematic region. If the gauge sector of the standard electroweak interactions is correctly described, detailed measurements of cross sections and helicity asymmetries for the production of $W^{\pm}Z^0$, $W^{\pm}\gamma$, Z^0Z^0, $Z^0\gamma$ and W^+W^- pairs will also provide us with a good calibration of various combinations of $q\bar{q}$ luminosities. In particular we will introduce two *universal curves* which allow a direct understanding of the single helicity asymmetry in several processes we will consider below and in the subsequent sections.

[2] For predictions at lower energies, up to 1 or 2 TeV, see [HID81].

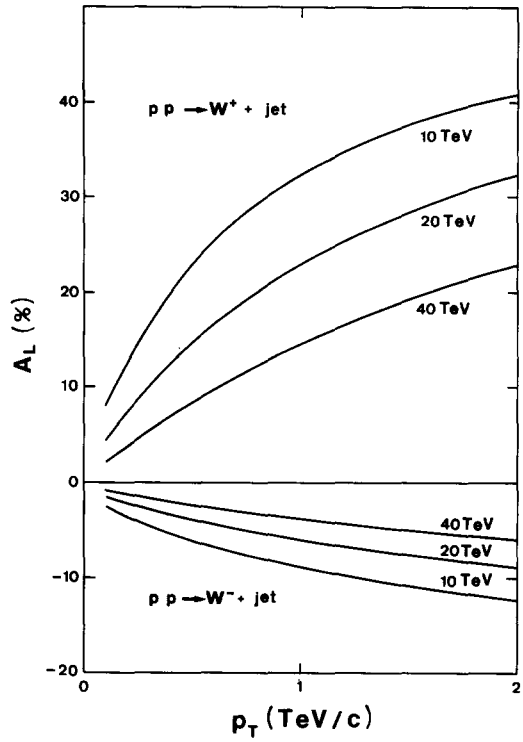

Fig. 5.6. A_L in $pp \to W^{\pm}$ + jet at $y = 0$ versus p_T at three different energies.

5.3.1. The universal curves

Since the W is a purely left-handed current we have seen that the single helicity asymmetry in W^+ production has the simple form in terms of luminosities given above in eq. (5.13). More generally let us consider a reaction dominated by the subprocess

$$q_i\bar{q}_j \to W(M) \to \text{any final state}, \tag{5.21}$$

with the production of an off-shell W of invariant mass M decaying into a W and a neutral object. The single helicity asymmetry as a function of M will be given for W^+ by

$$a_L^+(M) = \frac{\sum_{ij} \frac{\tau}{M^2}\left(\frac{d\mathscr{L}_{\Delta q_i\bar{q}_j}}{d\tau} - \frac{d\mathscr{L}_{\Delta\bar{q}_j q_i}}{d\tau}\right)}{\sum_{ij} \frac{\tau}{M^2}\frac{d\mathscr{L}_{q_i\bar{q}_j}}{d\tau}}, \tag{5.22}$$

where $q_i\bar{q}_j$ has charge +1. In the same way as for eq. (5.13) one gets

$$a_L^+(M) = \frac{\frac{\tau}{M^2}\left(\frac{d\mathscr{L}_{\Delta u\bar{d}}}{d\tau} - \frac{d\mathscr{L}_{\Delta\bar{d}u}}{d\tau}\right)}{\frac{\tau}{M^2}\frac{d\mathscr{L}_{u\bar{d}}}{d\tau} + \text{hfc}}, \tag{5.23}$$

which can be approximated, since $u\bar{d}$ dominates, by

$$a_L^+ \simeq a_u(\bar{d}) - a_{\bar{d}}(u) \quad \text{at } \sqrt{\hat{s}} = M . \tag{5.24a}$$

Similarly for W^- by permuting u and d one has

$$a_L^- \simeq a_d(\bar{u}) - a_{\bar{u}}(d) \quad \text{at } \sqrt{\hat{s}} = M . \tag{5.24b}$$

The flattening of a_L^+ for large M at 10 TeV is due to the increasing effect of $a_{\bar{d}}$ (see fig. 3.17). The two universal curves $a_L^{\pm}(M)$ as a function of M are represented in fig. 5.7 at three different energies and they will often be referred to in the following. A straightforward application is the production of $\ell^{\pm}\nu_\ell$ from an off-shell $W^{\pm}$ of mass M.

5.3.2. Production of $W^{\pm}Z^0$ and $W^{\pm}\gamma$ pairs

A substantial yield of these pairs is anticipated at supercollider energies and for example at the SSC we expect a total number of 4×10^5 $W^{\pm}Z^0$ events/year and 4×10^4 $W^{\pm}\gamma$ events/year provided that $W^{\pm}$, Z^0 and γ all satisfy $|y| < 2.5$ (see figs. 126 and 136 of EHLQ). Needless to recall that the cross sections, which fall rapidly with increasing mass of the pair, are dominated by quark–antiquark annihilation

$$q_i(h_1)\bar{q}_j(h_2) \rightarrow W^{\pm}Z^0 \text{ or } W^{\pm}\gamma . \tag{5.25}$$

This process gets contributions from the $\hat{t}$- and $\hat{u}$-channel quark exchange and from the $\hat{s}$-channel $W^{\pm}$ gauge boson exchange, so for $W^{\pm}Z^0$ it is a probe of the trilinear coupling WWZ fully specified by the gauge structure of the electroweak interactions [BRO79]. In particular the angular distribution in hard

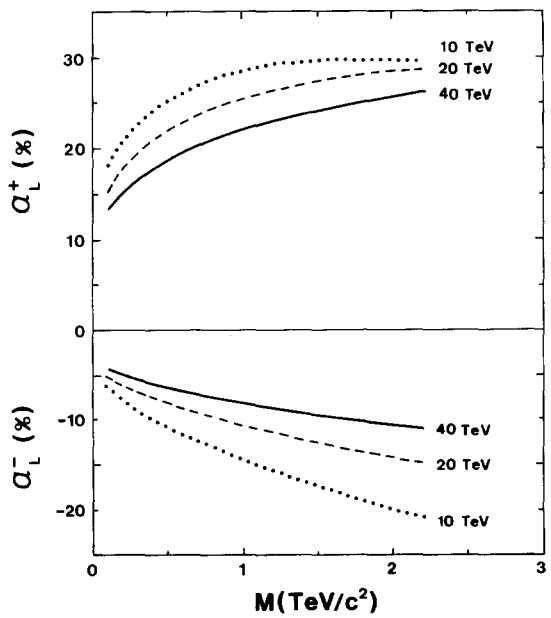

Fig. 5.7. The two universal curves $a_L^{\pm}(M)$ versus M at three different energies.

photon production is highly sensitive to the value of the magnetic moment parameter κ of the W [BRO79a] and deviations from the standard WWZ vertex, even restricted by unitarity, will give clean signals in WZ production [ZEP88]. A non-standard structure of the WWγ vertex can also have direct consequences in Wγ production [BAU88]. We will discuss later some theoretical considerations which lead to anomalous magnetic moments (see section 7).

The cross sections corresponding to eq. (5.25) are

$$\hat{\sigma}_{ij}(h_1, h_2) = \hat{\sigma}_{ij}(\text{unpol})(1 - h_1)(1 + h_2)\,, \tag{5.26}$$

where the unpolarized cross sections are given in [BRO79a]. From the simple form of eq. (5.26) we see that the single helicity asymmetry associated to the total yield $d\sigma/dM$ with no rapidity cut is clearly given by the universal curves $a_L^{\pm}(M)$ because in the ratio one can drop $\hat{\sigma}_{ij}(\text{unpol})$, which is a function of $\hat{s}$ only. From fig. 5.7 we see that for example at $\sqrt{s} = 10\,\text{TeV}$ a W^+Z^0 (or $W^+\gamma$) pair of mass $M = 0.5\,\text{TeV}/c^2$ will have $A_L = 25\%$, whereas a W^-Z^0 (or $W^-\gamma$) pair of the same mass will have $A_L = -10\%$. Clearly in a realistic experimental situation one should make rapidity cuts, which decrease the expected event rates, but we have checked that these cuts have almost no effect on A_L, whose magnitude is only slightly reduced.

5.3.3. Production of ZZ and Zγ pairs

These pair production reactions are useful and with a reasonable rapidity cut $|y| < 2.5$ we expect for each channel 2×10^5 events/year at the SSC. The production mechanism

$$q_i(h_1)\bar{q}_i(h_2) \rightarrow ZZ \text{ or } Z\gamma \tag{5.27}$$

does not involve the trilinear coupling and for the integrated cross sections we have

$$\hat{\sigma}_i(\hat{s}) = [(1 - h_1h_2)K_i + (h_2 - h_1)N_i]I(\hat{s})\,, \tag{5.28}$$

where $I(\hat{s})$ can be deduced e.g. from eqs. (4.69) and (4.79) of EHLQ. This has a spin structure similar to that of eq. (5.6), so the single helicity asymmetry is given by eq. (5.8) with for ZZ

$$K_i = (a_i^2 + b_i^2)^2 + 4a_i^2b_i^2\,, \qquad N_i = 4a_ib_i(a_i^2 + b_i^2)\,, \tag{5.28a}$$

and for Zγ

$$K_i = e_i^2(a_i^2 + b_i^2)\,, \qquad N_i = 2e_i^2a_ib_i\,, \tag{5.28b}$$

where e_i is the electric charge of the quark q_i and a_i, b_i are given in eq. (5.4). The results of the calculation of A_L with no rapidity cut are shown in fig. 5.8 versus M, the invariant mass of the pair, for three different energies. The polarization of the d-quark is negative, and since $a_d b_d$ is positive, the d-quark polarization reduces appreciably the polarization of the u-quark to give a rather small positive A_L in the case of ZZ. A_L is also positive for Zγ but larger as a consequence of the electric charge of the quarks, which reduces the effect of the d-quark. In all cases A_L decreases with increasing energy. A possible background for Zγ production is the standard direct photon production (see section 4), which has a larger cross section, but it does not contribute to A_L.

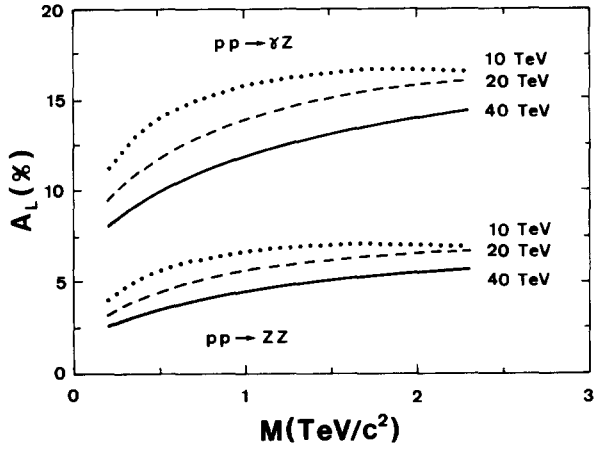

Fig. 5.8. A_L in pp→ZZ and pp→Zγ with no rapidity cut versus M at three different energies.

5.3.4. *Production of W^+W^- pairs*

This process gives the highest production rate and at SSC we expect about 10^6 events/year with $|y|<2.5$ (see fig. 120 of EHLQ). It is dominated by the subprocess

$$q_i(h_1)\bar{q}_i(h_2)\rightarrow W^+W^- , \tag{5.29}$$

which gets contributions from $\hat{s}$-channel γ, Z exchange involving the WWZ coupling g_Z and from $\hat{t}$-channel quark exchange. The cross section to produce a W^+W^- pair of invariant mass M with no rapidity cut for the W's is [BRO79]

$$\frac{d\sigma}{dM} = \left(\frac{8\pi\alpha^2}{M}\right)\frac{1}{3}\sum_i K_i\left(\frac{\tau}{M^2}\frac{d\mathscr{L}_{q_i\bar{q}_i}}{d\tau}\right), \tag{5.30}$$

where

$$K_i = e + i_i + a_i ,$$

with

$$e = \frac{1}{16x_w^2}\left[\frac{2\beta}{3}\left(\frac{1}{\varepsilon^2}+\frac{5}{\varepsilon}-3\right)+(2-\varepsilon)\ln\frac{1+\beta}{1-\beta}\right]$$

the quark exchange contribution,

$$a_i = [e_i^2 + 2e_i a_i g_Z M^2 \,\mathrm{Re}\, D_Z + (a_i^2+b_i^2)g_Z^2 M^4 |D_Z|^2]\beta^3\left(\frac{1}{3\varepsilon^2}+\frac{5}{3\varepsilon}+\frac{1}{4}\right)$$

the boson exchange contribution, and

$$i_i = \frac{\pm 1}{4x_w}[e_i + g_Z(a_i+b_i)M^2 \,\mathrm{Re}\, D_Z]\left[\beta\left(\frac{2}{3\varepsilon^2}+\frac{3}{\varepsilon}-\frac{7}{6}-\frac{\varepsilon}{4}\right)-\varepsilon(1+\tfrac{1}{8}\varepsilon)\ln\frac{1+\beta}{1-\beta}\right]$$

the interference term, where + (−) is for the d- (u-) quark [BRO79]. Here $\varepsilon = 4M_W^2/M^2$, $\beta = \sqrt{1-\varepsilon}$ and $g_Z = \operatorname{cotg}\theta_w$. The integrated cross section corresponding to eq. (5.29) reads

$$\hat{\sigma}_i(h_1, h_2) = \frac{4\pi\alpha^2}{\hat{s}} [(1 - h_1h_2)K_i + (h_2 - h_1)N_i] , \tag{5.31}$$

where

$$N_i = e + i_i + a_i' ,$$

with

$$a_i' = (2e_ib_ig_ZM^2 \operatorname{Re} D_Z + 2a_ib_ig_Z^2M^4|D_Z|^2)\left[\beta^3\left(\frac{1}{3\varepsilon^2} + \frac{5}{3\varepsilon} + \frac{1}{4}\right)\right]$$

and consequently the single helicity asymmetry A_L has a simple expression in terms of luminosities given by eq. (5.8). The results of the calculation of A_L versus M are shown in fig. 5.9 at three different energies. For $\varepsilon \ll 1$ we note that $K_u \sim N_u \sim K_d \sim N_d$, so together with the result $\mathcal{L}_{u\bar{u}} \simeq 2\mathcal{L}_{d\bar{d}}$ following from eq. (3.6), we have the very simple approximate expression

$$A_L \sim \tfrac{2}{3}a_u(\bar{u}) + \tfrac{1}{3}a_d(\bar{d}) - a_{\bar{q}}(q) . \tag{5.32}$$

We also show in fig. 5.9 the resulting asymmetries in the absence of the trilinear coupling, i.e. with $g_Z = 0$. In this case

$$i_u = 2i_d , \qquad a_u = 4a_d , \qquad a_u' = a_d' = 0 , \tag{5.33}$$

so A_L is smaller and flatter because the effect of the d-quark polarization becomes more important. Clearly it is possible to distinguish between $g_Z = 0$ and $g_Z = \operatorname{cotg}\theta_w$ and the perturbation introduced by the decoupling of the Z is more substantial for M very much above threshold. The asymmetries with a

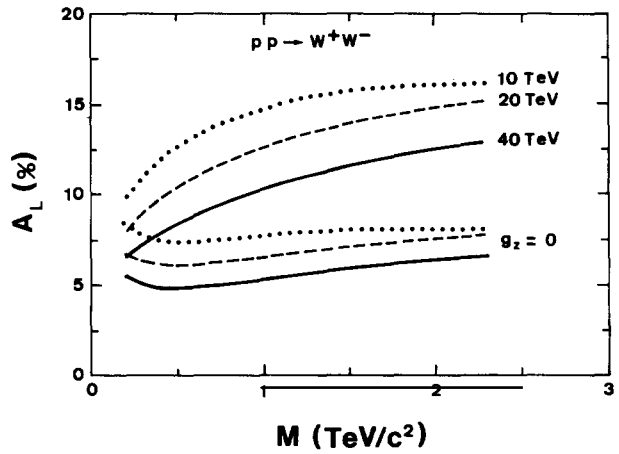

Fig. 5.9. A_L in $pp \to W^+W^-$ with no rapidity cut versus M at three different energies, for $g_Z \neq 0$ and $g_Z = 0$.

rapidity cut[3] have been calculated and as already mentioned in previous cases we found the same trend with the magnitude reduced by 1% or so compared to the case with no rapidity cut. Finally we have calculated the asymmetry corresponding to the cross section integrated over the pair mass M and the results are shown in fig. 5.10 for the two values of g_Z. The effects are smaller and less easy to discriminate.

5.4. Higgs boson production

The Higgs boson predicted by the standard electroweak theory is a neutral scalar particle whose mass M_H is not specified. However, according to some consistency arguments one can derive a lower bound [WEI76, LIN76] and an upper bound [LEE77] allowing the following range:

$$7\,\mathrm{GeV}/c^2 \leq M_H \leq 1000\,\mathrm{GeV}/c^2\,. \tag{5.34}$$

One could have $M_H > 1\,\mathrm{TeV}/c^2$ for any model where the electroweak symmetry is broken by a new strongly interacting sector [CHA85a] but since the width of the Higgs grows with M_H, it would become very large, making the Higgs not easy to identify as a resonance[4]. Higgs production in pp collisions occurs via several mechanisms, quark–antiquark annihilation, gluon–gluon fusion via a quark loop [GEO78] and gauge boson fusion [CAH84].

The first of these leads to the unpolarized cross section

$$\mathrm{d}\sigma(\mathrm{pp}\to \mathrm{H}+\mathrm{X}) = \frac{\pi G_F}{3\sqrt{2}} \sum_i m_i^2 \beta_i^3 \left(\frac{\tau}{M_H^2} \frac{\mathrm{d}\mathscr{L}_{q_i\bar{q}_i}}{\mathrm{d}\tau}\right), \tag{5.35}$$

with $\beta_i = (1 - 4m_i^2/M_H^2)^{1/2}$, which is dominant for heavy quarks because of the factor m_i^2, so we now need to specify the top quark distribution. It is consistent with that given in the erratum of EHLQ and

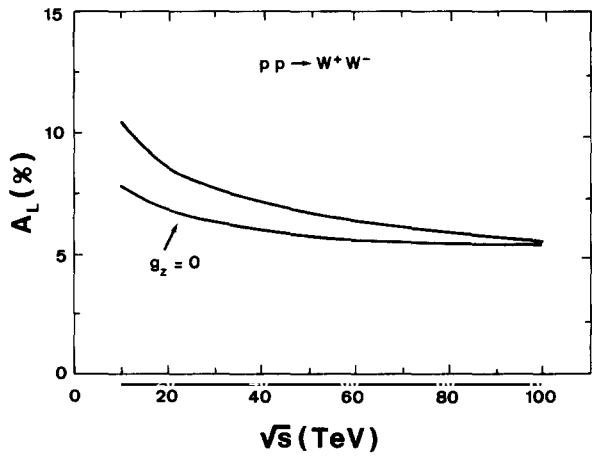

Fig. 5.10. Integrated A_L in $\mathrm{pp}\to \mathrm{W^+W^-}$ versus $\sqrt{s}$, for $g_Z \neq 0$ and $g_Z = 0$.

[3] The expressions for K_i and N_i with a rapidity cut can be deduced from appendix B.

[4] The shape of the Higgs resonance produced at the SSC has been studied in [BEN86].

following our simple parametrizations of section 3 [see eq. (3.7)] we propose to take for the unpolarized (top or antitop) distribution

$$xt(x, S_t) = \tfrac{1}{2}[(S_t/b)\ln(1/x)]^{1/2} xF(x, S_t)\,, \tag{5.36}$$

with

$$xF(x, S_t) = a_1 \exp[a_2\sqrt{S_t}(1-\sqrt{S_t})]\exp[12a_3\sqrt{(S_t/b)\ln(1/x)}]\,(1-x)^6\,,$$

$$S_t = \ln[\ln(Q^2/\Lambda^2)/\ln(4M_t^2/\Lambda^2\ln(1/x))]\,,$$

which takes into account the threshold due to the top quark mass M_t; for $M_t = 40\,\mathrm{GeV}/c^2$ this parametrization is valid for $Q^2 \geq 7\times 10^3\,\mathrm{GeV}^2$. The three parameters a_1, a_2, a_3 have been fitted and we found

$$a_1 = 4.95\times 10^{-4}\,,\quad a_2 = 14.48\,,\quad a_3 = 2.75\,. \tag{5.37}$$

The smallness of a_1 reflects the tiny amount of top quark in the proton. The polarized distribution $x\,\Delta t(x, S_t)$ was obtained from $xt(x, S_t)$ assuming, as for the light flavors, the universal behavior given by eq. (3.15). The differential top–antitop luminosities at $\sqrt{s} = 40\,\mathrm{TeV}$ are shown in fig. 5.11 and from eq. (5.35) we can estimate the event rate it leads to, according to the value of $\sqrt{\hat{s}} = M_H$. For small $\sqrt{\hat{s}}$ the singly and doubly polarized luminosities are largely suppressed, so for a light Higgs we expect very small helicity asymmetries from this mechanism.

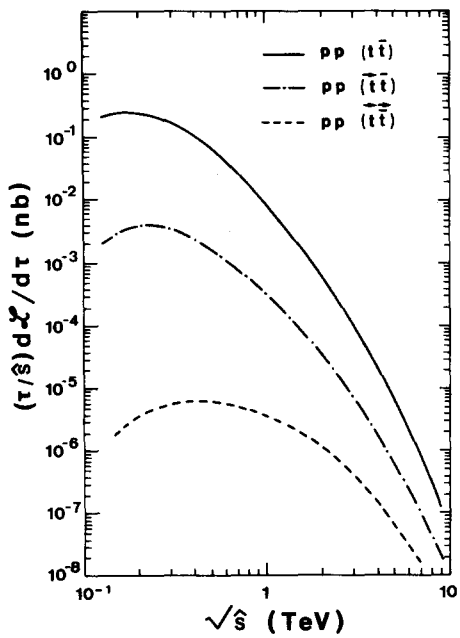

Fig. 5.11. The quantity $(\tau/\hat{s})\,\mathrm{d}\mathscr{L}/\mathrm{d}\tau$ versus $\sqrt{\hat{s}}$ for $t\bar{t}$ interactions in pp collisions at $\sqrt{s} = 40\,\mathrm{TeV}$. Solid curve, unpolarized distributions; dashed–dotted curve, singly polarized (t or $\bar{t}$) distributions; dashed curve, doubly polarized distributions.

Gluon–gluon fusion is also very sensitive to the mass of the quark loop and the corresponding Higgs production cross section [see eq. (4.90) of EHLQ] involves the gluon–gluon luminosity (see fig. 3.7a, b). As a result it dominates over direct quark–antiquark annihilation for $M_H < 700\,\mathrm{GeV}/c^2$ or so with $M_t = 40\,\mathrm{GeV}/c^2$ and $\sqrt{s} = 10\,\mathrm{TeV}$. For these two production mechanisms parity is conserved and one should consider only the double helicity asymmetry A_{LL}. At the level of the subprocesses one has

$$\hat{a}_{LL} = (1 - 4M_t^2/M_H^2)^{-1} \quad \text{for } t\bar{t}, \qquad \hat{a}_{LL} = +1 \quad \text{for gg}. \tag{5.38}$$

Consequently A_{LL} resulting from the combination of the two mechanisms is positive and from the relative size of the two cross sections we expect it to follow the behavior of $a_{\bar{q}}$ (see fig. 3.17) for large values of M_H independently of the value of M_t. This is indeed the case as shown in fig. 5.12, where A_{LL} is represented at $\sqrt{s} = 10\,\mathrm{TeV}$ up to $M_H = 3.5\,\mathrm{TeV}/c^2$ just for illustration. At $\sqrt{s} = 40\,\mathrm{TeV}$, A_{LL} is less than 1% and is not worth drawing. It is well known that if $M_H < 2M_W$ and if the Higgs decays mainly in $t\bar{t}$ due to the enormous background, there is no way to detect it at supercollider energies and we see that polarized beams would not help. For $M_H > 2M_W$ the WW/ZZ fusion mechanism dominates over gluon–gluon fusion for $M_H \geq 300\,\mathrm{GeV}/c^2$ if $M_t = 40\,\mathrm{GeV}/c^2$; we will come back to this in section 9. In this mass range the Higgs boson may be observed up to $M_H \sim 800\,\mathrm{GeV}/c^2$ in the decay mode $H \to ZZ$ with both Z's decaying to e^+e^- or $\mu^+\mu^-$, but other experimental signatures have also been considered [CAH88].

Polarized beams might be more useful for associated production of a Higgs boson with a vector gauge boson W or Z as we will discuss now. They occur by direct formation and decay of a virtual gauge boson in

$$q_i\bar{q}_j \to HW^{\pm}, \qquad q_i\bar{q}_i \to HZ. \tag{5.39a, b}$$

The cross section corresponding to eq. (5.39a) has an expression similar to eq. (5.26) and therefore the single helicity asymmetry A_L for $HW^{\pm}$ production is given by the universal curves $a_L^{\pm}(M)$ (see fig. 5.7), where M is the invariant mass of the produced HW system. The cross section corresponding to eq.

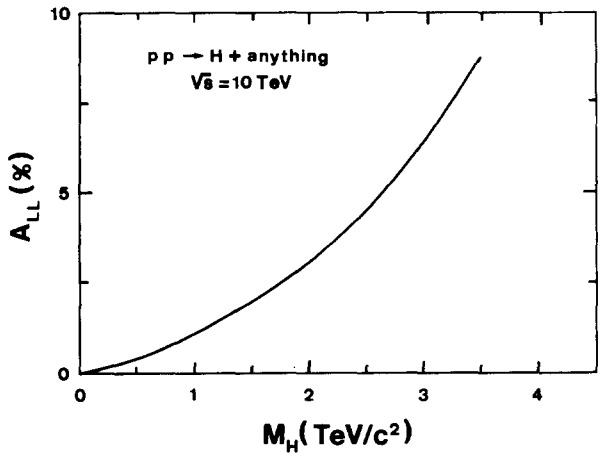

Fig. 5.12. A_{LL} versus M_H for $pp \to H$ + anything at $\sqrt{s} = 10\,\mathrm{TeV}$. The curves for $M_t = 40\,\mathrm{GeV}/c^2$ and $M_t = 100\,\mathrm{GeV}/c^2$ are indistinguishable.

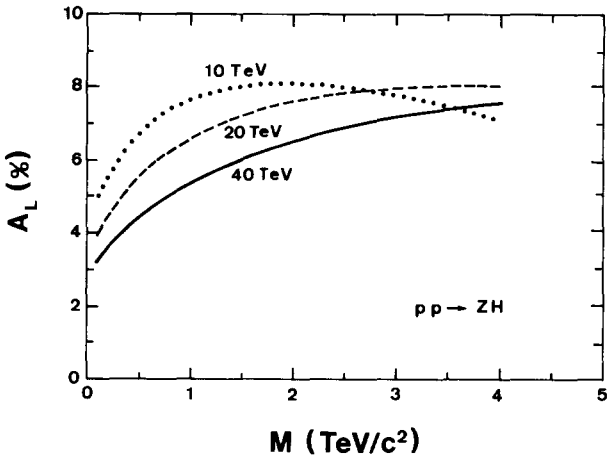

Fig. 5.13. A_L in pp→HZ versus M at three different energies.

(5.39b) is similar to eq. (5.28) with

$$K_i = a_i^2 + b_i^2 , \qquad N_i = 2a_i b_i , \tag{5.40}$$

allowing a simple calculation of A_L. The result is shown in fig. 5.13 at three different energies. Here again at $\sqrt{s} = 10$ TeV, A_L is larger and the effect of the d-quark polarization reduces its value for high M, the invariant mass of the HZ system.

We have seen that the Standard Model of electroweak interactions at LHC and SSC energies leads to definite predictions for single helicity asymmetries in gauge boson production providing better information on the couplings of $W^{\pm}$ and Z^0 and a good calibration of the polarized proton structure functions. We have also calculated some helicity asymmetries in Higgs production from quark and gluon collisions, but in this situation at least polarized beams do not allow a better identification of the signal for a light Higgs. We will now study nonstandard scenarios and we will see that polarization may be even necessary to discover deviations from the Standard Model.

6. Minimal extensions of the Standard Model

The simplicity of the $SU(3)_C \otimes SU(2)_L \otimes U(1)_Y$ Standard Model is remarkable but its Higgs sector, which is the least understood, makes it very puzzling. Although the Standard Model works impressively well at CERN collider energy, something else could be present in the multi-TeV energy range. Many attempts have been made to enlarge the gauge group; minimal extensions are obtained by the consideration of new quarks and new leptons, heavier than the usual known fermions, interacting with new heavy gauge bosons in a similar fashion to the standard electroweak theory. We shall only study a few typical examples of such minimal extensions to show the relevance of polarized beams to identify a bump in a cross section. Needless to recall that helicity asymmetries are less sensitive to systematic errors and allow one to get valuable information on the couplings of these new objects. We will consider the cases of charged Higgs $H^{\pm}$ production, pair production of heavy leptons and production of new gauge bosons.

6.1. Charged Higgs production

As soon as one adds more Higgs doublets to the standard electroweak theory, it implies the existence of charged physical Higgs $H^{\pm}$, non-standard Higgs bosons[1]. Ignoring all the details of possible versions for the enlargement of the Higgs sector [LAN82, LAN84, ANS85], we should not forget that, as for neutral Higgs, the production and the detection of these particles in pp collisions are difficult and strongly related to their mass. The main production mechanism is the Drell–Yan process $q_i(h_1)\bar{q}_i(h_2)\to\gamma, Z\to H^+H^-$ whose corresponding integrated cross section, similarly to eq. (5.6), reads for scalar particles

$$\hat{\sigma}_i(h_1, h_2) = \frac{4\pi\alpha^2}{3M^2}\,\frac{\beta^3}{4}\,[(1-h_1h_2)\tilde{K}_i + (h_2-h_1)\tilde{N}_i]\,, \tag{6.1}$$

with

$$\tilde{K}_i = e_i^2 + 2e_ia_ig_{ZH^+H^-}M^2\,\mathrm{Re}\,D_Z + (a_i^2+b_i^2)g^2_{ZH^+H^-}M^4|D_Z|^2\,, \tag{6.2}$$

$$\tilde{N}_i = 2e_ib_ig_{ZH^+H^-}M^2\,\mathrm{Re}\,D_Z + 2a_ib_ig^2_{ZH^+H^-}M^4|D_Z|^2\,, \tag{6.3}$$

where M is the invariant Higgs pair mass, $M_{H^\pm}$ is the Higgs mass and $\beta = (1-4M^2_{H^\pm}/M^2)^{1/2}$. The ZH^+H^- coupling is, in the minimal extension,

$$g_{ZH^+H^-} = \frac{1-2x_w}{2x_w^{1/2}(1-x_w)^{1/2}}\,. \tag{6.4}$$

The single helicity asymmetry has therefore a simple expression analogous to eq. (5.8) and is independent of $M_{H^\pm}$. The result of the calculation is shown in fig. 6.1 at three different energies. A_L is positive, it has the same trend as in dilepton production (see fig. 5.1) but with a larger magnitude

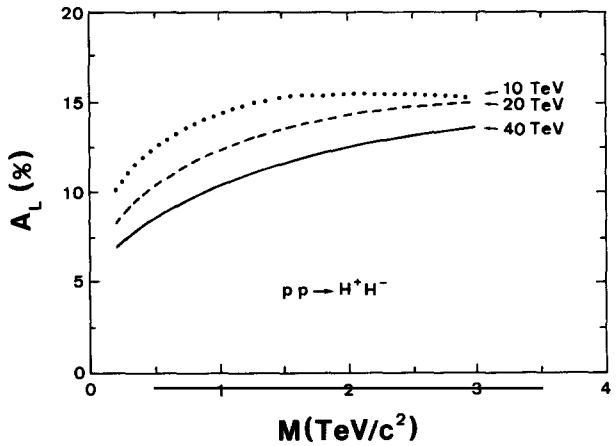

Fig. 6.1. A_L in $pp\to H^+H^-$ versus M at $\sqrt{s} = 10$, 20 and 40 TeV.

[1] This is a typical feature of supersymmetric models (see section 8).

because of the value of $g_{ZH^+H^-}$ and the absence of the suppression of the vector coupling in lepton pair production. If the most prominent decay of $H^\pm$ is into a pair of hadron jets, this parity violating asymmetry will be present in the four-jet cross section.

Another obvious Higgs pair production mechanism is $pp \to W^\pm(M) \to H^\pm H^0$, which occurs by direct formation and decay of a virtual $W^\pm$. In this case A_L is given by the universal curves (see fig. 5.7). If charged Higgs bosons exist, it is tempting to search them in production associated with the standard $W^\pm$ and Z^0. In the Standard Model there are no H^+W^-Z and $H^+W^-\gamma$ couplings at the tree level, so they should be ignored in first approximation. Although they are small the HWZ couplings exist in left–right symmetric models [GUN86].

6.2. Heavy lepton pair production

In the absence of a basic understanding of the pattern of the fermion generations, one should be open to the possible existence of new heavy fermions. From what we learnt in section 4, the production of heavy quarks is not expected to be strongly affected by the use of polarized beams, so we will consider only the case of new heavy leptons. Let us consider a new lepton doublet (L, ν_L). The mass M_L of the charged lepton is assumed to be such that $M_L - M_{\nu_L} > M_W$, where M_{ν_L} denotes the neutrino mass. The cross sections for the production of heavy leptons at the SSC are rather small and the relevant mechanism is from $q\bar{q}$ annihilation via γ, Z for a L^+L^- pair and via W for a $L\nu_L$ pair. For $M_L = 200\,\mathrm{GeV}/c^2$ we expect 10^4 L^+L^- events per year and 5×10^5 $L\nu_L$ events per year if ν_L is taken massless. The L^+L^- signal could be observed by an excessive W^+W^- rate with W^+ and W^- on opposite sides of the beam with an unbalanced p_T. Gauge boson fusion and gluon–gluon fusion via a quark loop give larger cross sections for very high values of M_L [AND88], but here we will restrict ourselves to the Drell–Yan mechanism $q_i(h_1)\bar{q}_i(h_2) \to \gamma, Z \to L^+L^-$, whose integrated cross section is given by eq. (5.6) with

$$K_i = \beta\{(\tfrac{3}{4} + \tfrac{1}{4}\beta^2)[e_i^2 - 2e_i a_\ell a_i M^2 \,\mathrm{Re}\, D_Z + (a_\ell^2 + b_\ell^2)(a_i^2 + b_i^2)M^4 |D_Z|^2] + 3(M_L^2/M^2)[e_i^2 - 2e_i a_\ell a_i M^2 \,\mathrm{Re}\, D_Z + (a_\ell^2 - b_\ell^2)(a_i^2 + b_i^2)M^4 |D_Z|^2]\}\,, \tag{6.5a}$$

$$N_i = \beta\{(\tfrac{3}{4} + \tfrac{1}{4}\beta^2)[-2e_i a_\ell b_i M^2 \,\mathrm{Re}\, D_Z + 2a_i b_i (a_\ell^2 + b_\ell^2)M^4 |D_Z|^2] + 3(M_L^2/M^2)[-2a_i a_\ell b_i M^2 \,\mathrm{Re}\, D_Z + 2a_i b_i (a_\ell^2 - b_\ell^2)M^4 |D_Z|^2]\}\,, \tag{6.5b}$$

where $\beta = (1 - 4M_L^2/M^2)^{1/2}$ and M denotes the lepton pair mass. Clearly when $M_L \ll M$ we recover the standard Drell–Yan expression independent of M_L with eqs. (5.3) and (5.7). One uses eq. (5.8) to calculate A_L and the result at $\sqrt{s} = 40\,\mathrm{TeV}$ is shown in fig. 6.2 for different values of M_L, where we also recall the result for the standard A_L from fig. 5.1. The effect is small and probably very hard to observe.

6.3. New gauge bosons

There are many proposals to incorporate the standard electroweak gauge group $SU(2)_L \otimes U(1)_Y$ in a larger framework. One possibility, assuming that parity violation is a low-energy phenomenon, is to construct left–right symmetric models [MOH83, SEN84] based on $SU(2)_L \otimes SU(2)_R \otimes U(1)$ in which one recovers parity invariance at high energies. In this case one predicts the existence of two new

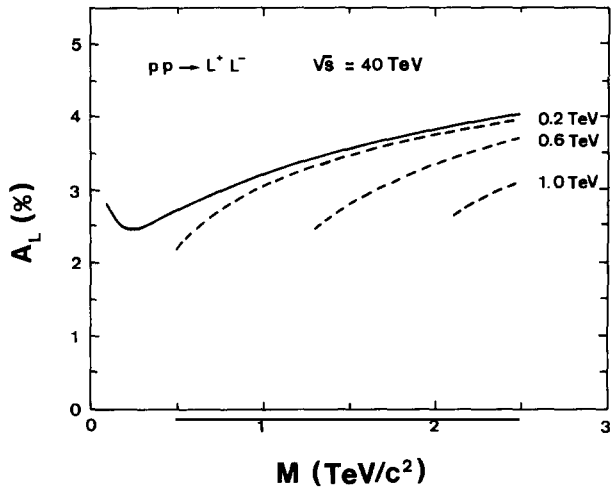

Fig. 6.2. A_L in $pp \to L^+L^-$ versus M at $\sqrt{s} = 40$ TeV for $M_L = 0.2$, 0.6 and 1.0 TeV/c^2 (dashed curves). The solid curve is A_L for light lepton pair production.

bosons $W_R^{\pm}$, associated to right-handed charged currents, and one additional new neutral gauge boson. The mass of $W_R^{\pm}$ is at least 300 GeV/c^2 and if one requires the production of 10^3 events in the rapidity range $|y| < 1.5$, one year running of SSC would be capable to discover $W_R^{\pm}$ with a mass up to 6.5 TeV/c^2 as reported in EHLQ. These heavy W would have a pure V + A coupling to quarks and leptons; if we assume for simplicity that the $SU(2)_L$ and $SU(2)_R$ couplings are equal, then the signature of new W's is extremely clear: it leads to obvious predictions for A_L in $pp \to W_R^{\pm}X$ given by the universal curves (see fig. 5.7), that is $-a_L^+(M)$ for W_R^+ of mass M and $-a_L^-(M)$ for W_R^- because of the sign change of the axial coupling. Therefore the use of polarized beams in this situation is one excellent method allowing a complete study of the couplings of new charged bosons. This is also true, as we will see now, for new neutral gauge bosons, whose characteristic couplings to ordinary quarks and leptons are far from being uniquely constrained. In addition to left–right symmetric models, grand unified and superstring theories lead us to expect additional neutral weak currents. We have chosen to examine the corresponding new bosons which are suggested by the phenomenology of the so-called E_6 superstring inspired models [PEC86]. Superstrings in 10 dimensions may, after compactification, lead to a four-dimensional E_6 gauge group of strong and electroweak interactions. Since E_6 has rank 6 and the standard gauge group $SU(3)_C \otimes SU(2)_L \otimes U(1)_Y$ has rank 4, it contains two extra U(1)'s orthogonal to $U(1)_Y$, whose corresponding Z bosons are called Z_ψ and Z_χ. Their mass eigenstates are any linear combination

$$Z(\alpha) = Z_\psi \cos\alpha + Z_\chi \sin\alpha\,, \tag{6.6}$$

and the orthogonal state. The mixing angle α specifies a particular model and clearly $\alpha = 0°$, 90° correspond to pure Z_ψ, Z_χ. As usual, weak bosons acquire their masses through spontaneous breakdown of the symmetry and if E_6 is broken to a rank-5 subgroup at the Planck scale, α is uniquely determined [LAN84a, LON86] and has the value $\alpha = \text{arctg}(\sqrt{3/5}) = 37.78°$. The corresponding boson is denoted Z′ and the boson orthogonal to Z′ associated to $\alpha = -\text{arctg}(\sqrt{5/3}) = 127.78°$ is called Z_I. The effective neutral current Lagrangian for such a model is

$$\mathcal{L} = eA_\mu J^\mu_{\rm em} + g_{\rm L}(1-x_{\rm w})^{-1/2} Z_\mu J^\mu_{\rm Z} + g' Z(\alpha)_\mu J^\mu_{{\rm Z}(\alpha)}\,, \tag{6.7}$$

where

$$J^\mu_{\rm em} = \sum_f \bar{f}\gamma^\mu Q_f f\,, \qquad J^\mu_{\rm Z} = \sum_f \bar{f}\gamma^\mu (a_f - b_f\gamma_5) f$$

are the standard electroweak currents and

$$J^\mu_{{\rm Z}(\alpha)} = \sum_f \bar{f}\gamma^\mu (a^\alpha_f - b^\alpha_f \gamma_5) f \tag{6.8}$$

is the new neutral current. $g_{\rm L}$ is the $SU(2)_{\rm L}$ gauge coupling related to g_Y, the $U(1)_Y$ coupling, as usual, $e = g_{\rm L}(x_{\rm w})^{1/2} = g_Y(1-x_{\rm w})^{-1/2}$, and g' is the new U(1) coupling, which takes the value

$$g' = \sqrt{5/3}\, e(1-x_{\rm w})^{-1/2}\,, \tag{6.9}$$

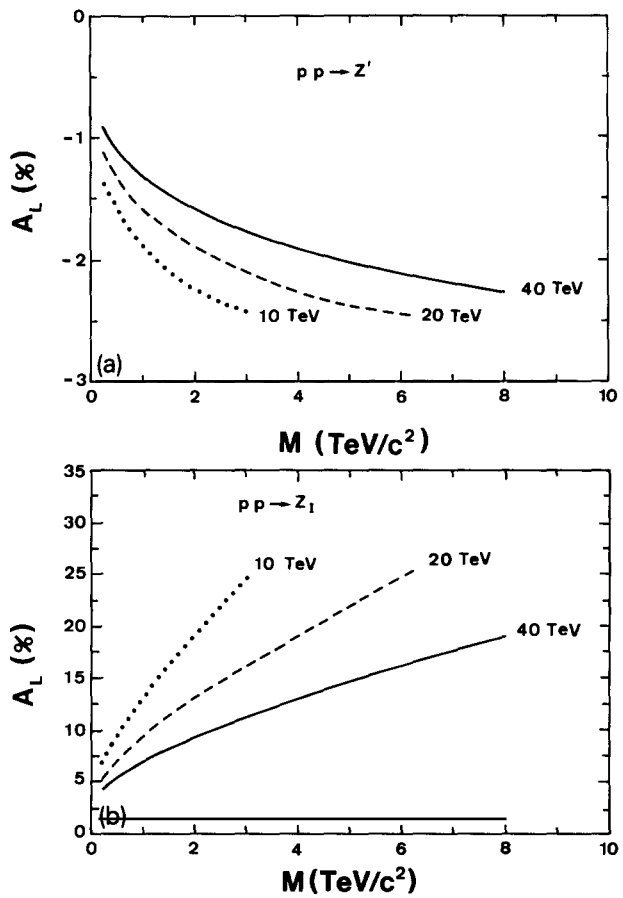

Fig. 6.3. $A_{\rm L}$ (a) in pp→Z', (b) in pp→$Z_{\rm I}$, versus M at three different energies.

normalized such that in the E_6 symmetry limit, when $x_w = 3/8$, g' is equal to g_L. We have

$$a_u^\alpha = 0\,, \qquad b_u^\alpha = \frac{g'}{2}\left(\frac{\cos\alpha}{\sqrt{6}} + \frac{\sin\alpha}{\sqrt{10}}\right) \quad \text{for up quarks}\,,$$
$$a_d^\alpha = g'\frac{\sin\alpha}{\sqrt{10}}\,, \qquad b_d^\alpha = \frac{g'}{2}\left(\frac{\cos\alpha}{\sqrt{6}} - \frac{\sin\alpha}{\sqrt{10}}\right) \quad \text{for down quarks}\,. \tag{6.10}$$

An extra Z must be sufficiently heavy in order not to give rise to departures of available neutral current data and according to experimental limits [GEE86] we will take $M_{Z'} > 200\ \mathrm{GeV}/c^2$. SSC would be an excellent source[2)] for producing Z′ and according to reasonable estimates [BAR87] we expect 2×10^5 events per year if $M_{Z'} = 500\ \mathrm{GeV}/c^2$ and ten times less if $M_{Z'} = 1\ \mathrm{TeV}/c^2$. The production mechanism is the Drell–Yan process and clearly the single helicity asymmetry A_L is given by eq. (5.16) using eq. (6.10). The results of the calculation are displayed in fig. 6.3a for Z′ and in fig. 6.3b for Z_I. Since $a_u^\alpha = 0$ in all cases, the size of the numerator in eq. (5.16) is determined by $2a_d^\alpha b_d^\alpha$, which is negative for Z′ and positive for Z_I. Moreover for Z_I u-quarks decouple and we have a pure V − A coupling to the d-quarks giving a much larger magnitude for A_L. We see that these asymmetries can be used at SSC and LHC to probe the couplings of these new bosons probably more accurately than with forward–backward asymmetries in $\mu^+\mu^-$ pair production [ADE86, ROS87].

7. Compositeness

Compositeness is one of the approaches to the outstanding problems left unanswered by the Standard Model. It supposes that all or at least some of the particles considered up to now as elementary and point-like, are in fact composite and extended objects [PES81, HAR84, PES85].

The idea that leptons could be composite is as old as the discovery of the muon, whose "raison d'être" is not yet understood. Later on the lepton–quark analogy and the proliferation of quarks and leptons has strongly supported this hypothesis. The mass generation problem, i.e. the origin and the mechanism for the wide spectrum of lepton, quark and gauge boson masses, has led to the proposal that the Higgs boson could be composite. This is the technicolor idea. Finally the peculiar gauge symmetry breaking which distinguishes the massive $W^\pm$ and Z^0 from the massless photon and gluons might lead us to the assumption that $W^\pm$ and Z^0 are composite objects satisfying a global SU(2) symmetry and mediating weak interactions appearing as residual effects of the underlying substructure.

Presently there is no experimental indication of compositeness in any of the three sectors mentioned above, which is not very encouraging. In spite of this, very interesting mechanisms have been proposed for the understanding of the intriguing aspects of the lepton and quark spectrum and the properties of composite intermediate vector bosons. Although several scenarios appear to be appealing, no model has yet been fully satisfactory and this is the reason for the development of phenomenological studies whose aims are, on the one hand, the search of the possible experimental signals for compositeness effects (new particles and interactions) and, on the other hand, the description of the processes in order to establish limits on the magnitude of the parameters measuring the interaction scales or the extension of the expected composite particles. Another aspect, as a consequence of the absence of a unique composite model, is the "effective" character of the parameters introduced in these phenomenological

[2)] Event rates at LHC from various models are also given in [AGU87].

descriptions, their model dependence and hence their limited significance. Therefore the experimental limits obtained from the various processes cannot be numerically compared without ambiguity and one needs to establish a complete set of limits in order to test various possible compositeness effects.

We will follow the strategy often used which consists in separately treating the effects coming from the three sectors, establishing a hierarchy in compositeness: composite Higgs bosons (technicolor), composite vector bosons (alternative models), composite quarks and leptons (substructure).

7.1. Technicolor

In this approach the spontaneous gauge symmetry breaking with the Higgs mechanism is replaced by a dynamical symmetry breaking. The existence of a whole spectrum of new fermions pertaining to a new gauge group G_{TC} is assumed [WEI76a, WEI79, SUS79]. The chiral symmetry associated to the peculiar assignments of these fermions is broken at an energy scale Λ_{TC} of the order of 1 TeV. As a consequence, among the various J^{PC} fermion–antifermion bound states, called the technimesons, whose masses are in principle of the order of Λ_{TC}, there appear some massless objects, the technipions ($J^{PC}=0^{-+}$). Three of them ($\pi_T^{\pm}, \pi_T^0$), coupled to the gauge bosons $W^{\pm}$, Z^0 by weak interactions, provide the degrees of freedom necessary to form the longitudinal states and generate the mass terms. The resulting $W^{\pm}$, Z^0 properties are then totally identical to the standard ones. The best test of this basic technicolor idea is the observation of massive technimeson states like techni-rhos ($\rho_T^{\pm}, \rho_T^0$), techni-omega (ω_T) etc. These vector states can be especially produced by the Drell–Yan mechanism,

$$q_i(h_1)\bar{q}_i(h_2)\to\gamma, Z\to\rho_T^0\,, \qquad q_i(h_1)\bar{q}_j(h_2)\to W^{\pm}\to\rho_T^{\pm}\,, \tag{7.1}$$

whose corresponding integrated cross sections are therefore for ρ_T^0

$$\hat{\sigma}_i(h_1,h_2)=\frac{\pi^2\alpha}{3M^4}\,\delta(M^2-m_{\rho_T}^2)[(1-h_1h_2)K_i+(h_2-h_1)N_i]\,, \tag{7.2}$$

with

$$K_i=e_i^2g_{\gamma\rho_T}^2+2e_ia_ig_{\gamma\rho_T}g_{Z\rho_T}M^2\,\mathrm{Re}\,D_Z+(a_i^2+b_i^2)g_{Z\rho_T}^2M^4|D_Z|^2\,, \tag{7.3}$$

$$N_i=2e_ib_ig_{\gamma\rho_T}M^2\,\mathrm{Re}\,D_Z+2a_ib_ig_{Z\rho_T}^2M^4|D_Z|^2\,, \tag{7.4}$$

and for $\rho_T^{\pm}$

$$\hat{\sigma}_{ij}^{\pm}(h_1,h_2)=2(1-h_1)(1+h_2)g_{W\rho_T}^2\,\frac{\pi^2\alpha}{3x_w}\,\delta(M^2-m_{\rho_T}^2)|D_W|^2\,, \tag{7.5}$$

where m_{ρ_T} is the mass of the techni-rho and

$$(g_{\gamma\rho_T}, g_{Z\rho_T}, g_{W\rho_T})=\frac{m_{\rho_T}^2}{g_{\rho\pi\pi}}\left(1, \frac{1-2x_w}{2x_w^{1/2}(1-x_w)^{1/2}}, \frac{1}{2x_w^{1/2}}\right). \tag{7.6}$$

The normalization of these couplings by $m_{\rho_T}^2/g_{\rho\pi\pi}$ is only relevant for the calculation of the production

cross sections and here we have used vector dominance with the natural assumption that the usual coupling $\rho\pi\pi$ is the same for the corresponding technimesons. Production rates in the case of unpolarized beams have been given in EHLQ; from ρ_T^0 ($\rho_T^\pm$) one expects a small enhancement of the W^+W^- ($W^\pm Z$) cross section in a kinematic region where the standard rate is only a few hundred events per year at the SSC. Polarized beams might then help to extract a convincing signal. For example, it allows one to distinguish the production of a neutral Higgs, $H^0 \to W^\pm W^-$, which has $A_L = 0$ (see section 5), from that of a neutral techni-rho, $\rho_T^0 \to W^+W^-$, for which A_L is not zero. For $\rho_T^\pm$ production, as a consequence of eq. (7.5), A_L is given by the universal curves $a_L^\pm(m_{\rho_T})$ (see fig. 5.7) and for ρ_T^0, by comparing eq. (7.6) and eq. (6.4), we see that A_L can be read off from fig. 6.1 with $M = m_{\rho_T}$. All these asymmetries are sizeable in the mass range of interest here, that is, above $1\,\mathrm{TeV}/c^2$. They are mainly related to m_{ρ_T} but not directly sensitive to the value of Λ_{TC}.

This minimal technicolor mechanism has been extended in order to generate also mass terms for leptons and quarks. This is done by assuming the existence of a larger gauge group G_{ETC} containing G_{TC} involving gauge bosons which couple leptons and quarks to technifermions. The resulting lepton and quark masses are then of the order of

$$m = \Lambda_{TC}^3/\Lambda_{ETC}^2 , \tag{7.7}$$

and to generate all mass terms the chiral flavor group must be rather large. In the Farhi–Susskind model [FAR79] one starts with the symmetry $SU(8)_L \otimes SU(8)_R \otimes U(1)_V$, which is spontaneously broken down to $SU(8)_V \otimes U(1)_V$ leading to $8^2 - 1$ massless technipions. There are 32 color-octet quark–antiquark bound states P_8^+, P_8^0, P_8^- and $P_8^{0'}$, 24 color-triplet quark–lepton bound states P_3 sometimes called leptoquarks, and 7 color singlets of which three ($\pi_T^+, \pi_T^0, \pi_T^-$) become the $W^\pm$, Z^0 longitudinal states, the remaining four being denoted P^+, P^0, P^- and $P^{0'}$. Except for the π_T's, all these states should then acquire small masses (as compared to Λ_{TC}) from radiative correction effects of electroweak, strong and ETC interactions. Initially it was expected that they could be light enough so that they could be observed at PEP or PETRA energies. Present lower limits [ADE85] are now of the order of $20\,\mathrm{GeV}/c^2$, still consistent with ETC models. In fact, one of the serious problem of ETC models is the prediction of unacceptably large flavor changing neutral currents and so far attempts to cure this difficulty led to modify the model in a rather unrealistic way.

From a purely phenomenological point of view one may still assume that this is solved and that it is worthwhile to search for such technipion states. A detailed review of the production processes has been given by EHLQ (see also [EIC86]). For single production of technipions the most important process is the production of the neutral technipions $P^{0'}$ and $P_8^{0'}$ via gluon–gluon fusion. Pair production of color-triplet or octet technipions can occur through both quark–antiquark annihilation and two-gluon fusion, the second process being dominant. In all these cases parity is conserved so there is no single helicity asymmetry and the double helicity asymmetries are small due to the smallness of the gluon polarization (see figs. 3.7a and b). However, color-singlet charged technipions can be produced in pairs P^+P^- by the Drell–Yan mechanism and in this case there is a single helicity asymmetry, which is the same as for charged Higgs (see fig. 6.1) regardless of the mass of these $P^\pm$ objects.

7.2. Composite $W^\pm$ and Z bosons

7.2.1. Anomalous magnetic moments

Compositeness of W, Z bosons could manifest itself through several types of anomalous properties (mass shifts, form factors, anomalous couplings of various kinds and existence of composite partners

and excited states). One class of anomalous couplings which has received much attention is the one concerning the vector boson trilinear couplings γW^+W^- and ZW^+W^- (and also the four-linear couplings, which we will not discuss here). In the general case one expects [GAE79] ten different types of trilinear couplings to exist; restricting ourselves to *CP* conservation and to pure spin-one currents, the only ones that can contribute in processes involving light leptons and quarks (for the case of heavy quarks see [CHA87]) leaves only four types of couplings. For simplicity we will also restrict ourselves to dimension-four, parity and charge conjugation conserving terms (the most conservative cases of departure from the standard situation), which means two types of couplings, the charge one and the magnetic one. For γW^+W^-, the charged coupling constant is fixed to e, and the magnetic moment κ_γ is left free. For ZW^+W^- both the charge coupling constant g_Z and the magnetic moment κ_Z are a priori left free. In the standard case $g_Z = \cot g\, \theta_w$ and $\kappa_\gamma = \kappa_Z = 1$. In a purely phenomenological way one can vary these three parameters independently and observe the effect on various experimental observables with unpolarized beams [BRO79a]. As soon as one departs from the standard values of the coupling constants, one observes an increase in the cross section as a consequence of the loss of the cancelations among the various diagrams, a typical feature of the standard gauge model. In general the single helicity asymmetry is also affected by such departures as we will see now in some detail[1]. The subprocess cross section $q_i(h_1)\bar{q}_i(h_2) \to W^+W^-$ was given in section 5.3.4. Clearly the exchange contribution e is unchanged but a_i, a_i' and i_i are generalized as follows. For the annihilation terms we have now

$$a_i = e_i^2 f_A(\kappa_\gamma, \kappa_\gamma) + 2e_i a_i g_Z f_A(\kappa_\gamma, \kappa_Z) M^2 \,\mathrm{Re}\, D_Z + (a_i^2 + b_i^2) g_Z^2 f_A(\kappa_Z, \kappa_Z) M^4 |D_Z|^2 , \tag{7.8}$$

$$a_i' = 2e_i b_i g_Z f_A(\kappa_\gamma, \kappa_Z) M^2 \,\mathrm{Re}\, D_Z + 2a_i b_i g_Z^2 f_A(\kappa_Z, \kappa_Z) M^4 |D_Z|^2 , \tag{7.9}$$

with

$$f_A(\kappa_a, \kappa_b) = \beta^3 \left(\frac{\kappa_a \kappa_b}{3\varepsilon^2} + \left[\tfrac{1}{3}(1 + \kappa_a \kappa_b) + \tfrac{1}{2}(\kappa_a + \kappa_b) \right] \frac{1}{\varepsilon} + \frac{1}{4} \right), \quad a, b = \gamma, Z .$$

The interference term becomes

$$i_i = \frac{\pm 1}{4x_w} \left[e_i f_I(\kappa_\gamma) + g_Z (a_i + b_i) M^2 \,\mathrm{Re}\, D_Z \, f_I(\kappa_Z) \right], \tag{7.10}$$

with

$$f_I(\kappa_a) = \beta \left(\frac{2}{3} \frac{\kappa_a}{\varepsilon^2} + \frac{5 + 4\kappa_a}{3\varepsilon} - \kappa_a - \tfrac{1}{6} - \tfrac{1}{4}\varepsilon \right) - \varepsilon \left[\tfrac{1}{2}(1 + \kappa_a) + \tfrac{1}{8}\varepsilon \right] \ln \frac{1 + \beta}{1 - \beta}, \quad a = \gamma, Z .$$

We have assumed no rapidity cut for these expressions but they are given with a rapidity cut in appendix C. Then we can calculate N_i and K_i from eqs. (5.30) and (5.31) and use eq. (5.8) to obtain A_L. In the standard case, as explained in section 5.3.4, for $M^2 \gg M_W^2$, i.e. $\varepsilon \ll 1$, the $\gamma + Z$ conspiracy leads to a W^3 amplitude with purely left couplings to the initial quarks, so $N_i \sim K_i$ and the subprocess asymmetry $\hat{a}_L$ is almost 100%. This is also the case if $g_Z = (\kappa_\gamma/\kappa_Z) \cot g\, \theta_w$ for any κ_γ and κ_Z. The standard A_L for W^+W^- pair production is recalled in fig. 7.1a at $\sqrt{s} = 10$ and 40 TeV together with the

[1] Another way to test the structure of the trilinear couplings and possible deviations from the Standard Model is to measure the angular distribution of the density matrix elements of the gauge bosons [CHA88].

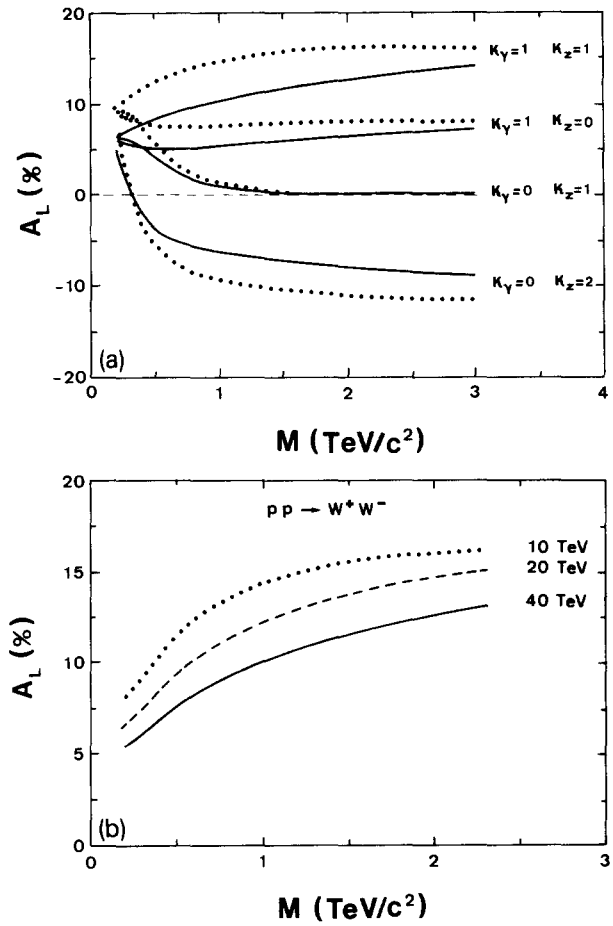

Fig. 7.1. (a) A_L in $pp \to W^+W^-$ versus M, the invariant mass of the pair, for different values of κ_γ and κ_Z, at $\sqrt{s} = 10$ TeV (dotted curves) and $\sqrt{s} = 40$ TeV (solid curves). (b) A_L in $pp \to W^+W^-$ versus M with the constraints (7.11) and $\kappa_\gamma = 2$ at three different energies.

results obtained using arbitrary values of κ_γ and κ_Z and holding $g_Z = \text{cotg}\,\theta_w$. We see that the measurement of A_L appears to be an interesting way to discriminate among several possibilities with anomalous magnetic moments. However, there exists a special class of models [KUR87, NEU87] characterized by specific constraints among κ_γ, κ_Z and g_Z. The following constraints:

$$g_Z = \frac{\kappa_\gamma - x_w}{x_w^{1/2}(1-x_w)^{1/2}}, \qquad \kappa_Z = \frac{\kappa_\gamma(1-x_w)}{\kappa_\gamma - x_w}, \tag{7.11}$$

were introduced in [NEU87] in order to kill the Λ^4 divergent behavior[2] of the boson loop contribution to the W, Z mass shifts, when anomalous couplings are considered. For $M^2 \gg M_W^2$ these constraints preserve approximately the purely left $\gamma + Z$ combination; therefore A_L stands very close to the standard value although the cross section is strongly modified. For illustration we show in fig. 7.1b the

[2] Λ is the ultraviolet cut-off interpreted as the mass scale at which new physical phenomena set in.

result corresponding to $\kappa_\gamma = 2$, giving $\kappa_Z = 0.876$ and $g_Z = 4.297$. By comparison with fig. 5.9 we see that A_L is very much the same for M above 1 TeV/c^2, but for low M the Z propagator effect breaks the $\gamma + Z$ conspiracy and A_L differs from the standard result.

7.2.2. Contact terms in W^+W^- production

Another possible consequence of the composite nature of $W^\pm$, Z bosons is the appearance of residual interaction terms (for example due to subconstituent rearrangements) in the process $q\bar{q} \to VV$ where V stands for a vector boson. Such effects have been studied in detail for the case $e^+e^- \to VV$ [MER87, MER88]. Here we will only illustrate the possibility of a residual term involving longitudinal vector boson states, which would be a strong signal in favor of anomalous dynamics in the vector boson sector (and not in the quark sector). Taking for definiteness the residual amplitude[3)]

$$R_{fi}^{(4)} = \frac{g^2}{\Lambda^4}\,\bar{v}(\bar{q})\,\frac{\not{p}' - \not{p}}{2}\,(c - d\gamma_5)u(q)\,\varepsilon' \cdot p\,\varepsilon \cdot p'\,, \tag{7.12}$$

with the chirality structure $c - d\gamma_5$ normalized to $c^2 + d^2 = 1$ and the effective compositeness scale Λ. g^2 is usually taken to be $g^2 = 4\pi$, p and ε (p' and ε') being the momentum and polarization vector of the W^+ (W^-). The subprocess cross section $q_i(h_1)\bar{q}_i(h_2) \to W^+W^-$ has now the following expression:

$$\hat{\sigma}_i(h_1, h_2) = \hat{\sigma}_i^{sm}(h_1, h_2) + \hat{\sigma}_i^{ct}(h_1, h_2)\,, \tag{7.13}$$

where $\hat{\sigma}_i^{sm}(h_1, h_2)$ is the standard integrated cross section given by eq. (5.31) and $\hat{\sigma}_i^{ct}(h_1, h_2)$ is the contact term integrated cross section, which reads

$$\begin{aligned}\hat{\sigma}_i^{ct}(h_1, h_2) = \frac{4\pi\alpha^2}{\hat{s}}\,\beta\Big(&[(1 - h_1h_2)(c^2 + d^2) + 2cd(h_2 - h_1)]C_4 \\ &+ (1 - h_1h_2)[(a_ic + b_id)C_{34}^Z + e_icC_{34}^\gamma] + (h_2 - h_1)[(a_id + b_ic)C_{34}^Z + e_idC_{34}^\gamma] \\ &+ \frac{1}{4x_w}\,(1 - h_1h_2 + h_2 - h_1)(c + d)C_{E4}\Big)\,.\end{aligned} \tag{7.14}$$

The coefficients C_4, C_{34}^γ, C_{34}^Z and C_{E4} are given in appendix D with a rapidity cut, but here one has to take them with $z_0 = 1$ since there is no rapidity cut in eq. (7.14). We show in figs. 7.2a and 7.2b at $\sqrt{s} = 40$ TeV the sensitivity of A_L to the choice of Λ and to the chirality structure of the interaction. Pure vector ($c = 1$, $d = 0$) and pure axial ($c = 0$, $d = 1$) lead to the same A_L as shown in fig. 7.2a, and when Λ increases departure from the standard $A_L(\Lambda = \infty)$ to $A_L = 0$ occurs for larger values of the invariant mass of the pair. Figure 7.2b shows the case of a right-handed interaction ($c = -d$). Clearly if the contact interaction is left-handed we do not expect any serious difference with the standard A_L. The results at $\sqrt{s} = 10$ and 20 TeV have the same trend with a slightly larger magnitude.

A similar study of contact terms for other gauge boson pair production processes could be done and, for example, the effects on the cross section in γZ^0 production have been reported in [RYZ87, KNE87].

[3)] Note that from dimensional arguments we have the fourth power of the scale as compared to the second power in the four-fermion case [see below eq. (7.17)].

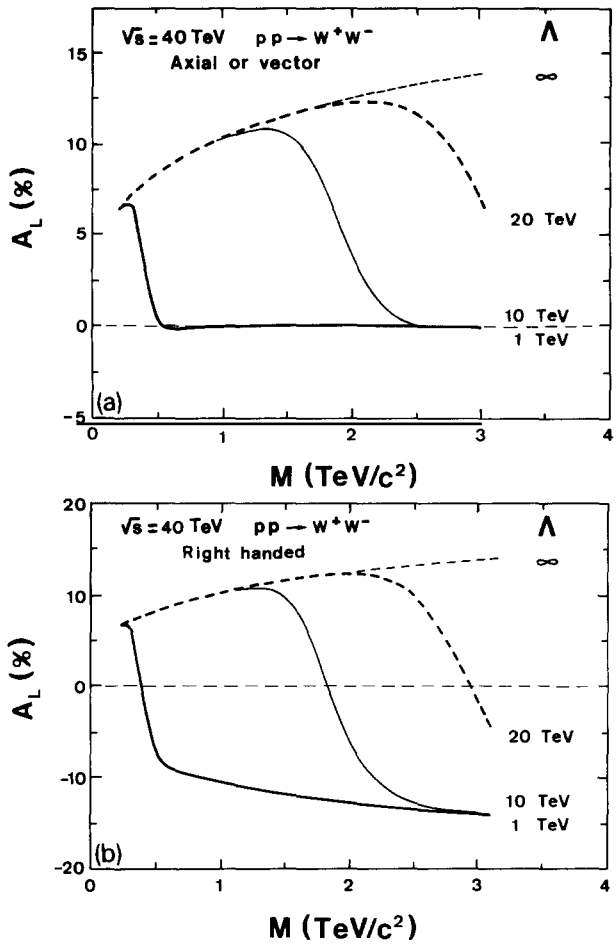

Fig. 7.2. A_L in $pp \to W^+W^-$ versus M at $\sqrt{s} = 40$ TeV, (a) with different values of the (axial or vector) contact interaction scale Λ, (b) with different values of the (right-handed) contact interaction scale Λ.

7.2.3. *Y and Z* bosons*

In composite models, by simple analogy with the known hadron spectrum it is natural to expect besides the isovector triplet W^+, W^-, W^3, a weak isoscalar vector boson Y. Phenomenological consequences associated to the existence of such a new state have been studied in [KUR85] for e^+e^- collisions at LEP or SLC. We would like to describe some implications in pp collisions with polarized beams at much higher energies. The Y boson can be produced by $q\bar{q}$ annihilation through the Drell–Yan mechanism and once more we will see that A_L provides a direct measurement of the $Yq\bar{q}$ couplings. Following [KUR85] we will assume that the Y boson couples to quarks according to two different models, either the isoscalar couples to the full hypercharge current (model A) or it couples to its left-handed part only (model B), in analogy with the left-handed isovector. However, these basic properties, in both cases, are spoiled by the mixing between the photon and the weak bosons in the same way as the W^3–γ mixing produces the Z boson with left- and right-handed couplings depending on Q_f and $\sin^2\theta_w$. The physical $Yq\bar{q}$ couplings now depend on additional mixing parameters and their general expressions are given in [KUR85, BAU87]. In the absence of a precise quantitative prediction

for the mixing we will consider two extreme cases [BAU86] with either weak or strong mixing. In the weak mixing case we have

$$a_i = g_Y(e_i - \tfrac{1}{2}I_i^3)\,, \qquad b_i = -g_Y I_i^3/2 \quad \text{(model A)}\,, \tag{7.15a}$$

$$a_i = b_i = \tfrac{1}{2} g_Y(e_i - I_i^3) \quad \text{(model B)}\,, \tag{7.15b}$$

where g_Y is the basic weak hypercharge coupling constant and I_i^3 is the third component of the quark isospin. We will refer to the choices of eqs. (7.15a) and (7.15b) as model 1 and model 2, respectively. The value of g_Y determines the size of the production rate. Assuming a similar strength for the weak isovector and hypercharge couplings, one estimates at the SSC the number of events per year in e^+e^- decay mode to be of the order of 10^6 for $M_Y = 0.5\,\text{TeV}/c^2$ [BAU86]. The corresponding asymmetry A_L is given by eq. (5.16) with M_Z replaced by M_Y, and by using eqs. (7.15a, b) we obtain the results displayed in figs. 7.3a, b. Clearly A_L is independent of g_Y and for model 1 it is negative and large whereas for model 2 it is positive and has the typical behavior of a purely left-handed object. For high

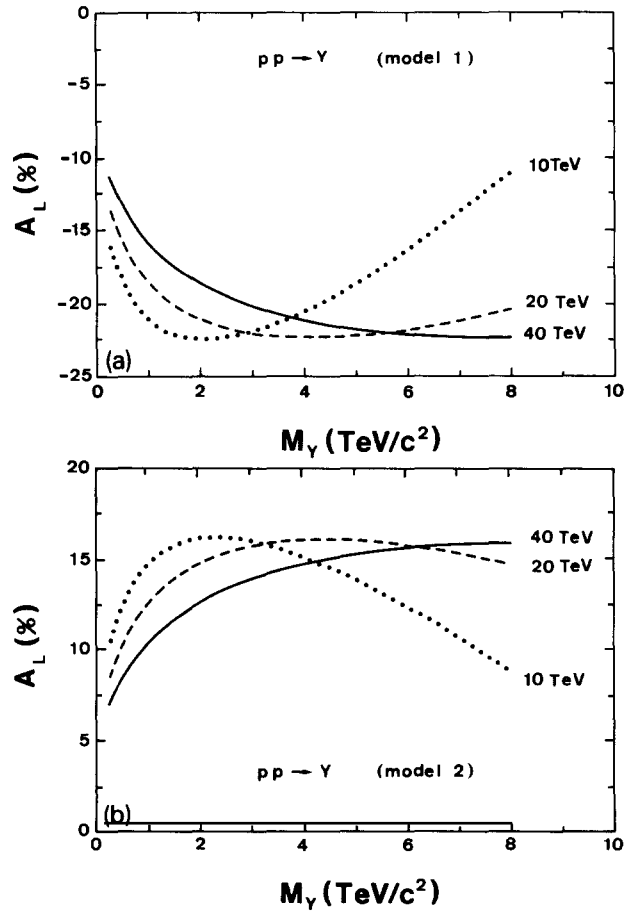

Fig. 7.3. A_L in pp→Y versus M_Y (a) for model 1, (b) for model 2 (see text) at three different energies.

M_Y at $\sqrt{s} = 10\,\text{TeV}$ the magnitude of A_L decreases in both cases due to the effect of the d-quark polarization. In the strong mixing case Y decouples in model A and becomes purely right-handed in model B, where we have

$$a_i = -b_i = -\tfrac{1}{2} g_Y e_i \,. \tag{7.16}$$

The result for A_L is similar to that of model 1.

In the case of an excited weak boson [BAU87a] one starts with a triplet of excited W* coupled to left-handed fermion doublets with a specific coupling constant g'_W. Again this purely left structure is spoiled by the W^3–W^{*3}–γ mixing leading to the physical Z* with left- and right-handed couplings depending on ratio g'_W/g_W as well as on a new mixing parameter λ'_W. So a priori it seems difficult to predict the typical chiral structure $\gamma^\mu(c - d\gamma^5)$ for the Z* couplings to $q\bar{q}$ states. For these reasons we restrict our illustration to large values of M_{Z^*}, say above $1\,\text{TeV}/c^2$, for which the mixing is expected to be small [BAU87a]. In this case one has to deal with a purely left-handed object, so the asymmetry A_L will be similar to the above model 2 (see fig. 7.3b). Therefore A_L allows a distinction between such an excited boson Z* and, for example, a new gauge boson Z′ as considered in section 6 (see fig. 6.3a). The measurement of A_L gives valuable information on the $q\bar{q}$ couplings to new objects and thus constitutes a severe test for current models.

7.3. Composite quarks and leptons

The composite nature of quarks and leptons could reveal itself through anomalous properties in a way very similar to those mentioned above in the case of $W^\pm$, Z bosons (anomalous magnetic $(g-2)$ or electric dipole moments, form factors, residual interactions) as well as through the discovery of new states (excited leptons or quarks, exotic states like colored leptons) which cannot be assigned to any standard multiplet.

Many lower limits have already been given for effective scales or masses of new states from various sources, in particular the value of the electron or muon $(g-2)$, the absence of flavor changing neutral currents (FCNC) like $\mu \to e\gamma$, the absence of a departure from standard predictions for e^+e^- and qq collisions, and the absence of a signal for any new state. Expectations of new limits accessible at SLC, LEP or HERA have also been obtained [TRE87, RÜC87]. It appears that there is still much room for improving these limits in a very fruitful way at pp supercolliders. Only special constraints have appeared to be required in a quasi-unavoidable way. FCNC seem to be forbidden up to very high scales (10^3 TeV), thus already setting important restrictions on subconstituent dynamics. Chirality plays a very important role in the magnitude of the lower limits obtained for the effective scales, for example, in $(g-2)$ factors, in $\mu \to e\gamma$ or in the search for excited leptons. The less model dependent limits on a possible non-zero extension of quarks and leptons come from the search of four-fermion residual interaction terms. At pp colliders one will have access to (qqqq) and $(qq\ell\ell)$ contact terms giving deviations from standard predictions for lepton pair, direct photon and hadronic jet production, which we will examine in turn. We will emphasize the advantages of polarized beams as was already pointed out in [ALB84].

7.3.1. Lepton pair production

If leptons and light quarks have common constituents, contact interactions will modify lepton pair production. Under this assumption we will add to the usual amplitude describing $q_i(h_1)\bar{q}_i(h_2) \to \ell^+\ell^-$,

the four-fermion residual amplitude[4)]

$$R_{\rm if}^{(4)} = (\pm)\,\frac{g^2}{4\Lambda^2}\,\bar{v}(\ell^+)\gamma^\mu(1-\eta\gamma_5)u(\ell^-)\bar{u}(q)\gamma_\mu(1-\eta'\gamma_5)v(\bar{q})\,, \tag{7.17}$$

and since the chirality structure is not known we will consider two extreme cases: $\eta=\eta'=1$ left–left (LL) coupling and $\eta=\eta'=-1$ right–right (RR) coupling. The integrated cross section reads as eq. (5.6) with

$$K_i = K_i^{\rm sm} + K_i^{\rm ct}\,, \qquad N_i = N_i^{\rm sm} + N_i^{\rm ct}\,, \tag{7.18}$$

where $K_i^{\rm sm}$ and $N_i^{\rm sm}$ are the Standard Model K_i and N_i given by eqs. (5.3) and (5.7), and

$$K_i^{\rm ct} = 2M^2C[-e_i + (a_\ell + b_\ell\eta')(a_i + b_i\eta)M^2\,{\rm Re}\,D_{\rm Z} + 2M^2C]\,, \qquad N_i^{\rm ct} = \eta K_i^{\rm ct}\,; \tag{7.19}$$

with $g^2 = 4\pi$ one has $C = 1/4\alpha\Lambda^2$.

Modifications in the lepton pair cross section due to this new interaction have been reported in [CHI88] and EHLQ and, for example, if the compositeness scale Λ is of the order of 10 TeV, then for a pair mass $M = 2\,{\rm TeV}/c^2$ the event rate at $\sqrt{s} = 40$ TeV is a factor four higher than the Standard Model rate. The single helicity asymmetry obtained from eq. (5.8) will be also strongly modified with respect to the standard model result (see fig. 5.1). The results for $A_{\rm L}$ are given in figs. 7.4a and b at $\sqrt{s} = 40$ TeV for different values of Λ. Here one important remark is in order. From the simple relation between $N_i^{\rm ct}$ and $K_i^{\rm ct}$ in eq. (7.19) we see that RR (LL) coupling will mimic a purely right- (left-) handed interaction producing the lepton pair. As a result, for small $\Lambda_{\rm RR}$, i.e. 1 TeV, which is probably not very realistic at SSC, the contact interaction dominates at large M and we recover the universal result of a purely right-handed interaction (see, for example, $\Lambda = 1$ TeV in fig. 7.2b) and similarly for small $\Lambda_{\rm LL}$ the universal result of a purely left-handed interaction (see, for example, $\Lambda = \infty$ in fig. 7.2b). For very large values of $\Lambda_{\rm RR}$ or $\Lambda_{\rm LL}$, $A_{\rm L}$ tends to the Standard Model result.

7.3.2. Direct photon production

Direct photon production at high $p_{\rm T}$ is also an interesting probe for the presence of subconstituents and the sensitivity of the cross section at the SSC, which has been investigated in [OWE84], shows that one can get access to compositeness scales of about 5 TeV. As we recalled in section 4, direct photons are produced via quark–antiquark annihilation and quark–gluon Compton scattering. In the presence of contact terms, the amplitude for $q_i(h_1)\bar{q}_i(h_2)\to g\gamma$ can be written as (see appendix E)

$$R_i(A) = R_i^{\rm sm}(A)\left(1 + \frac{\hat{u}\hat{t}}{2e_i\Lambda^4}\,(c - d\gamma_5)\right), \tag{7.20}$$

where $R_i^{\rm sm}(A)$ is the Standard Model annihilation amplitude, and the cross section becomes

[4)] The relative sign of this amplitude with respect to the standard one is unknown and + (−) refers to destructive (constructive) interference. We will take the + sign.

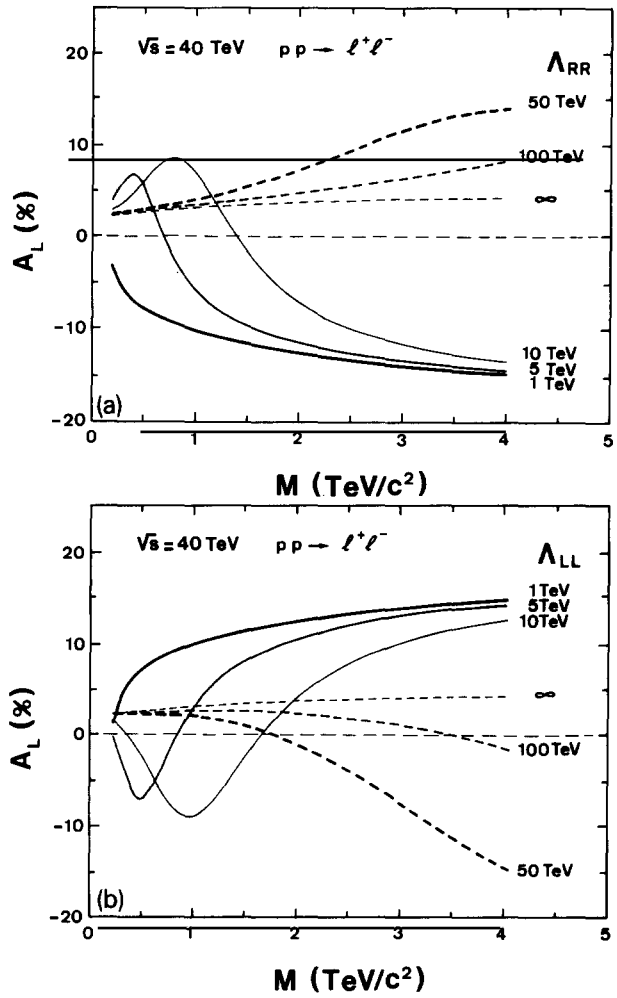

Fig. 7.4. A_L in $pp \to \ell^+\ell^-$ versus M at $\sqrt{s} = 40$ TeV with different values of (a) the right–right contact interaction scale Λ_{RR}, (b) the left–left contact interaction scale Λ_{LL}.

$$\frac{d\hat{\sigma}_i}{d\hat{t}}(h_1, h_2) = \frac{8\pi e_i^2 \alpha\alpha_s}{9\hat{s}^2}(\hat{u}/\hat{t} + \hat{t}/\hat{u})[(1 - h_1h_2)(C_i^2 + D_i^2) + 2(h_2 - h_1)C_iD_i], \tag{7.21}$$

$$C_i = 1 + \hat{u}\hat{t}c/2e_i\Lambda^4, \quad D_i = \hat{u}\hat{t}d/2e_i\Lambda^4.$$

For quark–gluon Compton scattering $q_i(h)g(\lambda) \to q_i\gamma$ by crossing symmetry ($\hat{s} \leftrightarrow \hat{t}$) we have

$$R_i(C) = R_i^{sm}(C)\left(1 + \frac{\hat{u}\hat{s}}{2e_i\Lambda^4}(c - d\gamma_5)\right), \tag{7.22}$$

and the cross section reads

$$\frac{d\hat{\sigma}_i}{d\hat{t}}(h,\lambda)=\frac{\pi e_i^2\alpha\alpha_s}{3\hat{u}\hat{s}^3}\{(\hat{u}^2+\hat{s}^2)(C_i^2+D_i^2-2C_iD_ih)-\lambda(\hat{u}^2-\hat{s}^2)[(C_i^2+D_i^2)h-2C_iD_i]\}\,. \quad (7.23)$$

For $\bar{q}_i(h)g(\lambda)\to\bar{q}_i\gamma$ the same formula holds but with $h\to -h$ and $\lambda\to -\lambda$. We recover the Standard Model results given in table 4.1 for $\Lambda=\infty$. Here also the chirality structure is arbitrary and for illustration we will take a left-handed interaction $c=d=1/\sqrt{2}$. The resulting A_L are shown in figs. 7.5a and b at $\sqrt{s}=10$ and 40 TeV versus p_T for different values of Λ. As usual the effect is larger in magnitude at $\sqrt{s}=10$ TeV and except for $\Lambda=1$ TeV, which is not very realistic, a clean signal is present up to $\Lambda=10$ TeV or so, whereas A_L vanishes for $\Lambda=\infty$. A_L changes sign with a right-handed contact interaction since $d\to -d$.

7.3.3. *Hadronic jet production*

High-p_T jet production can also give signals for compositeness and the influence of a contact interaction in quark–quark scattering producing an additional yield in the p_T distribution of a single outgoing jet has been studied in EHLQ and also in [BAR86]. It was shown that compositeness

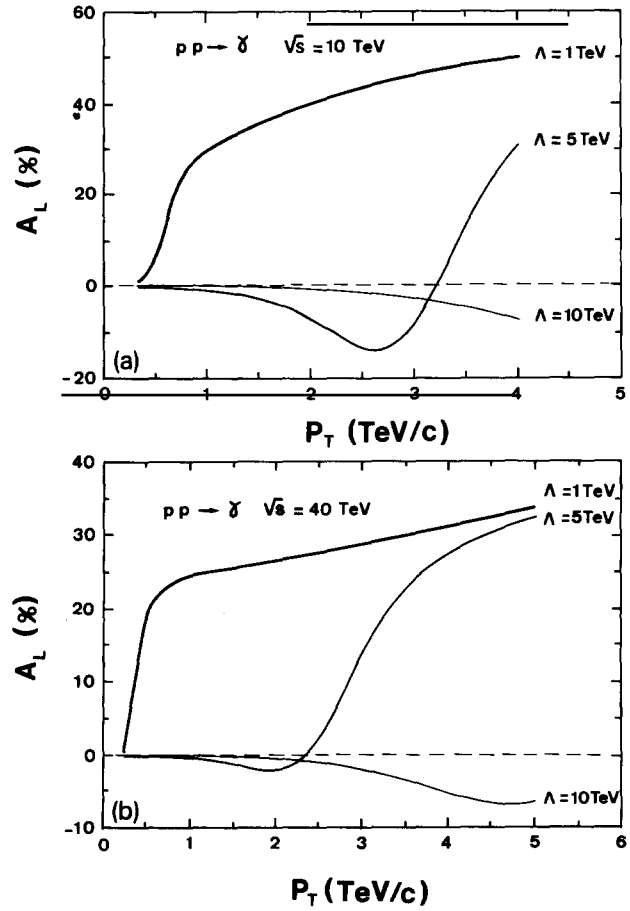

Fig. 7.5. A_L in $pp\to\gamma$ versus p_T (a) at $\sqrt{s}=10$ TeV, (b) at $\sqrt{s}=40$ TeV, with different values of the left-handed contact interaction scale Λ.

dominates over other exotic physics at the SSC, which may be sensitive to a compositeness scale as large as 20 TeV. Here we will examine this influence on the single helicity asymmetry, which is zero in the Standard Model (see section 4). The four-fermion residual amplitude is analogous to that used above for lepton pair production [see eq. (7.17)] and we assume a common axial coupling constant η. The differential cross section for quark–quark scattering now takes the form

$$\frac{\mathrm{d}\hat{\sigma}_i}{\mathrm{d}\hat{t}}(h_1, h_2) = \frac{\pi\alpha_s^2}{\hat{s}^2}\left[(1-h_1h_2)X_1 + (h_2-h_1)X_2 + (1+h_1h_2)X_1' + (h_2+h_1)X_2'\right], \tag{7.24}$$

and we have listed in table 7.1, where we should use $C = 1/\alpha_s\Lambda^2$, the expression of the X_i for the seven different processes[5]. Clearly for $\Lambda = \infty$ we recover the standard results given in table 4.1. The single-jet p_T distribution is obtained from eq. (4.1), whose explicit use allows the calculation of A_L, which is shown in figs. 7.6a and b at $y = 0$ for $\sqrt{s} = 40$ and 10 TeV. We have taken a left-handed contact interaction ($\eta = +1$) and the solid curves correspond to three values of Λ.

As we have seen in section 4, quark–quark scattering dominates jet production only at large p_T and a substantial part of the cross section comes from $gg \to gg$ and $gq \to gq$ scattering. Gluons are considered as elementary so there is no contact interaction in $gg \to gg$, but this is not the case for $gq \to gq$ or $gg \to q\bar{q}$. These last two contributions, which were ignored in EHLQ, have been calculated here[6]. Due to dimensional arguments, since we have two boson and two fermion fields, the residual amplitude goes like Λ^{-4} and the effects should die off faster than for $qq \to qq$ when Λ gets larger. The effect from $gg \to q\bar{q}$ on A_L is negligible and the effect of $qg \to gq$ is important only at $\sqrt{s} = 40$ TeV for Λ of the order of 1 TeV or so (see fig. 7.6a). At 10 TeV, to see an effect one should take Λ smaller than 250 GeV.

Table 7.1
List of the coefficients X_i entering in the cross section eq. (7.24) for various processes

	X_1	X_1'	X_2	X_2'
$q_i\bar{q}_j \to q_i\bar{q}_j$	$\frac{4}{9}\frac{\hat{u}^2}{\hat{t}^2} + \hat{u}^2C^2$	$\frac{4}{9}\frac{\hat{s}^2}{\hat{t}^2}$	$\hat{u}^2\eta C^2$	0
$q_iq_j \to q_iq_j$	$\frac{4}{9}\frac{\hat{u}^2}{\hat{t}^2}$	$\frac{4}{9}\frac{\hat{s}^2}{\hat{t}^2} + \hat{s}^2C^2$	0	$\hat{s}^2\eta C^2$
$\bar{q}_i\bar{q}_j \to \bar{q}_i\bar{q}_j$	$\frac{4}{9}\frac{\hat{u}^2}{\hat{t}^2}$	$\frac{4}{9}\frac{\hat{s}^2}{\hat{t}^2} + \hat{s}^2C^2$	0	$\hat{s}^2\eta C^2$
$q_iq_i \to q_iq_i$	$\frac{4}{9}\left(\frac{\hat{u}^2}{\hat{t}^2} + \frac{\hat{t}^2}{\hat{u}^2}\right)$	$\frac{4}{9}\left[\hat{s}^2\left(\frac{1}{\hat{t}^2} + \frac{1}{\hat{u}^2}\right) - \frac{2}{3}\frac{\hat{s}^2}{\hat{u}\hat{t}}\right] + \frac{8}{3}\hat{s}^2C^2$	0	$-\frac{8}{3}\hat{s}^2\left(\frac{1}{\hat{t}} + \frac{1}{\hat{u}}\right)\eta C - \frac{8}{3}\hat{s}^2\eta C^2$
$\bar{q}_i\bar{q}_i \to \bar{q}_i\bar{q}_i$	$\frac{4}{9}\left(\frac{\hat{u}^2}{\hat{t}^2} + \frac{\hat{t}^2}{\hat{u}^2}\right)$	$\frac{4}{9}\left[\hat{s}^2\left(\frac{1}{\hat{t}^2} + \frac{1}{\hat{u}^2}\right) - \frac{2}{3}\frac{\hat{s}^2}{\hat{u}\hat{t}}\right] + \frac{8}{3}\hat{s}^2C^2$	0	$+\frac{8}{3}\hat{s}^2\left(\frac{1}{\hat{t}} + \frac{1}{\hat{u}}\right)\eta C + \frac{8}{3}\hat{s}^2\eta C^2$
$q_i\bar{q}_i \to q_i\bar{q}_i$	$\frac{4}{9}\left(\frac{\hat{u}^2+\hat{t}^2}{\hat{s}^2} + \frac{\hat{u}^2}{\hat{t}^2} - \frac{2}{3}\frac{\hat{u}^2}{\hat{s}\hat{t}}\right) + \frac{8}{3}\hat{u}^2\left(\frac{1}{\hat{s}} + \frac{1}{\hat{t}}\right)C$	$\frac{4}{9}\frac{\hat{s}^2}{\hat{t}^2}$	$\frac{8}{3}\hat{u}^2\left(\frac{1}{\hat{s}} + \frac{1}{\hat{t}}\right)\eta C + \frac{8}{3}\hat{u}^2\eta C^2$	0
$q_i\bar{q}_i \to q_j\bar{q}_j$	$\frac{4}{9}\frac{\hat{u}^2+\hat{t}^2}{\hat{s}^2} + 2\hat{u}^2C^2$	0	$2\hat{u}^2\eta C^2$	0

[5] For the unpolarized cross sections given by $X_1 + X_1'$ we disagree with eqs. (8.13) and (8.15) of EHLQ for the C^2 terms, some of which do not satisfy the $\hat{u} \leftrightarrow \hat{t}$ crossing symmetry.

[6] Polarized cross sections are given in appendix E for completeness.

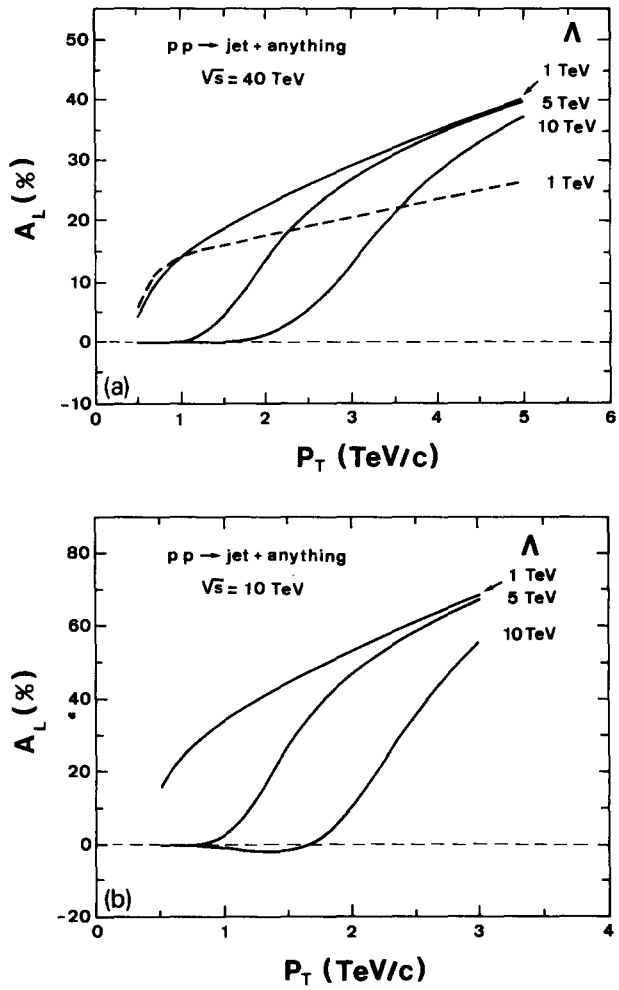

Fig. 7.6. A_L in pp→jet + anything versus p_T (a) at $\sqrt{s} = 40$ TeV, (b) at $\sqrt{s} = 10$ TeV, and $y = 0$ with different values of the left-handed contact interaction scale Λ. The dashed curve in (a) includes $gg \to q\bar{q}$ and $gq \to gq$ contact terms.

We have discussed some deviations to be expected from QCD predictions if quarks and leptons have internal structure with a characteristic size of Λ^{-1}. Although some uncertainties remain in our estimates we believe that polarized beams would increase notably our sensitivity to the manifestation of compositeness.

8. Supersymmetry

The idea of supersymmetric (SUSY) theories was proposed several years ago [GOL71, VOL73, WES74] but has become very popular more recently. Motivations for these theories have been reviewed in many places [FAY77, HAB85, NIL84] and a lot of studies have been devoted to search for supersymmetric particles (sparticles) at present [ELL88] or future hadronic colliders [EIC84, BAR86a,

SAV87, BAT87, MAN87, BAT88] as well as e^+e^- machines [LEP86, DIO87, DIO87a, CHE88]. SUSY implies the existence of partners of ordinary particles which differ from them by half a unit of spin. Thus in any minimal SUSY extension of the Standard Model, one finds scalars $\tilde{\ell}_L$, $\tilde{\ell}_R$ ($\tilde{q}_L, \tilde{q}_R$) associated to each helicity state of a lepton ℓ (or quark q): spin 1/2 gluinos ($\tilde{g}$), photinos ($\tilde{\gamma}$), winos ($\tilde{W}^{\pm}$) and zinos ($\tilde{Z}^0$), the partners of gluons, photons and the electroweak gauge bosons, respectively. Higgsinos are also present, as fermions associated to the two Higgs doublets which are now necessary to give masses to all particles. Experimental lower limits obtained up to now on the masses of these hypothetical sparticles lie in the range of a few tenths of GeV/c^2 (for more precision see [WU87, BAT88]) but these limits are not very relevant for the Supercollider energies considered here. Concerning a possible upper bound, let us just recall that the hope to solve the naturalness or hierarchy problem is a strong motivation to expect sparticles lying below the TeV range. For the experimental detection it is well known that, due to R-parity conservation [FAY75, SAL75], sparticles will be produced in pairs, each sparticle decaying by a cascade to the lightest sparticle (LSP) which is neutral and turns out to be the photino in many phenomenological models. Interacting very weakly with ordinary matter, the LSP will escape detection: this implies that the production of sparticles is always characterized by missing energy–momentum events. In spite of experimental progress, there is no doubt that such events, as in the recent past [HAL85], will remain difficult to interpret. We will see that, as in the case of e^+e^- interactions [CHI85a, CHI85b, SCH85], polarization could help to identify the nature of these events.

8.1. Strongly interacting SUSY particles

Gluinos and squarks should be copiously produced at Supercolliders, even in the case when their masses are quite high [EIC84, DAW85, SAV87, BAT87, BAT88]. For example, with an integrated luminosity of $10^{40}\,\mathrm{cm}^{-2}$, one gets 10^7 gluino pairs at the SSC and ten times less at the LHC for $m_{\tilde{g}} = 400\,\mathrm{GeV}/c^2$. This rate reduces to 10^4 pairs if $m_{\tilde{g}} = 1.5\,\mathrm{TeV}/c^2$ at the SSC or if $m_{\tilde{g}} = 1\,\mathrm{TeV}/c^2$ at the LHC.

In case of direct decay to the LSP, the signatures for squark and gluino production are very similar: multi-jets plus missing transverse momentum. The most important background is due to semileptonic decays of heavy quarks with energetic neutrinos and also $Z^0 \to \nu\bar{\nu}$ decays. Note that, in the case of very massive squarks and gluinos, decays involving winos and zinos tend to dominate if allowed [BAT88].

Since parity is conserved in the production of these new strongly interacting particles, we will only be concerned with double helicity asymmetries A_{LL} as in section 4. For the subprocesses where a pair of sparticles is produced in the final state: $gg \to \tilde{g}\tilde{g}$, $qg \to \tilde{q}\tilde{g}$, $gg \to \tilde{q}\bar{\tilde{q}}$, $qq \to \tilde{q}\tilde{q}$, . . . , the $\hat{a}_{LL}^{ij}$ are -100% in the limit of massless squarks and gluinos [CRA83, CRA83a] due to helicity conservation. This contrasts with the standard case where all the dominant $\hat{a}_{LL}^{ij}$ were *positive* and smaller in magnitude (see section 4). The invariant cross sections and the corresponding A_{LL}, in the case where only one SUSY particle is detected through one jet plus missing energy, can be calculated using eq. (4.1) and the subprocess cross sections, which can be found in EHLQ or in [CRA83]. For illustration, in the case of light sparticles, we display in fig. 8.1 A_{LL} versus p_T, calculated at zero rapidity by adding the dominant $gg \to \tilde{g}\tilde{g}$ and $qg \to \tilde{q}\tilde{g}$ contributions. As expected it is negative and larger in magnitude than in the standard case (see fig. 4.2). For heavier sparticles, using the formulas which can be found in [CRA83], we have checked that this pattern survives mass effects, apart from a slight decrease in magnitude.

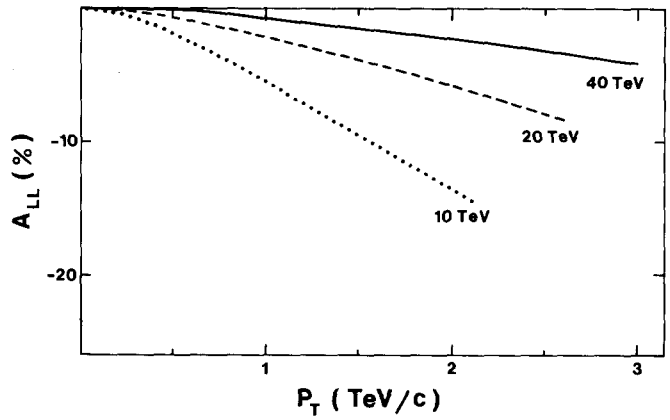

Fig. 8.1. The double helicity hadron asymmetry A_{LL} in the production of one light strongly interacting sparticle at $y = 0$ versus p_T for three different energies.

8.2. Non-strongly interacting SUSY particles

8.2.1. Slepton pair production

The elementary reaction is a simple generalization of the usual Drell–Yan process: $q\bar{q} \to \gamma, Z^0 \to \tilde{\ell}^+\tilde{\ell}^-$. If we assume the decay $\tilde{\ell}^\pm \to \ell^\pm\tilde{\gamma}$, the signature for such events is given by the production of a lepton pair plus missing energy. Production rates can be found, e.g., in EHLQ. The integrated cross section for the production of a $\tilde{\ell}_L^+\tilde{\ell}_L^-$ or $\tilde{\ell}_R^+\tilde{\ell}_R^-$ pair of invariant mass M is given by eq. (5.6) with

$$K_i = \tfrac{1}{4}\beta^3[e_i^2 + 2e_i a_i g_{L,R} M^2 \,\mathrm{Re}\, D_Z + g_{L,R}^2(a_i^2 + b_i^2)M^4|D_Z|^2], \tag{8.1}$$

$$N_i = \tfrac{1}{4}\beta^3[2e_i b_i g_{L,R} M^2 \,\mathrm{Re}\, D_Z + 2a_i b_i g_{L,R}^2 M^4|D_Z|^2], \tag{8.2}$$

where g_L (g_R) is the coupling of the Z^0 to a pair of left-handed (right-handed) sleptons. These couplings are given by

$$g_L = -(a_\ell + b_\ell), \qquad g_R = -(a_\ell - b_\ell), \tag{8.3}$$

with a_ℓ and b_ℓ defined in eq. (5.4), $\beta = (1 - 4m_{\tilde{\ell}}^2/M^2)^{1/2}$ as usual. Note that, for a given process ($\tilde{\ell}_L^+\tilde{\ell}_L^-$ or $\tilde{\ell}_R^+\tilde{\ell}_R^-$), β^3 disappears in the ratio when calculating the single helicity asymmetry, which consequently is independent of the slepton mass. In case of degenerate $\tilde{\ell}_L$ and $\tilde{\ell}_R$, from the above equations it is easy to see that, if we sum the two indistinguishable combinations, we recover the standard A_L for Drell–Yan pairs shown in fig. 5.1. The two different asymmetries for the production of a left-handed *or* right-handed slepton pair are displayed in fig. 8.2. Thus, in case of non-degeneracy, once a signal for scalar leptons is discovered, A_L should allow one to distinguish between left-handed and right-handed pair production.

Another process is $q_i\bar{q}_j \to W^\pm \to \tilde{\ell}^\pm\tilde{\nu}$, where $\tilde{\nu}$ is the scalar partner of the neutrino. Again, since the W is a purely left-handed current, the asymmetries are given by the two universal curves displayed in fig. 5.7.

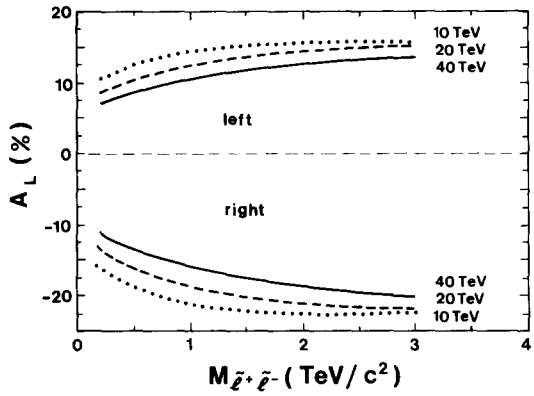

Fig. 8.2. The single helicity asymmetry A_L for pair production of a scalar lepton for three different energies (top curves left-handed, bottom curves right-handed).

8.2.2. Electroweak gauginos

This sector is characterized by a large model dependence, due to the various possible mixings which can occur between pure gaugino and pure higgsino states (charged or neutral). Those mixings are related to the SUSY breaking mechanism (see e.g. [HAB85]), which complicates the issue. Production mechanisms and possible signatures have been reviewed in EHLQ and more detailed investigations have been performed for SSC [DAW84, UKE86] or LHC]MAN87] energies.

The first process we consider is charged wino pair production arising from the subprocess $q\bar{q}\to\tilde{W}^+\tilde{W}^-$ with left-handed squark exchange and annihilation through γ and Z^0. Production rates are typical of an electroweak process (e.g. W^+W^- production) provided the masses are not too high. Moreover, the magnitude of the cross section and decays are very model dependent, according to the possible mixings and also to the spectrum of the other sparticles. Concerning spin effects, as in the standard W^+W^- case, due to the purely left chiral structure of the exchange diagram and due also to the γ–Z^0 conspiracy in the annihilation diagram, the subprocess single spin asymmetry turns out to be almost 100%. Consequently A_L for this process can be read from fig. 5.9 (upper curves), where now M is the invariant mass of the wino pair. For the above reasons, like in the e^+e^- case [CHI85b], A_L is not very sensitive to a particular choice of wino–higgsino mixing. For completeness, and to allow any elaborate estimates taking into account detection cuts, we give in appendix F the polarized differential cross section for this subprocess.

Next processes involving winos are $q_i\bar{q}_j\to\tilde{W}^\pm\tilde{\gamma}$ and $q_i\bar{q}_j\to\tilde{W}^\pm\tilde{Z}^0$. As they go through left-handed squark exchange and annihilation via a $W^\pm$ propagator, each subprocess gives an asymmetry of 100% and the resulting observable asymmetries are given by the universal curves defined in section 5 (see fig. 5.7).

We now turn to the production of a pair of neutralinos $q\bar{q}\to\tilde{\gamma}\tilde{\gamma}$, $\tilde{\gamma}\tilde{Z}$, $\tilde{Z}\tilde{Z}$, which proceeds by left-handed and right-handed squark exchange. Note that one should not forget to antisymmetrize the two diagrams due to the Majorana nature of these neutralinos. Again, rates are model dependent and detection will be rather tedious. In particular the observation of the $\tilde{\gamma}\tilde{\gamma}$ mode seems hopeless. Formulas for differential polarized cross sections can be found in appendix F. For illustration, we display the $\tilde{\gamma}\tilde{Z}$ case in fig. 8.3 for $\sqrt{s} = 10$ TeV; at higher energies A_L is smaller, as usual. Again the choice of zino–neutral higgsino mixing model is not crucial. In the extreme cases where one type of squark is very

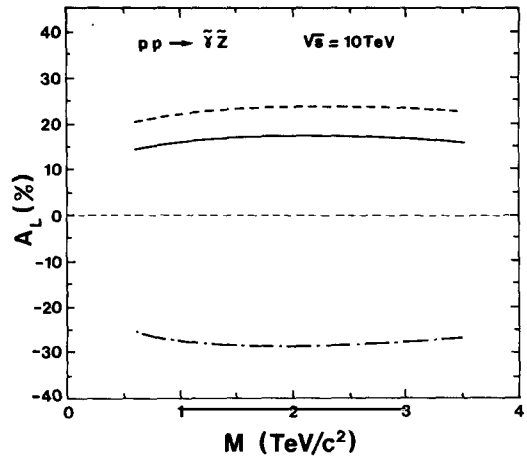

Fig. 8.3. The single helicity asymmetry A_L in $pp \to \tilde{\gamma}\tilde{Z}$ versus M at $\sqrt{s} = 10$ TeV. $m_{\tilde{q}_L} \gg m_{\tilde{q}_R}$ (dashed curve); $m_{\tilde{q}_R} \gg m_{\tilde{q}_L}$ (dashed-dotted curve); $m_{\tilde{q}_R} = m_{\tilde{q}_L}$ (solid curve).

much heavier than the other ($m_{\tilde{q}_L} \gg m_{\tilde{q}_R}$ or $m_{\tilde{q}_R} \gg m_{\tilde{q}_L}$) the subprocess asymmetries take their maximal (positive or negative) values. Then dilution effects give the upper and lower curves shown in fig. 8.3. If now $m_{\tilde{q}_L} = m_{\tilde{q}_R}$ we get the intermediate curve resulting from the weighted zino couplings to $\tilde{q}_L$ and $\tilde{q}_R$ (see appendix F). In the $\tilde{Z}\tilde{Z}$ process, we have the same pattern with smaller absolute magnitudes.

Finally, electroweak gauginos can also be produced in association with a squark or a gluino, like, e.g., in $q_i\bar{q}_j \to \tilde{W}^{\pm}\tilde{g}$ and $qg \to \tilde{W}^{\pm}\tilde{q}$. Indeed, rates for these processes are enhanced roughly by a factor α_s/α. The diagrams are the SUSY analogs of those entering in $W^{\pm}$ + jet production described in section 5. Consequently the asymmetries A_L turn out to be very similar to those shown in fig. 5.6.

9. WW collision processes

A new class of collision processes will be provided by very high energy pp (and also e^+e^- and ep) colliders: quasi-real vector boson–vector boson collisions [CAH84, DAW84a, KAN84, DAW85a, CHA85a, DUN86], where vector boson (V) means W^+, W^-, Z^0 or γ. They generalize the well-known $\gamma\gamma$ collision processes [BUD75] observed at e^+e^- colliders. They will constitute a new tool for exploring the deep properties of electroweak interactions, the true nature of $W^{\pm}$, Z^0 bosons, the origin of gauge symmetry breaking and the still unknown scalar sector. Typical channels to achieve this goal are: vector boson fusion into Higgs, higher vector boson or technimeson, vector boson–vector boson scattering processes and new fermion (or boson) pair production. Several works have already been devoted to V–V collisions at pp supercolliders [SNO86].

The effective vector boson approximation treats the intermediate vector boson as a real parton inside the proton. One starts, with the definition of vector boson distribution functions inside the proton $f_{V/p}(x)$ obtained by convoluting vector boson emission by quarks $f_{V/q}(z)$ with quark distributions inside the proton $q(y)$. One then defines luminosities for V–V collisions as in section 3.2 by convoluting vector boson distributions inside each of the colliding protons. This is done separately for each helicity combination of the V_λ–V_μ pair and invariant mass distributions $d\sigma/d\tau$ for $pp \to X + \cdots$ with $\tau = M_X^2/s$ are then obtained by products of V–V luminosities with cross sections for V_λ–V_μ subprocesses [see eq.

(3.17)]. The validity of this approximation depends on the off-mass-shell behavior of the vector boson dynamics. Several assumptions about its effect have led to different forms for vector boson distributions and luminosities [KAN84, DAW85a, LIN87a, CAP88]. They mainly differ in the low-x, $x = E_V/E_p$, and low-τ regions. An additional uncertainty about these processes comes from the possibility of producing the same final state X without going through V–V collisions or from the presence of a huge background simulating the same configurations. Because of all these features, detailed amplitude analyses will be required in order to extract reliable information about vector boson dynamics. For this purpose beam polarization should be particularly fruitful.

Firstly, monitoring V–V collision processes will certainly be mandatory, i.e., a test of the V–V luminosities to be used for measuring cross sections for subprocesses should be performed. This requires the use of a reaction for which the theoretical uncertainties and the experimental uncertainties are minimized. This may be partly realized by some of the VV→VV scattering processes (like $\gamma W \to \gamma W$, $ZW \to ZW$) where the Higgs boson is absent or negligibly contributing. One may also expect that SLC and LEP will substantially constrain the $W^{\pm}$ and Z properties so that a reasonable prediction can be made for such channels.

Secondly, disentangling of V–V processes from the background and of V–V processes among themselves will be provided by helicity asymmetries, which contain some signature of the type of vector boson (γ, Z, $W^{\pm}$) that is exchanged.

We now give a summary of the description of V–V collisions followed by a few typical examples of polarization effects.

9.1. *Vector boson distributions inside protons*

One first starts by vector boson emission from quark lines, $q_i \to q_j + V$. A helicity decomposition of vector boson exchange diagrams for example in quark–proton deep inelastic scattering, $q_i + p \to q_j + X$ [CAP88] leads to the definition of *three* different vector boson distributions inside quarks (or leptons): an averaged transverse $f^{T}_{V/q}(z)$, a longitudinal $f^{L}_{V/q}(z)$ and a parity violating transverse $f^{\tilde{T}}_{V/q}(z)$, where z is the reduced boson energy, $z = E_V/E_q$. This last distribution, introduced in [CAP88], has often been neglected in the literature [KAN84, DAW85a, LIN87a][1]. The various forms which have been proposed, assuming some off-mass-shell behavior for vector boson interactions, essentially agree in the limit of the effective W approximation (LEWA),

$$f^{T}_{V/q_i}(z) \to (a_i^2 + b_i^2 - 2a_i b_i h)\,\frac{\alpha}{2\pi}\,\frac{1+(1-z)^2}{z}\,L\,, \tag{9.1}$$

$$f^{L}_{V/q_i}(z) \to (a_i^2 + b_i^2 - 2a_i b_i h)\,\frac{\alpha}{\pi}\,\frac{1-z}{z}\,, \tag{9.2}$$

$$f^{\tilde{T}}_{V/q_i}(z) \to [2a_i b_i - (a_i^2 + b_i^2)h]\,\frac{\alpha}{2\pi}\,(2-z)L\,, \tag{9.3}$$

where h is the quark helicity, a_i and b_i are the standard Vqq vector and axial couplings and in the LEWA limit $L \to \log(4E_{q_i}^2/M_V^2)$ for $E_{q_i} \gg M_V$ and $z \ll 1$[2]. Vector boson distributions inside protons are

[1] However, see [RAL86a] for an alternative description in terms of left and right vector boson distributions.

[2] For a massless photon the mass M_V should be replaced by m_{q_i}.

then obtained by convoluting these $f_{V/q_i}(z)$ with the quark distributions inside protons given in section 3. For unpolarized beams we have

$$f_{V/p}^{T,L,\bar{T}}(x) = \int_x^1 \frac{dy}{y} \sum_i q_i(y) f_{V/q_i}^{T,L,\bar{T}}(x/y) , \tag{9.4}$$

where $x = E_V/E_p$ and the sum extends over all quark flavors inside the proton which can couple to the vector boson V, an average over quark helicity being understood. The cross section for $q_i + p \to q_j + X$ where none of the quarks or proton helicities is observed, is expressed in terms of

$$\frac{d\sigma}{dx} = f_{V/p}^{T}(x)\hat{\sigma}_T + f_{V/p}^{L}(x)\hat{\sigma}_L + f_{V/p}^{\bar{T}}(x)\hat{\sigma}_{\bar{T}} , \tag{9.5}$$

where $\hat{\sigma}_{T,L,\bar{T}}$ are simply related to the three cross sections $\hat{\sigma}(+)$, $\hat{\sigma}(0)$, $\hat{\sigma}(-)$ for the process $V + p \to X$ with helicity $+$, 0, $-$ of the vector boson, as follows:

$$\hat{\sigma}_T = \tfrac{1}{2}[\hat{\sigma}(+) + \hat{\sigma}(-)] , \qquad \hat{\sigma}_L = \hat{\sigma}(0) , \qquad \hat{\sigma}_{\bar{T}} = \tfrac{1}{2}[\hat{\sigma}(+) - \hat{\sigma}(-)] . \tag{9.6}$$

In the case of polarized proton beams, the interesting quantities suitable for computing polarization effects are

$$\Delta f_{V/p}^{T,L,\bar{T}}(x) = \int_x^1 \frac{dy}{y} \sum_i \Delta q_i(y)\, \Delta f_{V/q_i}^{T,L,\bar{T}}(x/y) , \tag{9.7}$$

where Δq_i is the quark helicity asymmetry given in section 3.1 and

$$\Delta f_{V/q_i}^{T,L,\bar{T}} = \tfrac{1}{2}[f_{V/q_i}^{T,L,\bar{T}}(h=-1) - f_{V/q_i}^{T,L,\bar{T}}(h=+1)] . \tag{9.8}$$

The resulting single helicity asymmetry with polarized protons emitting a vector boson V then reads

$$a_L^V(x) = \frac{\Delta f_{V/p}^{T}(x)\, \hat{\sigma}_T + \Delta f_{V/p}^{L}(x)\, \hat{\sigma}_L + \Delta f_{V/p}^{\bar{T}}(x)\, \hat{\sigma}_{\bar{T}}}{f_{V/p}^{T}(x)\hat{\sigma}_T + f_{V/p}^{L}(x)\hat{\sigma}_L + f_{V/p}^{\bar{T}}(x)\, \hat{\sigma}_{\bar{T}}} . \tag{9.9}$$

This asymmetry will give the driving effect for hadron asymmetries in proton collisions going through a vector boson subprocess.

All these distributions $f_{V/p}^{T,L,\bar{T}}(x)$ have been computed from eq. (9.4) with the LEWA expressions eqs. (9.1), (9.2), (9.3) as well as with the complete expression given in [CAP88], where the results are fully reported. As an example, the photon distributions are shown in fig. 9.1 in order to give a feeling about the order of magnitude of these distributions as well as about uncertainties in the theoretical predictions. The relative magnitudes of γ, Z, W^+ and W^- distributions follow from

- the mass term entering the leading log factor L,
- the magnitudes of the electroweak couplings a_i and b_i,
- the stronger probability of finding a u-quark (allowing W^+ emission) than a d-quark (allowing W^- emission) inside a proton.

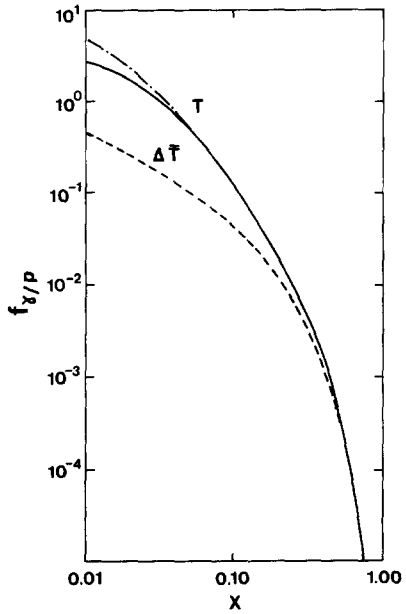

Fig. 9.1. Photon distributions inside a proton ($E_p = 20$ TeV). Complete expression (solid curve) and LEWA (dashed-dotted curve) for $f^{T}_{\gamma/p}(x)$. Complete expression for $\Delta f^{\bar{T}}_{\gamma/p}(x)$ (dashed curve).

In fig. 9.2 we have plotted the polarization asymmetry factors $\Delta f_{V/p}/f_{V/p}$ separately for T, L and $\bar{T}$, which can be compared to the parton polarizations obtained in section 3 (see figs 3.3 to 3.6). This allows us a priori to appreciate, independently of the subprocess considered, the spin dilution effect in the $p \to q \to V$ cascade. These asymmetry factors turn out to be large enough, in particular for the Z and W^+ cases[3] for high x values, to generate observable polarization effects.

9.2. Boson–boson and boson–parton luminosities in pp collisions

The first predictions were given in [KAN84, DAW85a, LIN87a] and a complete analysis has recently been provided in [CAP88] by generalizing the results previously obtained for $\gamma\gamma$ processes in e^+e^- collisions [BUD75, CRA83]. Again one starts by considering processes at the quark level, that is, a quark–quark collision $q + q' \to q + q' + VV'$ where each quark emits a soft vector boson followed by the process $VV' \to X$.

In general there are nineteen independent luminosity factors to be defined, which, however, reduce to nine where one considers cross sections integrated over the azimuthal angles of scattered quarks. For a given subprocess $VV' \to W$ the invariant mass distribution $d\sigma/d\xi$ (with $\xi = M_X^2/s_{qq'}$) reads

$$\frac{d\sigma}{d\xi} = \sum_{i=1,9} \mathscr{L}_i(\xi)\hat{\sigma}_i = \mathscr{L}_{TT}\hat{\sigma}_{TT} + \mathscr{L}_{LL}\hat{\sigma}_{LL} + \mathscr{L}_{TL}\hat{\sigma}_{TL} + \mathscr{L}_{LT}\hat{\sigma}_{LT}$$
$$+ \mathscr{L}_{\bar{T}\bar{T}}\hat{\sigma}_{\bar{T}\bar{T}} + \mathscr{L}_{T\bar{T}}\hat{\sigma}_{T\bar{T}} + \mathscr{L}_{\bar{T}T}\hat{\sigma}_{\bar{T}T} + \mathscr{L}_{\bar{T}L}\hat{\sigma}_{\bar{T}L} + \mathscr{L}_{L\bar{T}}\hat{\sigma}_{L\bar{T}}\,, \tag{9.10}$$

[3] Note that $\Delta f^{\bar{T}}_{Z/p}/f^{\bar{T}}_{Z/p}$ exceeds one near $x = 1$ as a consequence of the large factor $(a_i^2 + b_i^2)/2a_ib_i$ [see eq. (9.3)].

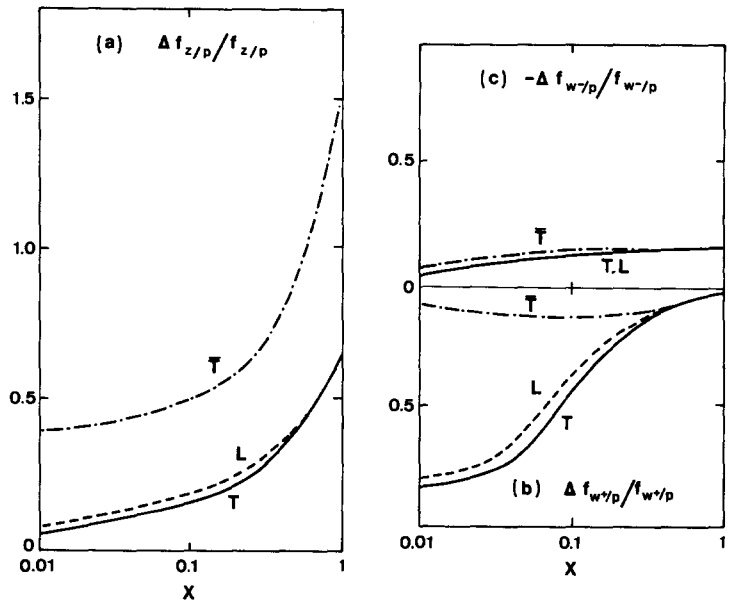

Fig. 9.2. Polarization asymmetries in Z, $W^{\pm}$ distributions inside a proton ($E_p = 20$ TeV). $\Delta f^T/f^T$ (solid curves), $\Delta f^L/f^L$ (dashed curves), $\Delta f^{\bar{T}}/f^{\bar{T}}$ (dashed–dotted curves). (a) Z, (b) W^+, (c) W^- (note the minus sign).

where the $\hat{\sigma}$'s are cross sections for the various VV′ helicity combinations, five parity conserving ones ($\hat{\sigma}_{TT}$, $\hat{\sigma}_{LL}$, $\hat{\sigma}_{TL}$, $\hat{\sigma}_{LT}$, $\hat{\sigma}_{\bar{T}\bar{T}}$) and four parity violating ones ($\hat{\sigma}_{T\bar{T}}$, $\hat{\sigma}_{\bar{T}T}$, $\hat{\sigma}_{\bar{T}L}$, $\hat{\sigma}_{L\bar{T}}$), defined in appendix G.

The nine luminosity factors $\mathcal{L}_i(\xi)$ can be explicitly computed from the square of the amplitude corresponding to the VV′ exchange diagram with full integration over the final qq′ phase space [BUD75, CRA83, CAP88]. A simpler approximation, in the spirit of the parton model, consists in defining $\mathcal{L}_i(\xi)$ as convolutions of single vector boson distributions inside each initial quark,

$$\mathcal{L}_i(\xi) \cong f * f' \equiv \int_{\xi}^{1} \frac{dz}{z} f(z) f'(\xi/z) ; \tag{9.11}$$

so for the nine possibilities considered above in eq. (9.10) we will have

$$\mathcal{L}_{ab} = f^a * f'^b , \quad a, b = T, L, \bar{T} . \tag{9.12}$$

The various approximate forms of $f_{V/q}$ mentioned previously lead to luminosities differing one from the other mainly in the low-ξ region. Apart from simplifying kinematical approximations, an unavoidable model dependence associated with the off-mass-shell behavior of the VV subprocesses affects the definitions of these luminosities (see discussion in [CAP88]). The leading high-energy (LEWA) forms of these nine luminosity factors at the quark–quark level are given in eq. (G.3) of appendix G.

One finally gets the invariant mass distribution $d\sigma/d\tau$ (with $\tau = M_X^2/s$) for $pp \to X + \cdots$ (via $VV' \to X$) in the same form as in eq. (9.10), replacing $\mathcal{L}_i(\xi)$ by $\mathcal{L}^{(ij)}_{VV'/pp}(\tau)$. These last luminosities can be obtained by convolution of the above $\mathcal{L}_i(\xi)$ with quark distributions inside protons. An alternative and simpler procedure consists in constructing $\mathcal{L}^{(ij)}_{VV'/pp}(\tau)$ directly as convolutions of vector boson

distributions inside protons $f^{(i)}_{V/p}(x)$ defined in eq. (9.4),

$$\mathscr{L}^{(ij)}_{VV'/pp}(\tau) = \int_\tau^1 \frac{dx}{x} f^{(i)}_{V/p}(x) f^{(j)}_{V'/p}(\tau/x)\,, \tag{9.13}$$

using the appropriate $f^{T,L,\bar{T}}_{V/p}$ distributions appearing in the definitions given in eq. (9.12) and where symmetrization is understood when necessary. This is done in a similar way as for the parton–parton luminosities introduced in section 3. When *one* proton beam is polarized, nine asymmetries factors can now be formed with

$$\Delta\mathscr{L}^{(ij)}_{VV'/pp}(\tau) = \int_\tau^1 \frac{dx}{x} \Delta f^{(i)}_{V/p}(x)\, f^{(j)}_{V'/p}(\tau/x)\,, \tag{9.14}$$

using the $\Delta f^{T,L,\bar{T}}_{V/p}$ defined in eq. (9.7)[4]. Corresponding asymmetries with *two* polarized proton beams have also been given in [CAP88] together with the computation of many of these boson–boson luminosities for $\gamma\gamma$, γZ, ZZ, γW^+, ZW^+ and W^+W^-. In fig. 9.3 we reproduce a sample for $\gamma\gamma$ luminosities at $\sqrt{s} = 40$ TeV, which have been calculated by convoluting the complete expressions of the photon distributions. They are the largest compared to any other VV′ pair but still several orders of magnitude smaller than the parton–parton luminosities of section 3 (see figs. 3.7 to 3.13) as well as the corresponding cross sections.

One can also consider single beam asymmetry factors defined as ratios

$$a^{(ij)}_V(V') = \Delta\mathscr{L}^{(ij)}_{VV'} / \mathscr{L}^{(ij)}_{VV'}\,, \tag{9.15}$$

similar to the parton polarizations considered in section 3 [see eq. (3.23)]. In fig. 9.4 we give some

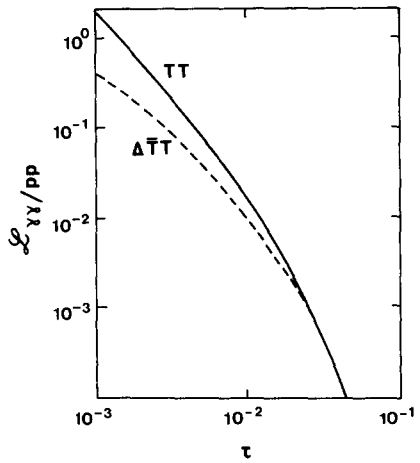

Fig. 9.3. $\gamma\gamma$ luminosities in pp collisions at $\sqrt{s} = 40$ TeV. $\mathscr{L}^{TT}_{\gamma\gamma}$ (solid curve) and $\Delta\mathscr{L}^{\bar{T}\bar{T}}_{\gamma\gamma}$ (dashed curve).

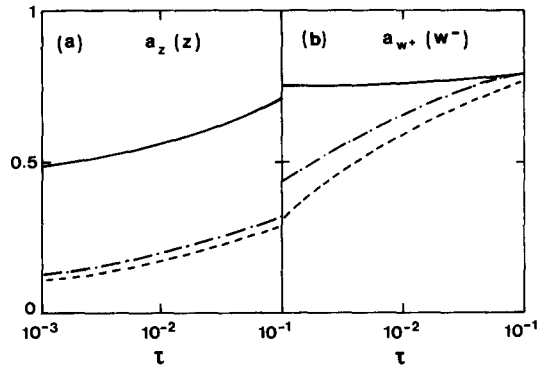

Fig. 9.4. Asymmetries $a^{(ij)}_V(V')$ in pp collisions at $\sqrt{s} = 40$ TeV. (a) $a^{L\bar{T}}_Z(Z)$ (solid curve), $a^{TT}_Z(Z)$ (dashed curve), $a^{LL}_Z(Z)$ (dashed–dotted curve). (b) $a^{\bar{T}\bar{T}}_{W^+}(W^-)$ (solid curve), $a^{L\bar{T}}_{W^+}(W^-)$ (dashed curve), $a^{LL}_{W^+}(W^-)$ (dashed–dotted curve).

[4] It is understood in the notation of eq. (9.14) that V is emitted from the proton which is polarized.

examples of these for $a_Z^{(ij)}(Z)$ and $a_{W^+}^{(ij)}(W^-)$. These asymmetries also have a universal character associated to Z or W^+ emission from a polarized proton beam. They differ from the ones established in section 5 from $q\bar{q}\to W$ or Z because of the different kinematics defining the scaling variable τ, in the present case involving a two-step process. Finally, if we want to study subprocesses involving boson–parton scattering, one has to construct boson–quark and boson–gluon luminosities [LIN87, CAP88] by considering

$$\mathscr{L}^{T,L,\bar{T}}_{Vc/pp}(\tau) = \int_\tau^1 \frac{dx}{x} f^{T,L,\bar{T}}_{V/p}(x) f_{c/p}(\tau/x)\,, \tag{9.16}$$

where c stands for quark or gluon. In the case of one polarized proton one has the analog of eq. (9.14) and the interesting quantities to evaluate are ratios $a^i_c(V)$ or $a^i_V(c)$ (with $i = T, L, \bar{T}$) defined as in eq. (9.15). Figure 9.5 illustrates some of these asymmetries. They all grow in the high-τ region and we see that W^+g gives the largest effects. [$a_{W^+}(g)$ is larger than $a_u(g)$ (see fig. 3.14) because the emission of a W^+ involves a u quark with a higher x and Δu increases with x.]

9.3. *Applications*

The possible use of these polarized luminosities to study boson–boson subprocesses will now be illustrated by a few applications.

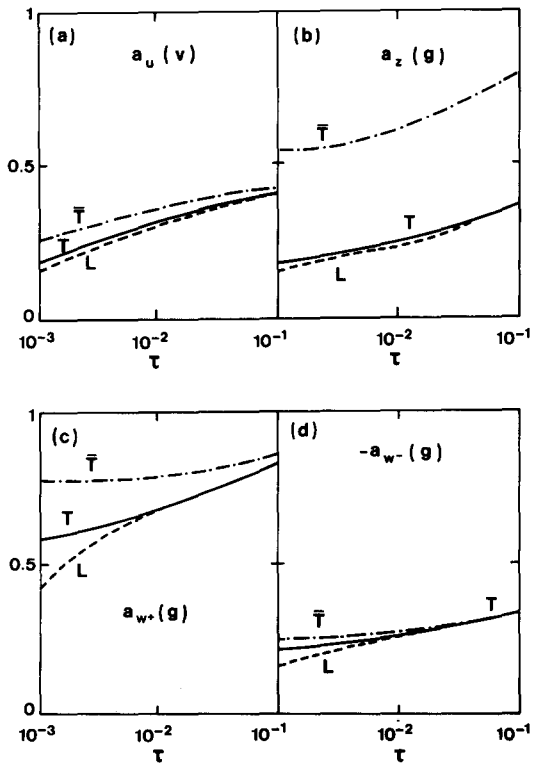

Fig. 9.5. Asymmetries $a^i_c(V)$ and $a^i_V(c)$ in pp collisions at $\sqrt{s} = 40$ TeV (T, solid curve; L, dashed curve; $\bar{T}$, dashed–dotted curve). (a) $a^i_u(V)$ ($V = \gamma, Z, W^+$), (b) $a^i_Z(g)$, (c) $a^i_{W^+}(g)$, (d) $-a^i_{W^-}(g)$.

9.3.1. Higgs production

Using standard couplings a heavy neutral Higgs boson can be produced by W^+W^-/ZZ fusion [PRO79, JON79, CAH84, DAW84a]. As recalled in section 5 these production processes dominate over $t\bar{t}$ and gg fusion as soon as $M_H > 300\ \mathrm{GeV}/c^2$ if $M_t = 40\ \mathrm{GeV}/c^2$. The subprocess cross sections to be used in eq. (9.10) are [CAP88]

$$\hat{\sigma}_{TT} = \hat{\sigma}_{\bar{T}\bar{T}} = \tfrac{1}{2}N\,, \qquad \hat{\sigma}_{LL} = N\,\frac{(\hat{s}-2M^2)^2}{4M^4}\,, \tag{9.17}$$

where M is the vector boson mass M_W or M_Z, and

$$N = \frac{2\pi}{4k\sqrt{\hat{s}}}\,g^2_{VVH}\delta(\hat{s}-M_H^2)\,,$$

$$k^2 = \tfrac{1}{4}\hat{s} - M^2\,, \qquad g_{W^+W^-H} = \frac{eM_W}{\sin\theta_w}\,, \qquad g_{ZZH} = \frac{eM_W}{\sin\theta_w\cos^2\theta_w}\,,$$

all other $\hat{\sigma}$'s being zero. It is obvious from eq. (9.17) and from the luminosity factors given in [CAP88], that production rates shown in fig. 9.6 are dominated by LL contributions as soon as $M_H > 2M_W$ and much larger than those from gluon–gluon fusion considered in section 5. Polarization asymmetries are then typical of pure W^+W^- or ZZ fusion processes as given in fig. 9.4 and they could be very useful to disentangle the background, which may be important [GUN87]. In a similar context, let us recall that it

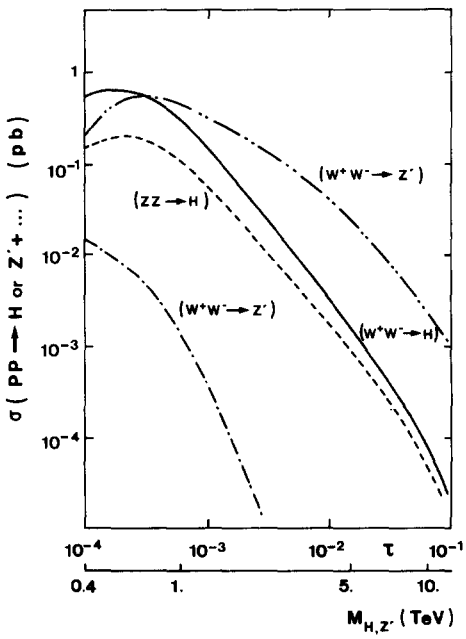

Fig. 9.6. Cross sections for Higgs or Z′ production from W^+W^-/ZZ fusion in pp collisions at $\sqrt{s} = 40$ TeV versus $M_{H,Z'}$ (or $\tau = M^2_{H,Z'}/s$). $W^+W^- \to H$ (solid curve), $ZZ \to H$ (dashed curve), $W^+W^- \to Z'$ with ϕ given by eq. (9.20) (dashed–dotted curve), W^+W^-Z with $|\sin\phi| = 0.1$ (dashed–double dotted curve).

was also shown [DUN86a] that, to establish the existence of a Higgs of several hundred GeV, in $pp \to H \to ZZ$, the determination of the polarization of one final Z is useful. A Z from the background $pp \to q\bar{q} \to ZZ$ is almost purely transverse where a Z from H decay is purely longitudinal.

9.3.2. Heavy Z′ production

A new neutral gauge boson [ROB82, LEU82, ROB84, CAN85, WIT85] associated to an additional U(1) gauge group can couple to W^+W^- through Z_0–Z_0' mixing and the standard $Z_0W^+W^-$ Yang–Mills couplings [COH85, ELL86a]. Defining

$$|Z'\rangle = |Z_0'\rangle \cos\phi + |Z_0\rangle \sin\phi\,, \tag{9.18}$$

the cross sections for the subprocess $W^+W^- \to Z'$ read according to [CAP88]

$$\hat{\sigma}_{TT} = \hat{\sigma}_{\bar{T}\bar{T}} = \tfrac{1}{2}N(\hat{s} - 4M_W^2)\,, \qquad \hat{\sigma}_{TL} = \hat{\sigma}_{LT} = N\frac{4k^2\hat{s}}{M_W^2}\,,$$

$$\hat{\sigma}_{LL} = \frac{N}{M_W^4}\left[(\hat{s} - 4M_W^2)(\hat{s} - 2M_W^2)^2 + 2k^2\hat{s}M_W^2\right], \tag{9.19}$$

$$N = \frac{(2\pi)e^2\,\mathrm{cotg}^2\,\theta_w \sin^2\phi}{4k\sqrt{\hat{s}}}\,\delta(\hat{s} - M_{Z'}^2)\,, \qquad k^2 = \tfrac{1}{4}\hat{s} - M_W^2\,.$$

The production rate is dominated by LL contributions as seen from eq. (9.19) and it depends essentially on the value of the mixing angle. Illustrations are given in fig. 9.6 using the mixing angle of [COH85, ELL86a],

$$|\mathrm{tg}\,\phi| = \tfrac{1}{3}\sqrt{x_w}\,\frac{M_Z^2}{M_{Z'}^2 - M_Z^2}\,\frac{(\bar{v}/v)^2 - 4}{(\bar{v}/v)^2 + 1}\,, \tag{9.20}$$

taking for definiteness the ratio of vacuum expectation values to be $\bar{v}/v = 0.5$. We see that in this case for $M_{Z'} > 400\ \mathrm{GeV}/c^2$ the mixing angle is very small ($\sim 1°$) and decreases for larger values of $M_{Z'}$. The production cross section is rather small, say 10^2 events/year for $M_{Z'} = 500\ \mathrm{GeV}/c^2$, and the identification of Z′ will be difficult[5]. The situation is much better with a constant mixing angle, for example $|\sin\phi| = 0.1$ (see fig. 9.6). In any case polarization asymmetries are typical of $W^\pm$ exchanges (see fig. 9.4b) and much bigger than the asymmetries obtained in section 6.3. In addition to obvious differences between Z′ and H production processes, there are also differences in the decay processes since Z′ does not couple to ZZ and Z′ couplings to fermion pairs are not related to fermion masses like for the Higgs couplings.

9.3.3. Boson–boson scattering

In the standard model the various $VV \to VV$ ($V = W^\pm, Z, \gamma$) scattering amplitudes are fully predicted in terms of e and $\sin^2\theta_w$ through Yang–Mills three-boson and four-boson couplings. Only the heavy Higgs boson coupled to W^+W^- and ZZ can modify some of these processes. So these reactions

[5] For a discussion of the background see [DES87].

constitute a unique set of tests of the true nature of $W^{\pm}$ and Z bosons, of their structure and of the origin of mass generation [CHA85a, DUN86]. Having verified to some accuracy the standard behaviour of Z and $W^{\pm}$ bosons these reactions (or at least some of them in well-defined kinematical domains which should not be affected by additional or anomalous terms) could then be used to monitor the whole set of VV collision processes, i.e. to measure vector boson luminosity factors at pp colliders.

Helicity amplitudes have been explicitly written down in [KUR87a] for the standard case as well as in more general models [MAA86, KUR87, BIL88] allowing, for example, for a $W^{\pm}$ anomalous magnetic moment. From them, one immediately computes the sub-cross sections $\hat{\sigma}_{TT}$, $\hat{\sigma}_{LL}$, $\hat{\sigma}_{TL}$, $\hat{\sigma}_{LT}$, and $\hat{\sigma}_{\bar{T}\bar{T}}$ (all other terms vanish because of parity conservation) for all VV→VV processes. In [KUR87a] the effect of a $W^{\pm}$ anomalous magnetic moment has been computed in the various subprocesses as well as in their manifestation in e^+e^- collisions. It appears to be very strong and this makes these processes potentially very fruitful for testing vector boson dynamics. The same study can be done for pp collisions [CAP88] and we just present in fig. 9.7 the typical example $W^+W^- \to W^+W^-$ with different choices of Higgs masses and of anomalous moment κ. In [KUR88] it was noticed that a given final state, e.g. W^+W^-, can be produced by different initial vector boson–vector boson states, e.g. $\gamma\gamma$, W^+W^- and ZZ, and that by varying the tagging conditions one could perhaps disentangle these various reactions. Obviously beam polarization, thanks to the different values of the polarization asymmetries typical of γ, Z, W^- or W^+ exchanges as shown in fig. 9.4, is another way of solving this problem.

9.3.4. Heavy fermion pair production

Boson–boson collisions also constitute an interesting source of new types of leptons, quarks, leptoquarks or other exotic states. They generalize the classical modes $\gamma\gamma \to L^+L^-$ or $Q\bar{Q}$ with new possibilities like $W^+W^- \to L^+L^-$, $W\gamma$ or $WZ \to U\bar{D}, \ldots$ [WIL85, WIL86, DAW86, DAW87, LIN87].

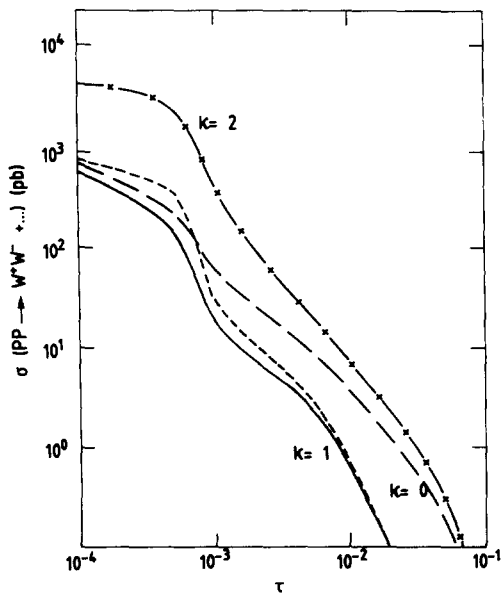

Fig. 9.7. Cross sections for W^+W^- production in pp collisions via $W^+W^- \to W^+W^-$ versus τ. Standard Model predictions with $M_H = 0.1\,\mathrm{TeV}/c^2$ (solid curve) and $M_H = 1\,\mathrm{TeV}/c^2$ (short-dashed curve). Alternative model predictions with $\kappa = 0$ (long-dashed curve) and $\kappa = 2$ (cross-dashed curve).

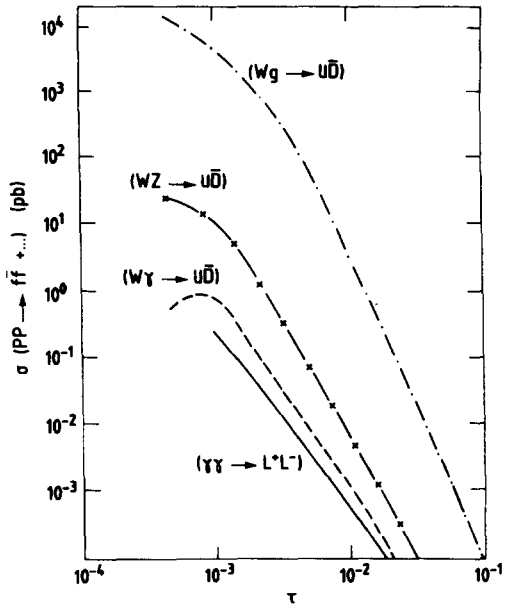

Fig. 9.8. Cross sections for fermion–antifermion production via VV collisions in pp collisions at $\sqrt{s} = 40$ TeV versus τ. $\gamma\gamma \to L^+L^-$ (solid curve), $W\gamma \to U\bar{D}$ (dashed curve), $WZ \to U\bar{D}$ (cross-dashed curve), $Wg \to U\bar{D}$ (dotted–dashed curve).

One of the most interesting cases appears to be $W^+g \to U\bar{D}$, which has the highest rate in this class of processes and which seems to be a competitive way of producing very heavy quarks. It was mentioned than the $U\bar{D}$ mode could be more easily identified than the $U\bar{U}$ one produced via gg fusion. Rates for these processes in pp collisions are shown in fig. 9.8. Dominant contributions come from longitudinal W or Z states, e.g. $W_L^+ g_T \to U\bar{D}$. So here also the polarization asymmetry is clearly typical of W_L^+ exchange and already shown in fig. 9.5. It would help for characterizing this process in distinction to QCD processes giving no such asymmetry.

Vector boson–vector boson collision processes indeed appear to be very powerful for studying the pure gauge sector and the scalar sector of the electroweak theory. Several processes are very sensitive to the presence of new particles (Higgs scalars, new gauge or composite vector bosons, new fermion pairs) or of new interactions (anomalous three-boson and four-boson couplings, residual interactions, . . .). However, the resulting production cross sections in pp collisions are sometimes rather difficult to identify and these interesting processes will be hidden in the background. Simultaneous use of all the available means to reduce this background or to enhance the signal will certainly be mandatory. Polarized beams which allow characterization of $W^{\pm}$ or Z^0 exchange by typical helicity asymmetries (see fig. 9.4) as compared to electromagnetic or chromodynamic processes will constitute one of these means. If it is associated to special cuts on the final phase space [GUN87], one can hope to be able to identify and study these new kinds of collision processes.

10. Conclusions

Projects for multi-TeV proton machines are being developed. They are strongly motivated by standard and new physics aspects which are expected to appear in the TeV range. However, these

projects have to face an increasing number of difficulties related to the very large number of particles produced during the collision. The analysis of such experiments will require new strategies, new methods, new ideas in order to disentangle the signals hidden in this huge background. This report aimed to answer the question: would polarized proton beams contribute to such a strategy?

We have assumed that longitudinally polarized proton beams will be available in these future hadron colliders such as SSC and LHC. The feasibility is indeed expected from the work of specialized study groups and it is based on the following scheme: a high-intensity polarized source and an acceleration set-up associated with devices such as Siberian Snakes to preserve the beam polarization.

We have chosen a set of spin dependent quark and gluon distributions inside a polarized proton in order to make predictions for hadron helicity asymmetries coming from a given subprocess. In many cases these asymmetries are simply expressed in terms of polarized luminosities multiplied by polarized subprocess asymmetries. The above set of distributions has the appealing feature of being given in terms of a simple analytical form compatible with our present knowledge of the proton structure. New developments initiated by the intriguing result of the EMC experiment might improve our knowledge in this field and yield a more accurate set of distribution functions. In such an event, in order to make new predictions it will be straightforward to reevaluate the polarized luminosities, keeping untouched the subprocess asymmetries established here.

A first application dealt with hard QCD processes which are parity conserving and lead essentially to double helicity asymmetries A_{LL}. These A_{LL} were found positive and small for jet and direct photon production and this is a test of QCD and of the spin content of the proton. Jet production will constitute the main part of the background in the search of new particles, so it will be characterized by the smallness of these asymmetries.

Single helicity asymmetries A_L appear with electroweak processes. Because of maximal parity violation, they can be large in some cases, in particular in any subprocess going through a $W^{\pm}$ gauge boson. The A_L's are universal quantities defined by simple combinations of ratios of luminosities. We have stressed that this is one of the best ways to calibrate directly spin dependent distributions in the kinematic range of interest at future supercolliders. On the other hand, there are several interesting channels allowing a test of some crucial features of the Standard Model, especially the structure of the trilinear gauge coupling in boson pair production and the existence of the Higgs produced in association with $W^{\pm}$. Here the information one obtains by means of polarized beams is rather unique.

We have applied the same method in order to characterize features of minimal extensions of the standard electroweak model. In this case also polarization should allow us to characterize immediately the nature of the new gauge boson, $W^{\pm}$ right-handed or Z' associated with a new U(1).

If we turn to genuine new physics let us turn first to compositeness. In the fermion sector it is likely that a residual interaction will involve a specific chiral structure, which will lead to spectacular effects in helicity asymmetries. We have illustrated the occurrence of strong departures from Standard Model predictions in lepton pair production, direct photon production and jet production. In the boson sector, A_L was shown to be able to discriminate between several models which predict anomalous self-boson couplings and which yield the same unpolarized cross sections. Composite partners like an isoscalar Y boson, an excited W* or techni-rhos will be clearly identified in the same way.

Other exotic partners are those predicted by supersymmetric theories. A negative A_{LL} is a typical feature of jets plus missing energy events coming from the production of squarks and gluinos. Moreover, A_L in slepton pair production and also in neutralino pair production is very sensitive to the mass spectrum of the left- and right-handed scalar partners.

A new class of processes which are accessible at supercollider energies are WW collisions. They have been advertised for the search of a very massive Higgs boson and for studying the behavior of $W_L W_L$

scattering but recognized as rather difficult to extract from the background. Here also polarization will help because of the purely left nature of $W^{\pm}$ exchanges compared to other gauge boson exchanges.

Polarization gives access to new observables A_L and A_{LL}, which contain a definite signature of the underlying dynamics. They provide an elegant way to reduce the background and to clarify signals for new physics. Polarized proton beams will undoubtedly be very useful and they may turn out to constitute key tools for the next generation of hadron supercolliders.

Acknowledgements

The motivation for this review originated at the Workshop on Polarized Beams at SSC (Ann Arbor, June 1985) and it is a pleasure to thank Alan Krisch and Owen Chamberlain who organized this meeting. We also wish to thank Maurice Jacob for his encouragement in undertaking this project and constructive suggestions. Mrs Antoinette Sueur deserves special thanks for her rapid and careful typing of the manuscript.

Appendices

Appendix A. The EMC effect, its various interpretations and consequences

In the parton model one introduces the spin dependent structure functions defined in terms of quark and antiquark helicity asymmetries as

$$g_1^p(x) = \frac{1}{2}\sum_i e_i^2[\Delta q_i(x) + \Delta\bar{q}_i(x)]$$
$$= \tfrac{1}{18}[4\,\Delta u(x) + 4\,\Delta\bar{u}(x) + \Delta d(x) + \Delta\bar{d}(x) + \Delta s(x) + \Delta\bar{s}(x)] \qquad (A.1)$$

for protons and similarly $g_1^n(x)$ for neutrons, obtained from $g_1^p(x)$ by the substitution $u \leftrightarrow d$. The total amount of the proton spin carried by quarks and antiquarks is

$$\Delta\Sigma = \Delta u + \Delta d + \Delta s\,, \qquad (A.2)$$

where

$$\Delta q_i \equiv \int_0^1 dx\,[\Delta q_i(x) + \Delta\bar{q}_i(x)]\,. \qquad (A.3)$$

Clearly the gluon helicity asymmetry and parton orbital angular momentum can also contribute to the proton spin with the obvious constraint

$$\tfrac{1}{2} = \tfrac{1}{2}\,\Delta\Sigma + \Delta G + \langle L_z\rangle\,. \qquad (A.4)$$

Through the light cone operator product expansion the Δq_i are related to the matrix elements of the quark axial-vector currents between longitudinally polarized protons. By making use of the SU(3)

flavor symmetry, good to a level of 10%, they can be evaluated in terms of the F and D axial parameters which describe the β-decays of the baryon octet, so we have

$$\Delta u - \Delta d = F + D\,, \tag{A.5}$$

$$\Delta u + \Delta d - 2\,\Delta s = 3F - D\,, \tag{A.6}$$

with $F = 0.477 \pm 0.011$ and $D = 0.755 \pm 0.011$ [BOU83]. The recent experimental result in polarized deep inelastic scattering obtained by the European Muon Collaboration, over the kinematical range $0.015 \leq x \leq 0.7$ and $1.5 \leq Q^2 \leq 70\ \mathrm{GeV}^2$ and shown in fig. 3.2, yields a very precise value for the integral of $g_1^{\mathrm{p}}(x, Q^2)$ [ASH88, HUG88],

$$\int_0^1 \mathrm{d}x\, g_1^{\mathrm{p}}(x, Q^2) = 0.116 \pm 0.009\ (\mathrm{stat}) \pm 0.019\ (\mathrm{syst})\,, \tag{A.7}$$

and it is essentially Q^2 independent. By combining (A.5), (A.6) and (A.7) one finds

$$\Delta u = 0.72 \pm 0.08\,, \qquad \Delta d = -0.51 \pm 0.08\,, \qquad \Delta s = -0.23 \pm 0.08\,, \tag{A.8}$$

so that

$$\Delta\Sigma = -0.02 \pm 0.24\,. \tag{A.9}$$

It is very surprising to find Δs so large and it is even more striking to be led to the conclusion that the proton spin is *not* carried by the quarks. At this stage it is interesting to recall that one can write

$$\int_0^1 \mathrm{d}x\, g_1^{\mathrm{p}}(x, Q^2) = \tfrac{1}{18}\left((9F - D) - \frac{\alpha_s(Q^2)}{\pi}\,(3F + D)\right) + \tfrac{1}{3}\,\Delta s = (0.189 \pm 0.005) + \tfrac{1}{3}\,\Delta s\,, \tag{A.10}$$

which is known as the Ellis–Jaffe sum rule [ELL74] in the absence of the QCD correction and assuming $\Delta s = 0$, in strong disagreement with eq. (A.8).

Several interpretations of the result (A.9) have been proposed including the possibility that the experiment is wrong, which we will ignore. First it has been suggested that the small-x extrapolation was incorrectly done [CLO88] and this could lead to a much larger value of $\Delta\Sigma$, but this argument is not very serious. Second, one might assume [ANS88] a rapid Q^2 dependence of the integral in eq. (A.7) which has to be negative at $Q^2 = 0$ due to the Drell–Hearn–Gerasimov sum rule, but the EMC data have no significant Q^2 dependence down to the lowest Q^2 values. According to another speculation, the result (A.9) is in perfect agreement with a skyrmion model based on the $1/N_c$ expansion and chiral symmetry [BRO88] and more recently [ELL88a] it was argued that $\Delta G = 0$ [see eq. (A.4)] so $\langle L_z \rangle = 1/2$ and the orbital angular momentum is essentially carried by the quarks. This possibility of no gluon polarization is certainly at variance with the consequences of another suggestion related to the anomaly of the axial-vector current. According to this observation first made in [EFR88] and reexamined later in [ALT88, CAR88], the Δq_i appearing in the naive parton model should be replaced by

$$\Delta q_i' = \Delta q_i - \frac{\alpha_s}{2\pi}\Delta G\,. \tag{A.11}$$

From this interpretation one can restore the agreement between eq. (A.7) and eq. (A.10) where Δs is replaced by $\Delta s'$ provided $\Delta s = 0$ and $\Delta G \sim (0.23) \times 2\pi/\alpha_s$. As a consequence one should expect a new phenomenology of spin effects at short distances driven by this sizable gluon polarization (i.e., $\Delta G \sim 6$–7), which also implies that a polarized proton has a significant amount of rotation since $\langle L_z \rangle$ is very large. However, by using the available experimental data on the strange quark content of the proton it was shown that the *measured* Δs [i.e. $\Delta s'$ in eq. (A.11)] is bounded and one has [PRE88]

$$|\Delta s| < 0.052^{+0.023}_{-0.052}\,, \tag{A.12}$$

which implies

$$\int_0^1 \mathrm{d}x\, g_1^{\mathrm{p}}(x, Q^2) > 0.183^{+0.017}_{-0.007}\,. \tag{A.13}$$

Clearly the EMC experiment has to be redone both on protons and on neutrons because the knowledge of $g_1^{\mathrm{n}}(x, Q^2)$ would enable us to check the Bjorken sum rule [BJO66], that is eq. (A.5) usually written as

$$\int_0^1 [g_1^{\mathrm{p}}(x) - g_1^{\mathrm{n}}(x)]\,\mathrm{d}x = \tfrac{1}{6}(-G_{\mathrm{A}}/G_{\mathrm{V}})\,, \tag{A.14}$$

which is predicted to be badly violated according to the approach considered in [GIA85]. There are several projects either with a conventional polarized target and a muon beam at CERN or by using a polarized jet target [DIC88] inside a polarized electron ring at LEP or at HERA, which is a new attractive possibility.

We will end this appendix by making a few remarks on the significance of having a polarized proton beam at HERA. The main physics issues [BJO82] include the measurement of $g_1^{\mathrm{p}}(x, Q^2)$ in the small-x region ($x \sim 10^{-3}$) for large Q^2 values and the access to the new structure function $g_2^{\mathrm{p}}(x, Q^2)$, which requires transversely polarized protons. From the two weak processes $\mathrm{e}^{\pm}\mathrm{p} \to \nu\mathrm{X}$ one can separate $\Delta u(x, Q^2)$ and $\Delta d(x, Q^2)$ and of course in the high-Q^2 range, if right-handed charged currents are found, it would be nice to learn more about their proton couplings from the use of polarization [CHI85]. Finally there are exciting possibilities of future polarized ep collisions with polarized LEP and polarized LHC up to an energy of 1.8 TeV [COR87].

Appendix B. Standard W^+W^- pair production with rapidity cuts

The unpolarized cross section to produce a $\mathrm{W}^+\mathrm{W}^-$ pair of invariant mass M such that both W's lie in the rapidity interval $(-Y, Y)$ is given by

$$\frac{\mathrm{d}\sigma}{\mathrm{d}M} = \frac{2M}{3s}\sum_i \int_{-Y}^{Y} \mathrm{d}y_{\mathrm{boost}}\,[q_i(x_{\mathrm{a}}, M^2)\bar{q}_i(x_{\mathrm{b}}, M^2) + (\mathrm{a} \leftrightarrow \mathrm{b})]\hat{\sigma}(z_0, M^2)\,, \tag{B.1}$$

where $y_{\text{boost}} = \frac{1}{2}\ln(x_a/x_b)$ is the rapidity of the parton c.m. frame with respect to the overall c.m. and

$$\hat{\sigma}(z_0, M^2) = \int_{-z_0}^{z_0} \mathrm{d}z \, \frac{\mathrm{d}\hat{\sigma}}{\mathrm{d}z} (q_i\bar{q}_i \to W^+W^-) , \tag{B.2}$$

$$\frac{\mathrm{d}\sigma}{\mathrm{d}z} = \beta \frac{\hat{s}}{2} \frac{\mathrm{d}\hat{\sigma}}{\mathrm{d}\hat{t}} , \qquad z_0 = \min(\beta^{-1}\tanh(Y - |y_{\text{boost}}|), 1) .$$

In the polarized case, it is straightforward to replace in (B.1) the unpolarized distributions by the polarized ones and to get the equivalent of eq. (5.8). K_i and N_i defined in eqs. (5.30) and (5.31) are now functions of z_0 and we have

$$e(z_0) = \frac{1}{16x_w^2}\left\{(2-\varepsilon)\frac{L}{2} + \beta z_0\left(\frac{1}{\varepsilon^2} + \frac{3}{\varepsilon} - 1 - \frac{z_0^2}{3\varepsilon^2}(1-\varepsilon) - \left[\left(1-\frac{2}{\varepsilon}\right)^2 - 4\frac{\beta^2 z_0^2}{\varepsilon^2}\right]^{-1}\right)\right\}, \tag{B.3}$$

$$i_i(z_0) = \frac{\pm 1}{4x_w}[e_i + g_Z(a_i + b_i)M^2 \operatorname{Re} D_Z] \times\left\{\beta z_0\left[-1 - \frac{\varepsilon}{4} + \frac{5}{2\varepsilon} + \frac{1}{\varepsilon^2} + z_0^2\left(-\frac{1}{6} + \frac{1}{2\varepsilon} - \frac{1}{3\varepsilon^2}\right)\right] - \frac{\varepsilon}{2}\left(1 + \frac{\varepsilon}{8}\right)L\right\}, \tag{B.4}$$

$$a_i(z_0) = [e_i^2 + 2e_i a_i g_Z M^2 \operatorname{Re} D_Z + (a_i^2 + b_i^2)g_Z^2 M^4 |D_Z|^2] \times\left(\frac{\beta^3 z_0}{2\varepsilon^2}[3\varepsilon + \tfrac{3}{4}\varepsilon^2 + 1 - \tfrac{1}{3}z_0^2(\tfrac{3}{4}\varepsilon^2 - \varepsilon + 1)]\right), \tag{B.5}$$

$$a_i'(z_0) = [2e_i b_i g_Z M^2 \operatorname{Re} D_Z + 2a_i b_i g_Z^2 M^4 |D_Z|^2] \times\left(\frac{\beta^3 z_0}{2\varepsilon^2}[3\varepsilon + \tfrac{3}{4}\varepsilon^2 + 1 - \tfrac{1}{3}z_0^2(\tfrac{3}{4}\varepsilon^2 - \varepsilon + 1)]\right), \tag{B.6}$$

where

$$L = \ln\left(\frac{\varepsilon - 2(1+\beta z_0)}{\varepsilon - 2(1-\beta z_0)}\right). \tag{B.7}$$

Appendix C. W^+W^- pair production with anomalous magnetic moments and rapidity cuts

The functions f_A and f_I defined in eqs. (7.9) and (7.10) become functions of z_0 (defined in appendix B) and read

$$f_A(\kappa_a, \kappa_b, z_0) = \beta^3 z_0\left[\frac{\kappa_a\kappa_b}{2\varepsilon^2} + [\tfrac{1}{4}(1 + \kappa_a\kappa_b) + \tfrac{1}{2}(\kappa_a + \kappa_b)]\frac{1}{\varepsilon} + \frac{3}{8} - z_0^2\left(\frac{\kappa_a\kappa_b}{6\varepsilon^2} - (1 + \kappa_a\kappa_b)\frac{1}{12\varepsilon} + \frac{1}{8}\right)\right], \tag{C.1}$$

$$f_1(\kappa_a, z_0) = \beta z_0\Big[\frac{\kappa_a}{\varepsilon^2} + \frac{3+2\kappa_a}{\varepsilon} - \kappa_a - \tfrac{1}{4}\varepsilon + z_0^2\Big(-\frac{\kappa_a}{3\varepsilon^2} + \frac{2\kappa_a+1}{6\varepsilon} - \frac{1}{6}\Big)\Big]$$
$$- \tfrac{1}{4}\varepsilon(1+\kappa_a+\tfrac{1}{4}\varepsilon)L\,, \qquad \text{(C.2)}$$

L being defined in eq. (B.7).

Appendix D. Contact terms in W^+W^- production

The coefficients entering eq. (7.14) are given by
- contact term:

$$C_4 = \Big(\frac{g^2}{\Lambda^4 e^2}\Big)^2 \frac{\hat{s}^4}{32\varepsilon^2}(1-\varepsilon)^2(1-\varepsilon-\tfrac{1}{3}\beta^2 z_0^2)\,; \qquad \text{(D.1)}$$

- interference between the contact term and the annihilation through a γ or a Z^0:

$$C_{34}^{\gamma} = \frac{g^2}{\Lambda^4 e^2}\,\frac{1}{\hat{s}}\Big(\frac{\hat{s}^3}{8\varepsilon^2}(1-\varepsilon)(1-\varepsilon-\tfrac{1}{3}\beta^2 z_0^2)\Big)\,, \qquad \text{(D.2)}$$

$$C_{34}^{Z} = \frac{g^2}{\Lambda^4 e^2}\, g_Z\,\mathrm{Re}\,D_Z\Big(\frac{\hat{s}^3}{8\varepsilon^2}(1-\varepsilon)(1-\varepsilon-\tfrac{1}{3}\beta^2 z_0^2)\Big)\,, \qquad \text{(D.3)}$$

- interference between the contact term and the quark exchange term:

$$C_{E4} = -\frac{1}{4}\Big(\frac{g^2}{\Lambda^4 e^2}\Big)\Big[\hat{s}^2(2-\varepsilon)\Big(3+\varepsilon+\frac{2}{\varepsilon}-\frac{4}{\varepsilon^2}\Big) + \frac{\hat{s}^2\varepsilon^2}{16}\Big(1+\frac{L}{\beta z_0}\Big) + \frac{\hat{s}^2\beta^2 z_0^2}{48}\Big(3+\frac{16}{\varepsilon^2}\Big)\Big]\,, \qquad \text{(D.4)}$$

where z_0 and L are defined in appendix B and $g_Z = \mathrm{cotg}\,\theta_w$. The above formulas are given in the case of rapidity cuts; then eq. (7.14) has to be inserted in eq. (B.1) to get the cross section and the asymmetry in an obvious way.

Appendix E. Contact terms in processes involving photons or gluons

The most general set of contact terms for two-fermion–two-vector-boson processes has been given in [MER87]. We have to restrict ourselves to the case where the vector bosons are true gauge bosons (γ and g). In this illustration, from the several forms of contact terms which are allowed we will choose the one with the lowest dimension and a spin structure which leads to strong interference with the standard amplitude. It is called R^2_{TT} in [MER87] and is defined with an effective compositeness scale Λ and a chiral structure $c - d\gamma_5$. It is also assumed that the color structure among quarks and gluons is the same for the contact term and for the standard amplitude.

In the case of $q\bar{q}\to\gamma g$ and $gq\to\gamma q$ the complete amplitude is given in the text [see eqs. (7.20) and (7.22)]. We give below the complete expressions for the cross sections in cases involving two gluons.

$q(h_1)\bar{q}(h_2)\to gg$:

$$\frac{d\hat{\sigma}}{d\hat{t}} = \Big(\frac{d\hat{\sigma}}{d\hat{t}}\Big)^{sm} + \frac{4\pi\alpha_s^2(\hat{u}^2+\hat{t}^2)}{3\hat{u}\hat{t}\hat{s}^2}\,[(1-h_1h_2)(C^2+D^2+\tfrac{2}{3}C)+(h_2-h_1)(2CD+\tfrac{2}{3}D)]\,; \qquad \text{(E.1)}$$

$\underline{g(\lambda)g(\lambda')\to q\bar{q}}$:

$$\frac{d\hat{\sigma}}{d\hat{t}} = \left(\frac{d\hat{\sigma}}{d\hat{t}}\right)^{sm} + \frac{\pi\alpha_s^2(\hat{u}^2+\hat{t}^2)}{8\hat{u}\hat{t}\hat{s}^2}\left((1-\lambda\lambda')[C+\tfrac{3}{2}(C^2+D^2)] - (\lambda'-\lambda)\frac{\hat{u}^2-\hat{t}^2}{\hat{u}^2+\hat{t}^2}(D+3CD)\right), \tag{E.2}$$

where we have taken $\hat{t} = (p_{\bar{q}} - p_{\lambda'})^2$;

$\underline{q(h)g(\lambda)\to qg}$:

$$\frac{d\hat{\sigma}}{d\hat{t}} = \left(\frac{d\hat{\sigma}}{d\hat{t}}\right)^{sm} + \frac{\pi\alpha_s^2}{-2\hat{u}\hat{s}^3}\{(\hat{u}^2+\hat{s}^2)[\tfrac{2}{3}(C'-D'h)+C'^2+D'^2-2C'D'h] + (\hat{u}^2-\hat{s}^2)\lambda[\tfrac{2}{3}(D'-C'h)+2C'D'-(C'^2+D'^2)h]\}. \tag{E.3}$$

For $\bar{q}(h)g(\lambda)\to\bar{q}g$, change $h\to -h$ and $\lambda\to-\lambda$.

In all the formulas, the corresponding standard cross sections $(d\hat{\sigma}/d\hat{t})^{sm}$ can be deduced from table 4.1 and we have defined $C = \hat{u}\hat{t}c/\Lambda^4$, $D = \hat{u}\hat{t}d/\Lambda^4$, $C' = \hat{u}\hat{s}c/\Lambda^4$ and $D' = \hat{u}\hat{s}d/\Lambda^4$.

Appendix F. Production of gaugino pairs

We give in this appendix the polarized differential cross sections $d\hat{\sigma}/d\Omega$ for the subprocesses $q_i(h_1)\bar{q}_i(h_2)\to\tilde{W}^+\tilde{W}^-$, $\tilde{Z}\tilde{Z}$, $\tilde{\gamma}\tilde{Z}$. The corresponding unpolarized integrated cross sections can be found in EHLQ (table IX) or in [DAW85] and in view of the simple structure described below, it is straightforward to obtain integrated cross sections in the polarized case. Cross sections for the processes $q_i\bar{q}_i\to\tilde{W}\tilde{Z}$, $\tilde{W}\tilde{\gamma}$, where the subprocess asymmetries are 100%, can be found in the same references. The general form of $d\hat{\sigma}/d\Omega$ for the above reactions can be written as

$$\frac{d\hat{\sigma}}{d\Omega} = \frac{\alpha^2\mathcal{S}}{\hat{s}^2}[(1-h_1h_2)X_1 + (h_2-h_1)X_2], \tag{F.1}$$

$$\mathcal{S} = [\hat{s}-(\tilde{M}+\tilde{M}')^2]^{1/2}[\hat{s}-(\tilde{M}-\tilde{M}')^2]^{1/2},$$

$\tilde{M}$ and $\tilde{M}'$ being the masses of the two outgoing gauginos.

(i) $q_i\bar{q}_i\to\tilde{W}^+\tilde{W}^-$:

$$X_1 = e + a + i, \tag{F.2}$$

$$X_2 = e + a' + i; \tag{F.3}$$

– exchange term:

$$e = \tfrac{1}{4}C_L^4[(\hat{t}-M_{\tilde{W}}^2)/(\hat{t}-m_{\tilde{q}_L}^2)]^2; \tag{F.4}$$

– annihilation terms:

$$a = \tfrac{1}{4}G_1(1+\beta_{\tilde{W}}^2\cos^2\theta) + \tfrac{1}{2}G_2\beta_{\tilde{W}}\cos\theta + G_3\,M_{\tilde{W}}^2/\hat{s}\,, \tag{F.5}$$

$$a' = \tfrac{1}{4}G_4(1+\beta_{\tilde{W}}^2\cos^2\theta) + \tfrac{1}{2}G_5\beta_{\tilde{W}}\cos\theta + G_6\,M_{\tilde{W}}^2/\hat{s}\,, \tag{F.6}$$

where $\beta_{\tilde{W}} = (1-4M_{\tilde{W}}^2/\hat{s})^{1/2}$ and

$$G_j = e_i^2 + 2e_ia_ia_{\tilde{W}}\hat{s}\,\mathrm{Re}\,D_Z + (a_i^2+b_i^2)(a_{\tilde{W}}^2+\varepsilon_jb_{\tilde{W}}^2)\hat{s}^2|D_Z|^2\,, \tag{F.7}$$

for $j=1,3$ with $\varepsilon_1 = -\varepsilon_3 = 1$,

$$G_j = 2e_iC_j\hat{s}\,\mathrm{Re}\,D_Z + D_j\hat{s}^2|D_Z|^2\,, \tag{F.8}$$

for $j=2,4,5,6$ with

$$\begin{aligned} &C_2 = b_ib_{\tilde{W}}\,, && D_2 = 4a_ib_ia_{\tilde{W}}b_{\tilde{W}}\,,\\ &C_4 = b_ia_{\tilde{W}}\,, && D_4 = 2a_ib_i(a_{\tilde{W}}^2+b_{\tilde{W}}^2)\,,\\ &C_5 = a_ib_{\tilde{W}}\,, && D_5 = 2a_{\tilde{W}}b_{\tilde{W}}(a_i^2+b_i^2)\,,\\ &C_6 = C_4\,, && D_6 = 2a_ib_i(a_{\tilde{W}}^2-b_{\tilde{W}}^2)\,; \end{aligned} \tag{F.9}$$

– interference between annihilation and exchange:

$$\begin{aligned} i = \frac{C_i^2}{2\hat{t}-m_{\tilde{q}}^2}\,&\{(e_i/\hat{s})[(\hat{t}-M_{\tilde{W}}^2)^2 + M_{\tilde{W}}^2\hat{s}]\\ &+ (a_i+b_i)\hat{s}\,\mathrm{Re}\,D_Z\,[(a_{\tilde{W}}-b_{\tilde{W}})(\hat{t}-M_{\tilde{W}}^2)^2 + (a_{\tilde{W}}+b_{\tilde{W}})M_{\tilde{W}}^2\hat{s}]\}\,. \end{aligned} \tag{F.10}$$

In the above formulas, e_i is the charge of quark q_i and a_i and b_i, the standard couplings of quarks to the Z^0, are defined in eq. (5.4). C_L is the coupling of the quark–squark–wino vertex occurring in the exchange term, $a_{\tilde{W}}$ and $b_{\tilde{W}}$ being the vector and axial couplings of the Z^0 to the $\tilde{W}^+\tilde{W}^-$ pair. The values of these supersymmetric couplings are model dependent. Some illustrations, following extreme cases of mixing, can be found, e.g., in [CHI85a]. In case of pure wino production one gets for example

$$a_{\tilde{W}} = -\mathrm{cotg}\,\theta_w\,, \qquad b_{\tilde{W}} = 0\,, \qquad C_L = \frac{-1}{\sqrt{2}\sin\theta_w}\,. \tag{F.11}$$

(ii) $q_i\bar{q}_i \to \tilde{Z}\tilde{Z}$, $\tilde{\gamma}\tilde{Z}$:

$$X_1 = e_L + e_R + \bar{e}_L + \bar{e}_R + i_L + i_R\,, \tag{F.12}$$

$$X_2 = e_L - e_R + \bar{e}_L - \bar{e}_R + i_L - i_R\,; \tag{F.13}$$

• $\tilde{Z}\tilde{Z}$:

$$e_{L,R} = \tfrac{1}{4}C_{L,R}^4[(\hat{t} - M_{\tilde{Z}}^2)/(\hat{t} - m_{\tilde{q}_{L,R}}^2)]^2\,, \qquad \bar{e}_{L,R} = e_{L,R} \text{ with } \hat{t} \leftrightarrow \hat{u}\,, \tag{F.14}$$

$$i_{L,R} = -\tfrac{1}{2}C_{L,R}^4 \frac{M_{\tilde{Z}}^2 \hat{s}}{(\hat{t} - m_{\tilde{q}_{L,R}}^2)(\hat{u} - m_{\tilde{q}_{L,R}}^2)}\,; \tag{F.15}$$

• $\tilde{\gamma}\tilde{Z}$:

$$e_{L,R} = e_i^2 C_{L,R}^2\,(l_i \cdot p_f)(l_i' \cdot p_f')/(\hat{t} - m_{\tilde{q}_{L,R}}^2)^2\,, \qquad \bar{e}_{L,R} = e_{L,R} \text{ with } \hat{t} \leftrightarrow \hat{u},\ p_f \leftrightarrow p_f'\,, \tag{F.16}$$

$$i_{L,R} = -\tfrac{1}{2}e_i^2\, C_{L,R}^2 \frac{M_{\tilde{Z}} M_{\tilde{\gamma}} \hat{s}}{(\hat{t} - m_{\tilde{q}_{L,R}}^2)(\hat{u} - m_{\tilde{q}_{L,R}}^2)}\,, \tag{F.17}$$

where l_i and l_i' are the momenta of the initial quark and antiquark, p_f and p_f' being those of the outgoing gauge bosons. The dot denotes here the scalar product. In the pure zino case the couplings at the vertex q_i–$\tilde{q}_{L,R}$–$\tilde{Z}^0$ are given by

$$C_L = -(a_i + b_i)\,, \qquad C_R = -(a_i - b_i)\,. \tag{F.18}$$

Appendix G. Collection of definitions and technical expressions for WW collision processes

As we mentioned in section 9.2, the invariant mass distribution $d\sigma/d\xi$ for $q + q' \to q + q' + VV'$ involves 9 terms [see eq. (9.10)]. The nine sub-cross sections occurring in eq. (9.10) are simply related [CAP88] to the nine cross sections $\hat{\sigma}(++)$, $\hat{\sigma}(+-)$, $\hat{\sigma}(+0)$, $\hat{\sigma}(0+)$, $\hat{\sigma}(0-)$, $\hat{\sigma}(00)$, $\hat{\sigma}(-+)$, $\hat{\sigma}(--)$, $\hat{\sigma}(-0)$ for the process $VV' \to X$ with all possible helicities for the two vector bosons. The five parity conserving sub-cross sections are

$$\begin{aligned}
&\hat{\sigma}_{TT} = \tfrac{1}{4}[\hat{\sigma}(++) + \hat{\sigma}(--) + \hat{\sigma}(-+) + \hat{\sigma}(+-)]\,, \qquad \hat{\sigma}_{LL} = \hat{\sigma}(00)\,,\\
&\hat{\sigma}_{TL} = \tfrac{1}{2}[\hat{\sigma}(+0) + \hat{\sigma}(-0)]\,, \qquad \hat{\sigma}_{LT} = \tfrac{1}{2}[\hat{\sigma}(0+) + \hat{\sigma}(0-)]\,,\\
&\hat{\sigma}_{T\bar{T}} = \tfrac{1}{4}[\hat{\sigma}(++) + \hat{\sigma}(--) - \hat{\sigma}(-+) - \hat{\sigma}(+-)]\,,
\end{aligned} \tag{G.1}$$

and the four parity violating ones are

$$\begin{aligned}
&\hat{\sigma}_{T\bar{T}} = \tfrac{1}{4}[\hat{\sigma}(++) - \hat{\sigma}(--) - \hat{\sigma}(-+) + \hat{\sigma}(+-)]\,,\\
&\hat{\sigma}_{\bar{T}T} = \tfrac{1}{4}[\hat{\sigma}(++) - \hat{\sigma}(--) + \hat{\sigma}(-+) - \hat{\sigma}(+-)]\,,\\
&\hat{\sigma}_{\bar{T}L} = \tfrac{1}{2}[\hat{\sigma}(+0) - \hat{\sigma}(-0)]\,, \qquad \hat{\sigma}_{L\bar{T}} = \tfrac{1}{2}[\hat{\sigma}(0+) - \hat{\sigma}(0-)]\,.
\end{aligned} \tag{G.2}$$

We also need the corresponding luminosity factors, which can be obtained in the LEWA limit by using eqs. (9.1), (9.2), (9.3) in eq. (9.11). They read

$$\mathcal{L}_{TT} = A_h A'_{h'} \left(\frac{\alpha}{2\pi}\right)^2 \frac{1}{\xi} [(2+\xi)^2 \log(1/\xi) - 2(1-\xi)(3+\xi)] LL' ,$$

$$\mathcal{L}_{LL} = A_h A'_{h'} \left(\frac{\alpha}{\pi}\right)^2 \frac{1}{\xi} [(1+\xi) \log(1/\xi) - 2(1-\xi)] ,$$

$$\mathcal{L}_{TL} = A_h A'_{h'} \left(\frac{\alpha^2}{2\pi^2}\right) \frac{1}{\xi} [2(1+\xi) \log(1/\xi) - \tfrac{1}{2}(1-\xi)(7+\xi)] L ,$$

$$\mathcal{L}_{LT} = A_h A'_{h'} \left(\frac{\alpha^2}{2\pi^2}\right) \frac{1}{\xi} [2(1+\xi) \log(1/\xi) - \tfrac{1}{2}(1-\xi)(7+\xi)] L' ,$$

$$\mathcal{L}_{\bar{T}\bar{T}} = B_h B'_{h'} \left(\frac{\alpha}{2\pi}\right)^2 [(4+\xi) \log(1/\xi) - 4(1-\xi)] LL' , \qquad \text{(G.3)}$$

$$\mathcal{L}_{T\bar{T}} = A_h B'_{h'} \left(\frac{\alpha}{2\pi}\right)^2 \frac{1}{\xi} [3(1-\xi^2) + \xi(4+\xi) \log \xi] LL' ,$$

$$\mathcal{L}_{\bar{T}T} = B_h A'_{h'} \left(\frac{\alpha}{2\pi}\right)^2 \frac{1}{\xi} [3(1-\xi^2) + \xi(4+\xi) \log \xi] LL' ,$$

$$\mathcal{L}_{\bar{T}L} = B_h A'_{h'} \left(\frac{\alpha^2}{2\pi^2}\right) \frac{1}{2\xi} [3 - 2\xi - \xi^2 + 4\xi \log \xi] L ,$$

$$\mathcal{L}_{T\bar{T}} = A_h B'_{h'} \left(\frac{\alpha^2}{2\pi^2}\right) \frac{1}{2\xi} [3 - 2\xi - \xi^2 + 4\xi \log \xi] L' ,$$

where we define $A_h = a^2 + b^2 - 2abh$ and $B_h = 2ab - (a^2 + b^2)h$; h (h') the helicity of the initial quark q (q'); a, b (a', b') the standard Vqq (V'q'q') vector and axial couplings; $L \to \log(4E_q^2/M_V^2)$ and $L' \to \log(4E_{q'}^2/M_{V'}^2)$.

References

[ADE85] B. Adeva et al., Phys. Lett. B 152 (1985) 439, and references therein.

[ADE86] B. Adeva, F. Del Aguila, D.V. Nanopoulos, M. Quiros and F. Zwirner, in: Proc. 1986 Summer Study on the Physics of the SSC (Snowmass, 1986), eds R. Donaldson and J. Marx, p. 257.

[AGU87] F. Del Aguila, M. Quiros and F. Zwirner, in: Proc. Workshop on Physics at Future Accelerators (La Thuile and Geneva, 1987), ed. J. Mulvey, CERN Yellow Report 87-07, Vol. II, p. 165.

[AHN88] C. Ahn et al., Opportunities and Requirements for experimentation at a very high energy e^+e^- collider, SLAC Report 329 (May 1988).

[ALB84] C.H. Albright et al., in: Proc. 1984 Summer Study on the Design and Utilization of the SSC (Snowmass, CO), eds R. Ronaldson and J. Morfin, p. 27.

[ALE88] G. Alexander et al., eds, Polarization at LEP, CERN Report 88-06, Vols. I and II (Sept. 1988).

[ALT77] G. Altarelli and G. Parisi, Nucl. Phys. B 126 (1977) 298.

[ALT88] G. Altarelli and G.G. Ross, Phys. Lett. B 212 (1988) 391.

[AND83] B. Andersson, G. Gustafson, G. Ingelman and T. Sjöstrand, Phys. Rep. 97 (1983) 31.

[AND88] G. Anderson and I. Hinchliffe, in: Proc. Workshop on Experiments, Detectors and Experimental Areas for the Supercollider, eds R. Donaldson and M.G.D. Gilchriese (World Scientific, Singapore, 1988) p. 282.

[ANS85] A.A. Ansel'm, N.G. Ural'tsev and V.A. Khoze, Sov. Phys. - Usp. 28 (1985) 113.

[ANS88] M. Anselmino, B.L. Ioffe and E. Leader, preprint NSF-ITP-88-94 (June 1988).

[ANT80] J. Antille et al., Phys. Lett. B 94 (1980) 523.
[APP85] UA2 Collab., J.A. Appel et al., Phys. Lett. B 160 (1985) 349.
[ARM85] T.A. Armstrong et al., Nucl. Phys. B 262 (1985) 356.
[ARN83] UA1 Collab., G. Arnison et al., Phys. Lett. B 122 (1983) 103; B 126 (1983) 398.
[ARN86] UA1 Collab., G. Arnison et al., Phys. Lett. B 172 (1986) 461.
[ART82] A.S. Artamonov et al., Phys. Lett. B 118 (1982) 225.
[ART84] N. Arteaga-Romero, A. Nicolaidis and J. Silva, Phys. Rev. Lett. 52 (1984) 172.
[ASH88] J. Ashman et al., Phys. Lett. B 206 (1988) 364.
[AUE77] I.P. Auer et al., Phys. Lett. B 70 (1977) 475.
[BAB79] J. Babcock, E. Monsay and D. Sivers, Phys. Rev. D 19 (1979) 1483.
[BAG83] UA2 Collab., P. Bagnaia et al., Phys. Lett. B 129 (1983) 130.
[BAL81] F. Baldracchini et al., Fortschr. Phys. 30 (1981) 505.
[BAN83] UA2 Collab., M. Banner et al., Phys. Lett. B 122 (1983) 476.
[BAR86] I. Bars and I. Hinchliffe, Phys. Rev. D 33 (1986) 704.
[BAR86a] R.M. Barnett, in: Proc. 1986 Summer Study on the Physics at the SSC (Snowmass, 1986), eds R. Donaldson and J. Marx, p. 262.
[BAR87] V. Barger, N.G. Deshpande, J.L. Rosner and K. Whisnant, Phys. Rev. D 35 (1987) 2893.
[BAR88] V. Barger, J.L. Lopez and W. Putikka, preprint Univ. of Wisconsin MAD/PH/406 (January 1988).
[BAT87] R. Batley, in: Proc. Workshop on Physics at Future Accelerators (La Thuile and Geneva, 1987), ed. J. Mulvey, CERN 87-07, Vol. II, p. 109.
[BAT88] R. Batley, Supersymmetric particle searches at future hadron colliders, CERN-EP/88-19.
[BAU83] G. Baum et al., Phys. Rev. Lett. 51 (1983) 1135.
[BAU86] U. Baur and K.H. Schwarzer, Phys. Lett. B 180 (1986) 163.
[BAU87] U. Baur, M. Lindner and K.H. Schwarzer, Nucl. Phys. B 291 (1987) 1.
[BAU87a] U. Baur, D. Schildknecht and K.H. Schwarzer, Phys. Rev. D 35 (1987) 297.
[BAU88] U. Baur and D. Zeppenfeld, Nucl. Phys. B 308 (1988) 127.
[BEN86] H.U. Bengtsson, in: Proc. 1986 Summer Study on the Physics at the SSC (Snowmass, 1986), eds R. Donaldson and J. Marx, p. 167.
[BIL88] C. Bilchak, M. Kuroda and D. Schildknecht, Nucl. Phys. B 299 (1988) 7.
[BJO66] J.D. Bjorken, Phys. Rev. 148 (1966) 1467.
[BJO70] J.D. Bjorken, Phys. Rev. D 1 (1970) 1376.
[BJO82] J.D. Bjorken, in: Proc. 5th Intern. Symp. on High Energy Spin Physics (Brookhaven Natl. Lab., NY, 1982), ed. G.M. Bunce, AIP Conf. Proc. 95, p. 268.
[BLO87] A. Blondel, in: Proc. Workshop on Physics at Future Accelerators (La Thuile and Geneva, 1987), ed. J.H. Mulvey, CERN Report 87-07, Vol. II, p. 173.
[BOU80] C. Bourrely, E. Leader and J. Soffer, Phys. Rep. 59 (1980) 95.
[BOU83] M. Bourquin et al., Z. Phys. C 21 (1983) 27.
[BOU87] C. Bourrely, J. Soffer and P. Taxil, Phys. Rev. D 36 (1987) 3373.
[BOU87a] C. Bourrely, J. Soffer and T.T. Wu, Phys. Rev. Lett. 59 (1987) 2009.
[BRO79] R.W. Brown and K.O. Mikaelian, Phys. Rev. D 19 (1979) 922.
[BRO79a] R.W. Brown, D. Sahdev and K.O. Mikaelian, Phys. Rev. D 20 (1979) 1164.
[BRO82] G.M. Bunce, ed., Proc. 5th Intern. Symp. on High Energy Spin Physics (Brookhaven Natl. Lab., NY, 1982), (AIP Conf. Proc. 95).
[BRO88] S.J. Brodsky, J. Ellis and M. Karliner, Phys. Lett. B 206 (1988) 309.
[BUD75] V.M. Budnev et al., Phys. Rep. 15 (1975) 181.
[BUK78] A.D. Bukin et al., Yad. Fiz. 27 (1978) 976.
[CAH84] R.N. Cahn and S. Dawson, Phys. Lett. B 136 (1984) 196.
[CAH88] R.N. Cahn et al., in: Proc. Workshop on Experiments, Detectors and Experimental Areas for the Supercollider, eds R. Donaldson and M.G.D. Gilchriese (World Scientific, Singapore, 1988) p. 20.
[CAM85] P.R. Cameron et al., Phys. Rev. D 32 (1985) 3070.
[CAN85] P. Candelas et al., Nucl. Phys. B 258 (1985) 46.
[CAP88] M. Capdequi Peyranère et al., Z. Phys. C 41 (1988) 99.
[CAR77] R. Carlitz and J. Kaur, Phys. Rev. Lett. 38 (1977) 1116;
J. Kaur, Nucl. Phys. B 128 (1977) 219.
[CAR88] R. Carlitz, J.C. Collins and A.H. Mueller, Phys. Lett. B 214 (1988) 229.
[CER88] UA6 Collab., Study of spin effects in pp and pp interactions at the SPS using a polarized atomic hydrogen beam target, letter of intent, CERN/SPSC/88-9, SPSC/I 168.
[CHA85] M. Chaichian, M. Hayashi, K. Yamagishi and J. Soffer, Nuovo Cimento 90 (1985) 327.
[CHA85a] M.S. Chanowitz and M.K. Gaillard, Nucl. Phys. B 261 (1985) 379.
[CHA86] M.S. Chanowitz, Weak Interactions at the SSC, invited talk presented at the Workshop on Standard Model Physics at the SSC (1986) preprint LBL-21290 (1986).

[CHA87] C.H. Chang and S.C. Lee, Phys. Lett. B 197 (1987) 220.
[CHA88] C.H.. Chang and S.C. Lee, Phys. Rev. D 37 (1988) 101.
[CHE88] M. Chen et al., Phys. Rep. 159 (1988) 201.
[CHI85] P. Chiappetta, J.Ph. Guillet and J. Soffer, Nucl. Phys. B 262 (1985) 187.
[CHI85a] P. Chiappetta, F. Renard, J. Soffer, P. Sorba and P. Taxil, Nucl. Phys. B 259 (1985) 365.
[CHI85b] P. Chiappetta, F. Renard, J. Soffer, P. Sorba and P. Taxil, Nucl. Phys. B 262 (1985) 495; Erratum Nucl. Phys. B 279 (1987) 824.
[CHI87] P. Chiappetta, J.Ph. Guillet and J. Soffer, Phys. Lett. B 183 (1987) 213.
[CHI88] R.S. Chivukula and L. Randall, Phys. Lett. B 202 (1988) 429.
[CLO88] F.E. Close and R.G. Roberts, Phys. Rev. Lett. 60 (1988) 1471.
[COH85] E. Cohen et al., Phys. Lett. B 165 (1985) 76.
[COL84] J.C. Collins, in: Proc. 1984 Summer Study on the Design and Utilization of the SSC (Snowmass, CO), eds R. Donaldson and J. Morfin, p. 251.
[COR87] F. Cornet and R. Rückl, in: Proc. Workshop on Physics at Future Accelerators (La Thuile and Geneva, 1987), ed. J. Mulvey, CERN Report 87-07, Vol. II, p. 287.
[COU84] E.D. Courant, in: Proc. 6th Intern. Symp. on High Energy Spin Physics (Marseille, 1984), ed. J. Soffer, J. Physique Colloq. 46, 713.
[CRA83] N.S. Craigie, K. Hidaka, M. Jacob and F.M. Renard, Phys. Rep. 99 (1983) 69.
[CRA83a] N.S. Craigie, K. Hidaka and P. Ratcliffe, Phys. Lett. B129 (1983) 310.
[DAW84] S. Dawson and A. Savoy-Navarro, in: Proc. 1984 Summer Study on the Design and Utilization of the SSC (Snowmass, 1984), eds R. Donaldson and J. Morfin, p. 263.
[DAW84a] S. Dawson and J. Rosner, Phys. Lett. B 148 (1984) 497.
[DAW85] S. Dawson, E. Eichten and C. Quigg, Phys. Rev. D 31 (1985) 1581.
[DAW85a] S. Dawson, Nucl. Phys. B 249 (1985) 42.
[DAW86] S. Dawson, G. Kane, C.P. Yuan and S.S.D. Willenbrock, in: Proc. 1986 Summer Study on the Physics of the SSC (Snowmass, 1986), eds R. Donaldson and J. Marx, p. 235.
[DAW87] S. Dawson and S.S. Willenbrock, Nucl. Phys. B 284 (1987) 449.
[DEG85] T. Degrand, J. Markkanen and H. Miettinen, Phys. Rev. D 32 (1985) 2445.
[DER77] Y.A. Derbenev et al., in: Proc. 10th Intern. Conf. on High Energy Accelerators (Protvino, USSR, 1977), Vol. 2, p. 70; Part. Accel. 10 (1980) 177.
[DES87] N.G. Deshpande, J.F. Gunion and F. Zwirner, preprint LBL-23774 (1987).
[DIC88] L. Dick and W. Kubischta, preprint CERN-EP/88-135.
[DIO87] C. Dionisi, in: Proc. ECFA Workshop on LEP 200, CERN 87-08, p. 380.
[DIO87a] C. Dionisi and M. Dittmar, in: Proc. Workshop on Physics at Future Accelerators (La Thuile and Geneva, 1987), ed. J. Mulvey, CERN 87-07, Vol. II, p. 149.
[DUN86] M.J. Duncan, G.L. Kane and W.W. Repko, Nucl. Phys. B 272 (1986) 517.
[DUN86a] M.J. Duncan, Phys. Lett. B 179 (1986) 393.
[EFR88] A.V. Efremov and O.V. Teryaev, JINR preprint EL-88-287.
[EIC84] E. Eichten, I. Hinchliffe, K. Lane and C. Quigg, Rev. Mod. Phys. 56 (1984) 579; Erratum 58 (1986) 1065 (referred to as EHLQ).
[EIC86] E. Eichten, I. Hinchliffe, K.D. Lane and C. Quigg, Phys. Rev. D 34 (1986) 1547.
[EIN86] M.B. Einhorn and J. Soffer, Nucl. Phys. B 274 (1986) 714.
[ELL74] J. Ellis and R.L. Jaffe, Phys. Rev. D 9 (1974) 1444.
[ELL86] R.K. Ellis and J.C. Sexton, Nucl. Phys. B 269 (1986) 445.
[ELL86a] J. Ellis et al., Nucl. Phys. B 276 (1986) 14.
[ELL88] J. Ellis and F. Pauss, Search for new physics, in: Proton–Antiproton Collider Physics (World Scientific, Singapore, 1988).
[ELL88a] J. Ellis and M. Karliner, Phys. Lett. B 213 (1988) 73.
[FAR79] E. Farhi and L. Susskind, Phys. Rev. D 20 (1979) 3404.
[FAY75] P. Fayet, Nucl. Phys. B 90 (1975) 104.
[FAY77] P. Fayet and S. Ferrara, Phys. Rep. 32 (1977) 249.
[FNA88] E. Berger, J.G. Morfin, A.L. Read and A. Yokosawa, eds, Proc. Symp. on Future Polarization Physics at Fermilab (FNAL, June 1988).
[GAE79] K.J.F. Gaemers and G.J. Gounaris, Z. Phys. C 1 (1979) 259, and references therein.
[GEE86] S. Geer, in: Proc. 23rd Intern. Conf. on High Energy Physics (Berkeley, 1986), ed. S.C. Loken (World Scientific, Singapore, 1987) p. 982.
[GEO78] H. Georgi et al., Phys. Rev. Lett. 40 (1978) 692.
[GIA85] A. Giannelli, L. Nitti, G. Preparata and P. Sforza, Phys. Lett. B 150 (1985) 214.
[GLA61] S.L. Glashow, Nucl. Phys. 22 (1961) 579.
[GLU88] M. Glück and E. Reya, Z. Phys. 39 (1988) 569.
[GOL71] Y.A. Gol'fand and E.P. Likhtmann, JETP Lett. 13 (1971) 323.
[GOU86] S.A. Gourlay et al., Phys. Rev. Lett. 56 (1986) 2244.
[GRI83] L. Gribov, E. Levin and M. Ryskin, Phys. Rep. 100 (1983) 1.

[GUI88] J.Ph. Guillet, Z. Phys. C 39 (1988) 75.
[GUN86] J. Gunion et al., in: Proc. 1986 Summer Study on the Physics of the SSC (Snowmass, 1986), eds R. Donaldson and J. Marx, p. 197.
[GUN87] J.F. Gunion and A. Tofighi-Niaki, Phys. Rev. D 36 (1987) 2671.
[HAB85] H. Haber and G.L. Kane, Phys. Rep. 117 (1985) 75.
[HAL85] L.J. Hall, R.L. Jaffe and J.L. Rosner, Phys. Rep. 125 (1985) 103.
[HAR84] H. Harari, Phys. Rep. 104 (1984) 159, and references therein.
[HID81] K. Hidaka, Nucl. Phys. B 192 (1981) 369.
[HUG88] W. Hughes et al., Phys. Lett. B 212 (1988) 511.
[JON79] D.R.T. Jones and S.T. Petcov, Phys. Lett. B 84 (1979) 440.
[KAN84] G.L. Kane, W.W. Repko and W.B. Rolnick, Phys. Lett. B 148 (1984) 367.
[KNE87] J.L. Kneur, S. Larbi and S. Narison, Phys. Lett. B 194 (1987) 147.
[KOD79] J. Kodaira, S. Matsuda, T. Muta, T. Uematsu and K. Sasaki, Phys. Rev. D 20 (1979) 627.
[KRI85] A.D. Krisch, in: Polarized Beams at SSC (Ann Arbor, 1985), eds. A.D. Krisch, M. Lin and O. Chamberlain, AIP Conf. Proc. 145, p. 11.
[KRI87] A.D. Krisch et al., Proposal. Experimental Test of the Siberian Snake Concept (1987).
[KUR85] M. Kuroda, D. Schildknecht and K.N. Schwarzer, Nucl. Phys. B 261 (1985) 432.
[KUR87] M. Kuroda, J. Maalampi, D. Schildknecht and K.H. Schwarzer, Nucl. Phys. B 284 (1987) 271.
[KUR88] M. Kuroda, F.M. Renard and D. Schildknecht, Z. Phys. C 40 (1988) 575.
[LAN82] K. Lane, in: Proc. 1982 Summer Study on Elementary Particle Physics and Future Facilities (Snowmass, 1982), eds R. Donaldson, R. Gustafon and F. Paige, p. 222.
[LAN84] P. Langacker, in: Proc. 1984 Summer Study on the Design and Utilization of the SSC (Snowmass, 1984), eds R. Donaldson and J.G. Morfin, p. 771.
[LAN84a] P. Langacker, R.W. Robinet and J.L. Rosner, Phys. Rev. D 30 (1984) 1470.
[LEA88] E. Leader and M. Anselmino, Z. Phys. C 41 (1988) 239.
[LEE77] B.W. Lee, C. Quigg and H.B. Thacker, Phys. Rev. D 16 (1977) 1519.
[LEP86] J. Ellis and R. Peccei, eds., Physics at LEP, CERN-86-02, Vols. I and II.
[LEU82] C.N. Leung and J.L. Rosner, Phys. Rev. D 29 (1982) 2132.
[LIN76] A. Linde, JETP Lett. 23 (1976) 64.
[LIN87] J. Lindfors, Z. Phys. C 33 (1987) 385.
[LIN87a] J. Lindfors, Z. Phys. C 35 (1987) 355.
[LON86] D. London and J.L. Rosner, Phys. Rev. D 34 (1986) 1530.
[LYN87] B.W. Lynn and C. Verzegnassi, Phys. Rev. D 35 (1987) 51.
[MAA86] J. Maalampi, D. Schildknecht and K.H. Schwarzer, Phys. Lett. B 166 (1986) 361.
[MAN87] B. Mansoulie, in: Proc. Workshop on Physics at Future Accelerators (La Thuile and Geneva, 1987), ed. J. Mulvey, CERN 87-07, p. 126.
[MAR84] J. Soffer, ed., Proc. 6th Intern. Symp. on High Energy Spin Physics (Marseille, 1984), J. Physique Colloq. 46.
[MER87] P. Mery, M. Perrottet and F.M. Renard, Z. Phys. C 36 (1987) 249.
[MER88] P. Mery, M. Perrottet and F.M. Renard, Z. Phys. C 38 (1988) 579.
[MIL88] D. Miller, Polarized p ($\bar{p}$) beams at Tevatron (E704), talk at Conf. on Spin and Polarization Dynamics in Nuclear and Particle Physics (Trieste, January 1988).
[MIN88] K. Heller, ed., Proc. 8th Intern. Symp. on High Energy Spin Physics (Minneapolis, Sept. 1988), AIP Conf. Proc.
[MOH83] R.N. Mohapatra, Lectures delivered at the NATO Summer School on Particle Physics (Munich, 1983), preprint Md DP-PP-84-0012, and references therein.
[MON84] B.W. Montague, Phys. Rep. 113 (1984) 1.
[NEU87] H. Neufeld, J.D. Stroughair and D. Schildnecht, Phys. Lett. B 198 (1987) 563.
[NIL84] H.P. Nilles, Phys. Rep. 110 (1984) 1.
[ORI79] Jade Collab., S. Orito, in: Proc. 1979 Intern. Symp. on Lepton and Photon Interactions, eds T.B.W. Kirk and H.D.I. Abarbanel, p. 52.
[OWE84] J.F. Owens, T. Ferbel, M. Dine and I. Bars, in: Proc. 1984 Summer Study on the Design and Utilization of the SSC (Snowmass, 1984), eds R. Donaldson and J. Morfin, p. 218.
[OWE87] J.F. Owens, Rev. Mod. Phys. 59 (1987) 465.
[PEC86] R.D. Peccei, in: Proc. 23rd Intern. Conf. on High Energy Physics (Berkeley, 1986), ed. S.C. Loken (World Scientific, Singapore, 1987) p. 3, and references therein.
[PES81] M.E. Peskin, in: Proc. 1981 Intern. Symp. on Lepton–Photon Interactions at High Energies (Bonn, 1981), ed. W. Pfeil, p. 880.
[PES85] M.E. Peskin, in: Proc. 1985 Intern. Symp. on Lepton–Photon Interactions at High Energies (Kyoto, 1985), eds M. Konuma and K. Takahashi, p. 714.
[PRE78] Y. Prescott et al., Phys. Lett. B 77 (1978) 347.
[PRE79] Y. Prescott et al., Phys. Lett. B 84 (1979) 524.
[PRE88] G. Preparata and J. Soffer, Phys. Rev. Lett. 61 (1988) 1167; Erratum Phys. Rev. Lett. 62 (1989) 1213.

[PRO79] A. van Proeyen, Phys. Rev. D 20 (1979) 813.
[RAL86] J.P. Ralston, Phys. Lett. B 172 (1986) 430.
[RAL86a] J.P. Ralston and F. Olness, in: Proc. 1986 Summer Study on the Physics of the SSC (Snowmass, 1986), eds R. Donaldson and J. Marx, p. 191.
[RAM88] G.P. Ramsey, D. Richards and D. Sivers, Phys. Rev. D 37 (1988) 3140.
[RAT83] P. Ratcliffe, Nucl. Phys. B 223 (1983) 45.
[RIC86] E. Richter-Was, Phys. Rev. D 34 (1986) 2893.
[ROB82] R.W. Robinet and J.L. Rosner, Phys. Rev. D 25 (1982) 3036.
[ROB84] R.W. Robinet and J.L. Rosner, Phys. Rev. D 30 (1984) 1470.
[ROS87] J.L. Rosner, Phys. Rev. D 35 (1987) 2244.
[RÜC87] R. Rückl, in: Proc. ECFA Workshop on LEP 200, CERN 87-08, p. 453.
[RUT84] R.D. Ruth, in: Proc. 6th Intern. Symp. on High Energy Spin Physics (Marseille, 1984), ed. J. Soffer, J. Physique Colloq. 46, 611.
[RYZ87] Z. Ryzak, Nucl. Phys. B 289 (1987) 301.
[SAL68] A. Salam, in: Proc. VIII Nobel Symp., ed. N. Svartholm (Almqvist and Wiksell, Stockholm, 1968) p. 367.
[SAL75] A. Salam and T. Strathdee, Nucl. Phys. B 87 (1975) 85.
[SAV87] A. Savoy-Navarro and N. Zaganidis, in: Proc. Workshop on Physics at Future Accelerators (La Thuile and Geneva, 1987), ed. J. Mulvey, CERN 87-07, p. 82.
[SCH75] R.F. Schwitters et al., Phys. Rev. Lett. 35 (1975) 1320, 1609.
[SCH84] P.W. Schmor, in: Proc. 6th Intern. Symp. on High Energy Spin Physics (Marseille, 1984), ed. J. Soffer, J. Physique Colloq. 46, 683.
[SCH85] D.H. Schiller and D. Wahner, Nucl. Phys. B 255 (1985) 505.
[SEN84] G. Senjanovic, in: Phenomenology of Unified Theories, eds H. Galić, B. Guberina and D. Tadić (World Scientific, Singapore, 1984) p. 133, and references therein.
[SER86] Proc. 7th Intern. Symp. on High Energy Spin Physics (Serpukhov, Protvino, 1986).
[SNO86] R. Donaldson and J. Marx, eds, Snowmass 86, Proc. 1986 Summer Study on the Physics of the SSC.
[SOF85] J. Soffer, in: Polarized Beams at SSC (Ann Arbor, 1985), eds A.D. Krisch, A.M.T. Lin and O. Chamberlain, AIP Conf. Proc. 145, p. 141.
[SOF87] J. Soffer, in: Proc. Workshop on The Elementary Structure of Matter (Les Houches, 1987), eds J.M. Richard, E. Aslanides and N. Boccara, Springer Proc. in Physics 26, p. 173.
[SOF87a] J. Soffer, in: Proc. EPS Intern. Conf. on High Energy Physics (Uppsala, 1987), ed. O. Bottner (Uppsala Univ.) p. 497.
[STU87] C. Stubenrauch, Thesis, CEA-N-2532 (1987).
[SUS79] L. Susskind, Phys. Rev. D 20 (1979) 2619.
[TER83] K. Terwilliger et al., in: Accelerator Physics for SSC (Ann Arbor, 1983), ed. M. Tigner, UM HE 84-1.
[TER88] K. Terwilliger, in: Proc. Symp. on Future Polarization Physics at Fermilab (FNAL, June 1988), eds E. Berger, J.G. Morfin, A.L. Read and A. Yokosawa, p. 107.
[TRE87] D. Treille, in: Proc. ECFA Workshop on LEP 200, CERN 87-08, p. 414.
[UKE86] F. Ukegawa, Y. Takaiwa and K. Kondo, in: Proc. 1986 Summer Study on the Physics at the SSC (Snowmass, 1986), eds R. Donaldson and J. Marx, p. 276.
[VAS88] A. Vasiliev, Proc. 8th Intern. Symp. on High Energy Spin Physics (Minneapolis, 1988), ed. K. Heller, AIP Conf. Proc.
[VOL73] D. Volkov and V.P. Akulov, Phys. Lett. B 46 (1973) 109.
[WEI67] S. Weinberg, Phys. Rev. Lett. 19 (1967) 1264.
[WEI76] S. Weinberg, Phys. Rev. Lett. 36 (1976) 294.
[WEI76a] S. Weinberg, Phys. Rev. D 13 (1976) 974.
[WEI79] S. Weinberg, Phys. Rev. D 19 (1979) 1277.
[WES74] J. Wess and B. Zumino, Nucl. Phys. B 70 (1974) 39.
[WIL85] S.S. Willenbrock and D. Dicus, Phys. Lett. B 156 (1985) 429.
[WIL86] S.S. Willenbrock and D. Dicus, Phys. Rev. D 34 (1986) 155.
[WIL87] C. Wilkinson et al., Phys. Rev. Lett. 58 (1987) 855.
[WIT85] E. Witten, Nucl. Phys. B 258 (1985) 75.
[WU87] S.L. Wu, in: Proc. 1987 Intern. Symp. on Lepton and Photon Interactions at High Energy (Hamburg, 1987), eds W. W. Bartel and R. Rückl, Nucl. Phys. B (Proc. Suppl.) 3 (1988) p. 39.
[YOK80] A. Yokosawa, Phys. Rep. 64 (1980) 47.
[ZEP88] D. Zeppenfeld and S. Willenbrock, Phys. Rev. D 37 (1988) 1775.